NRL Report 6607

AD 662189

Metallurgical Characteristics of High Strength Structural Materials

Twelfth Progress Report

R. J. Goode, R. W. Huber, D. G. Howe, R. W. Judy, Jr., T. W. Crooker, E. A. Lange, C. N. Freed, and P. P. Puzak

Strength of Metals Branch
Metallurgy Division

September 1967

NAVAL RESEARCH LABORATORY
Washington, D.C.

CONTENTS

PRECEDING PAGE BLANK

CONTENTS (Contd)

ABSTRACT

A progress report covering the research studies in high strength structural metals conducted during the period July 1966 through January 1967 is presented. The report includes fracture toughness studies on some new titanium alloys as well as results of an initial feasibility study aimed at raising the optimum strength and toughness limits for titanium alloys through an approach involving thick section composites. The results of salt water stress-corrosion-cracking studies on a number of titanium alloys are described including a study concerning the effect of vacuum heat treatment on stress-corrosion-cracking resistance of titanium alloys. Fatigue crack propagation studies in air and in salt water on the pressure vessel steels A302B, A201B, and A517F are discussed; and the results compared to the actual service performance of these same materials in PVRC program studies. Preliminary fracture toughness correlation diagrams are presented for high strength steels based upon fracture mechanics and engineering test methods. The latest versions of the Fracture Toughness Index Diagrams for steels, titanium alloys and aluminum alloys, a usual feature of this report series and which are based upon engineering test methods, are presented and the significance of the features briefly discussed. Fracture toughness studies on thick plates of 5Ni-Cr-Mo-V, and a "new" 9Ni-4Co steel are reported. In addition, the results are presented for similar studies on welds of 2Mn-2Ni in 5Ni-Cr-Mo-V steels and welds of 9Ni-4Co, 12Ni-3Cr-3Mo and 17Ni-2Co-3Mo compositions.

PROBLEM STATUS

This is a progress report; work is continuing.

AUTHORIZATION

NRL Problem F01-17; Project S-4607-11894
NRL Problem M01-05; Projects RR-007-01-46-5405, and SF-020-01-01-0724
NRL Problem M01-18; Projects RR-007-01-46-5420, SF-020-01-05-0731, and ENG-NAV-67-1
NRL Problem M03-01; Projects RR-007-01-46-5414, and SF-020-01-01-0850
NRL Problem M04-08B; ARPA 878

Manuscript submitted June 26, 1967.

METALLURGICAL CHARACTERISTICS OF HIGH STRENGTH STRUCTURAL MATERIALS

[Twelfth Progress Report]

INTRODUCTION

This report is the twelfth in the series of status reports covering the U.S. Naval Research Laboratory Metallurgy Division's long-range Advanced High Strength Structural Metals Program. This program is concerned with determining the performance characteristics of high strength metals and is directed to developing the necessary information to provide "guideline" principles for the metallurgical optimization of alloys, for processing and fabrication techniques and for reliable failure-safe utilization of these materials in large complex structures. Fracture toughness aspects of the failure-safe design problem are being studied with recently developed and conventional, long-established engineering test methods. The subcritical crack growth characteristics of the high strength metals are studied under conditions of low cycle fatigue. Environmental effects on subcritical crack growth and the application of fracture mechanics techniques for the spectrum of materials under investigation are also being studied.

The drop-weight tear and explosion tear tests and the Charpy V notch (for steels in particular) have been used to determine the fracture toughness characteristics of steels, titanium alloys, and aluminum alloys over wide ranges of yield strengths and have made possible the development of fracture toughness index diagrams for these materials. These diagrams which have been featured in this Progress Report Series, provide guideline information for purposes of design, alloy development, specification, and quality control. The latest versions of these diagrams for steels, titanium alloys and aluminum alloys are presented in this report.

Preliminary fracture toughness characteristics have been determined for the new alloys Ti-6Al-4V 2Mo, Ti-6Al-6V-2Sn-2Mo, Ti-4Al-3Mo-1V, Ti-2Al-4Mo-4Zr, and a new heat of Ti-6Al-4V. The results indicate that the Ti-4Al-3Mo-1V alloy has considerable potential for high toughness in the 120 ksi yield strength range although welding may be a problem. A Ti-6Al-2Cb-1Ta-0.8Mo alloy from a heat-treatment

study indicates a high level of fracture toughness below 110 ksi yield strength provided the interstitial content is kept low and proper heat-treatments are used.

Initial feasibility studies on the use of a composite approach to make high strength and higher toughness titanium plate material are presented. Explosive bonding and roll bonding techniques were employed to produce the plate. The results of the fracture toughness, metallographic, and ultrasonic studies have provided considerable encouragement at this early phase of what is envisioned as a long-range effort to provide a major advancement in this high and ultrahigh strength metals technology.

The effects of vacuum heat treatment on imparting essential immunity to salt water stress-corrosion-cracking to otherwise stress-corrosion-cracking sensitive titanium alloys are described. At the same time, the interstitial hydrogen level is reduced to very low levels due to the vacuum heat treatment whereas similar heat treatments in inert environments neither impart a similar high resistance to salt water nor reduce the interstitial hydrogen to the same low levels. The details are described for the Ti-8Al-1Mo-1V, Ti-7Al-1Mo-1V, Ti-6Al-4V, and Ti-7Al-2.5Mo alloys. In addition, the stress-corrosion-cracking characteristics of a number of additional titanium alloy plate and weldments in salt water have been determined and the results are presented along with the results of a fractographic study of fatigue crack surfaces developed during preparation of fracture mechanics type fracture toughness specimens. In some cases, cleavage and quasi-cleavage was noted to be present, but it was not possible to conclusively associate it with the fatiguing operation or the initial crack extension phase in the fracture mechanics test.

Low cycle fatigue crack propagation studies in the A201B, A302B, and A517F pressure vessel steels in air and in salt water are described in one section of this report. Since these steels represent pedigreed material obtained from failed pressure vessels, comparisons are made between the laboratory test results and actual structural experience with these materials. It was found that in air fatigue crack growth rates in A201B and A302B steels follow a common third power relationship with total strain range; a fourth power relationship was found for A517F. A201B possessed the greatest tolerance for cyclic plastic strain.

All of the steels showed some sensitivity to salt water but no gross effects were observed. Comparisons between the laboratory results and structural experience with these steels were in agreement for the A201B and A302B steels.

The results of a preliminary study on steels of the relationship between plane strain fracture toughness and the results obtained with engineering type fracture toughness tests, in this case, the drop-weight tear test, are reported. A number of high strength steels were investigated using the single-edge notched, side-grooved tension specimen and a remarkably good correlation was established between drop-weight tear test energy for fracture and the plane strain fracture toughness K_{Ic}, the strain energy release rate $\mathcal{G}_{Ic}$ and β_{Ic} (plastic zone size indicator). These correlations permit one to make reasonable estimates of K_{Ic}, $\mathcal{G}_{Ic}$, and β_{Ic} from measured drop-weight tear energy values.

The salt water stress-corrosion-cracking resistance of the aluminum alloys 7075-T7351, 7079-T6 and 7005-T63 is reported. The first two alloys appeared to be relatively sensitive to the environment in the "short transverse" direction whereas the 7005-T63 did not.

Fracture toughness studies of steel plates and welds characterized by strengths ranging from about 130 to 200 ksi yield strength have been conducted. The steels included 3/4 to 4-inch thick plates of 5Ni-Cr-Mo-V and 1-inch thick plates of a "new" version of the 9Ni-4Co-0.XXC quenched and tempered steel. Producer fabricated manual and metal-arc inert gas welds of the nominal 2Mn-2Ni alloy composition developed for welding the 5Ni-Cr-Mo-V steel, and NRL fabricated, fully-automatic, tungsten-arc inert gas welds of the 9Ni-4Co-0.XXC alloy and 12Ni-3Cr-3Mo and 17Ni-2Co-3Mo maraging steel weld metal compositions were also examined.

HIGH STRENGTH TITANIUM ALLOYS

(R. J. Goode and R. W. Huber)

Preliminary fracture toughness characteristics have been determined for the recently received new alloys Ti-6Al-4V-2Mo, Ti-6Al-6V-2Sn-2Mo, Ti-4Al-3Mo-1V, Ti-2Al-4Mo-4Zr, and a new heat of Ti-6Al-4V in the as-received condition; additional

data are also presented for several of the alloys after a solution annealing treatment in vacuum. In support of a heat treatment study being conducted by Reactive Metals Corporation, full thickness fracture toughness properties were determined for a Ti-6Al-2Cb-1Ta-0.8Mo alloy after heat treatment.

A new study concerning the properties and characteristics of thick section composites of titanium alloys has been initiated and fracture toughness data has been obtained for several composites representative of initial attempts at defining significant parameters and their control for cladding thick sections.

FRACTURE TOUGHNESS INDEX DIAGRAM FOR TITANIUM

The latest fracture toughness index diagram for titanium is shown in Fig. 1 along with the drop-weight tear test (DWTT) data points for all materials studied. The features of the diagram and their significance have been described in detail in earlier reports of this series and in References 1-3. Briefly, below 1500 ft-lb DWTT energy materials will propagate fractures through elastic stress regions; increasing levels of plastic strain are required for propagation of fractures for increasing DWTT energy values above 1500 ft-lb. The impingement of the elastic-to-plastic transition bond (1500-1700 ft-lb DWTT energy) with the optimum materials trend line (OMTL) indicates that for those materials having yield strengths above 140 ksi elastic stresses can be expected to sustain fracture propagation. Between 120-140 ksi yield strength (YS) only carefully optimized alloys will be capable of developing plastic strains before fracture occurs. The region below 120 ksi YS is characterized by a number of alloys that require high levels of plastic strain for propagation of fractures.

FRACTURE TOUGHNESS STUDIES

One-inch thick plates were recently received of the following alloys:

1. Ti-6Al-4V-2Mo (R-2) - a modification of the Ti-6Al-4V alloy

2. Ti-6Al-6V-2Sn-2Mo (R-4) - a modification of the Ti-6Al-6V-2Sn alloy

3. A high purity Ti-4Al-3Mo-1V alloy (R-3)

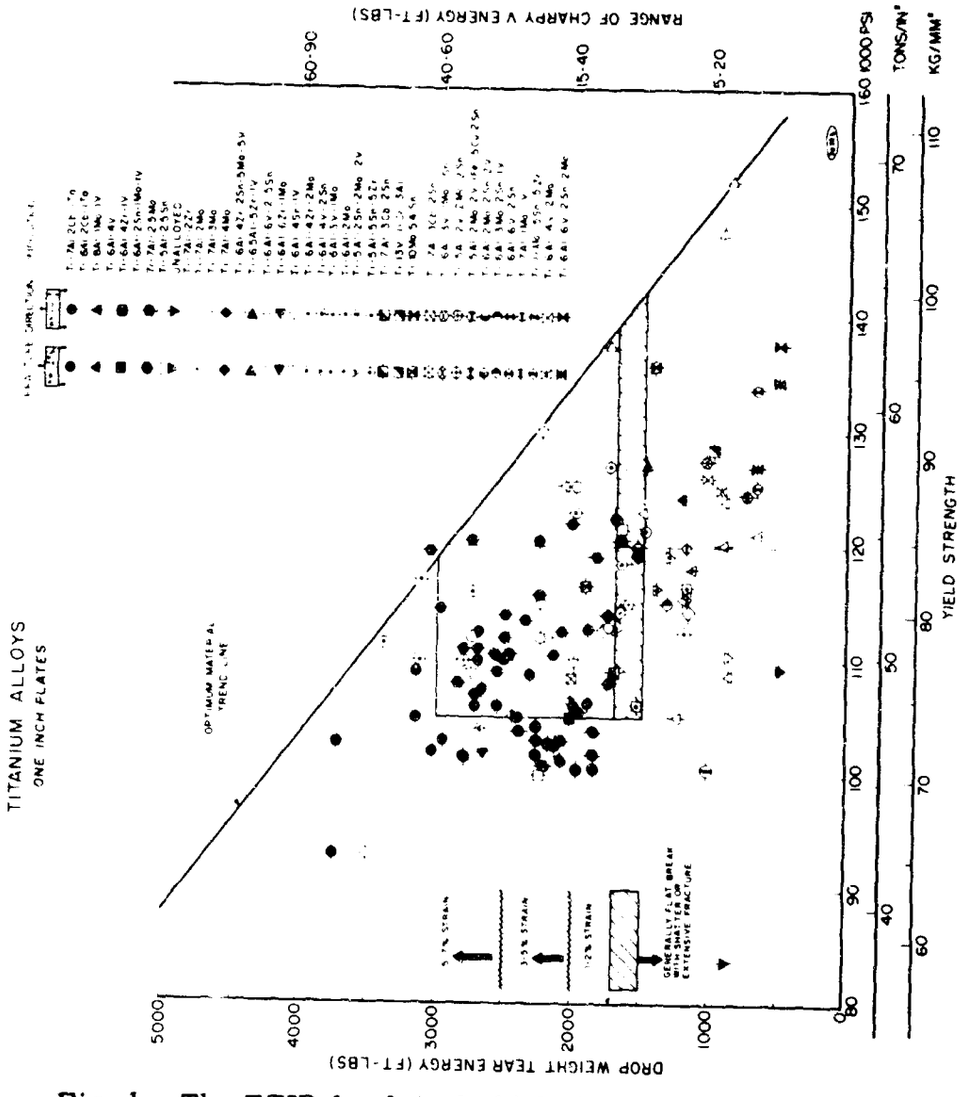

Fig. 1 - The FTID for 1-inch thick titanium alloys

4. Ti-2Al-4Mo-4Zr (R-5) - a new Titanium Metals Corporation of America alloy

5. Ti-6Al-2Mo (R-1) - represents an additional heat of a promising high strength, high toughness alloy previously studied.

The DWTT fracture toughness of the as-received material was determined for these alloys. In addition, a single DWTT specimen from the plates R-1,R-2, and R-4 were vacuum solution annealed for 1 or 2 hours in a cold wall vacuum furnace at temperatures judged to be just below the β transus of each alloy (β transus temperatures to be determined). The DWTT results are shown in Table 1 along with the tensile data provided by the producer as well as those presently determined at NRL. The DWTT energy data is plotted against the FTID features in Fig. 2 for the as-received material and since the tensile data is available for the Ti-6Al-6V-2Sn-2Mo alloy after the vacuum heat treatment. The NRL tensile data is used in this figure where possible. (It should be noted that these data do not necessarily represent the capabilities of these alloys but are related only to the beginning of an optimization study on these materials.)

The combination of 2325 ft-lb DWTT energy and about 115 ksi YS for the Ti-4Al-3Mo-1V alloy in the as-received condition indicates that this alloy may have considerable potential for high toughness in the 120 ksi YS range. However, the high content of beta forming elements may lead to difficulties in fusion welding. An indication that such a problem may exist was observed when an electron beam, bead-on-plate type of weld decreased the DWTT energy to 573 ft-lbs. More extensive, MIG type welding studies on this alloy as well as on the others is scheduled to begin as soon as like composition welding wire on order is received.

HEAT TREATMENT STUDY ON Ti-6Al-2Cb-1Ta-0.8Mo

The Eleventh Quarterly Report (7), contained data concerning the fracture toughness of DWTT specimens of a Ti-6Al-2Cb-1Ta-0.8Mo alloy (1-inch plate, HT No. 292555). The specimens represented a variety of heat-treated conditions and were evaluated in the DWTT at NRL for Reactive Metals Corporation in support of their Navy sponsored heat-treatment study on this alloy. Afterwards the broken halves were returned to Reactive Metals Corporation to provide material for determination of the related tensile and Charpy V (C_V) properties. These data have now been obtained

TABLE 1

Tensile and Fracture Toughness Properties of Some Titanium Alloys (Plates R-1 through R-5)

Alloy		DWTT		2% Y.S. (ksi) PROD	2% Y.S. (ksi) NRL	UTS (ksi) PROD	UTS (ksi) NRL	Elong (%) PROD	Elong (%) NRL	R. A. (%) PROD	R. A. (%) NRL
R-1	RW	1662	As rec'd	114.8	114.2	126.9	126.1	13.5	9.8	29.3	20.3
6Al-2Mo	WR	1601	As rec'd	111.9	117.5	124.9	126.6	14.5	10.5	29.8	27.1
	WR	2146	V.A. 1 Hr 1850°F He Cooled								
R-2	WR	931	As rec'd	130.9	125.3	145.6	141.1	13.0	10.0	24.4	19.0
6Al-4V-2Mo	RW	1052	As rec'd	126.1	126.0	143.4	141.0	12.5	10.0	21.6	21.0
	RW	811	V.A. 1 Hr 1850°F He Cooled								
R-3	RW	2325	As rec'd	114.6	-	122.2	-	16.5	-	40.6	-
4Al-3Mo-1V	WR	2325	As rec'd	115.5	-	123.5	-	15.0	-	38.8	-
R-4	RW	514	As rec'd	139.4	134.1	165.0	161.0	7.0	6.5	8.5	10.0
6Al-6V-2Sn-2Mo	WR	514	As rec'd	141.6	138.2	168.6	161.3	6.0	6.5	10.0	10.9
	WR	681	V.A. 1660°F 2 Hr He Cooled	-	126.8	-	148.1	-	10.0	-	10.0
R-5	WR	2325	As rec'd	104.3	-	115.8	-	20.0	-	51.2	-
2Al-4Mo-4Zr	RW	2498	As rec'd	94.2	-	111.8	-	20.5	-	43.8	-

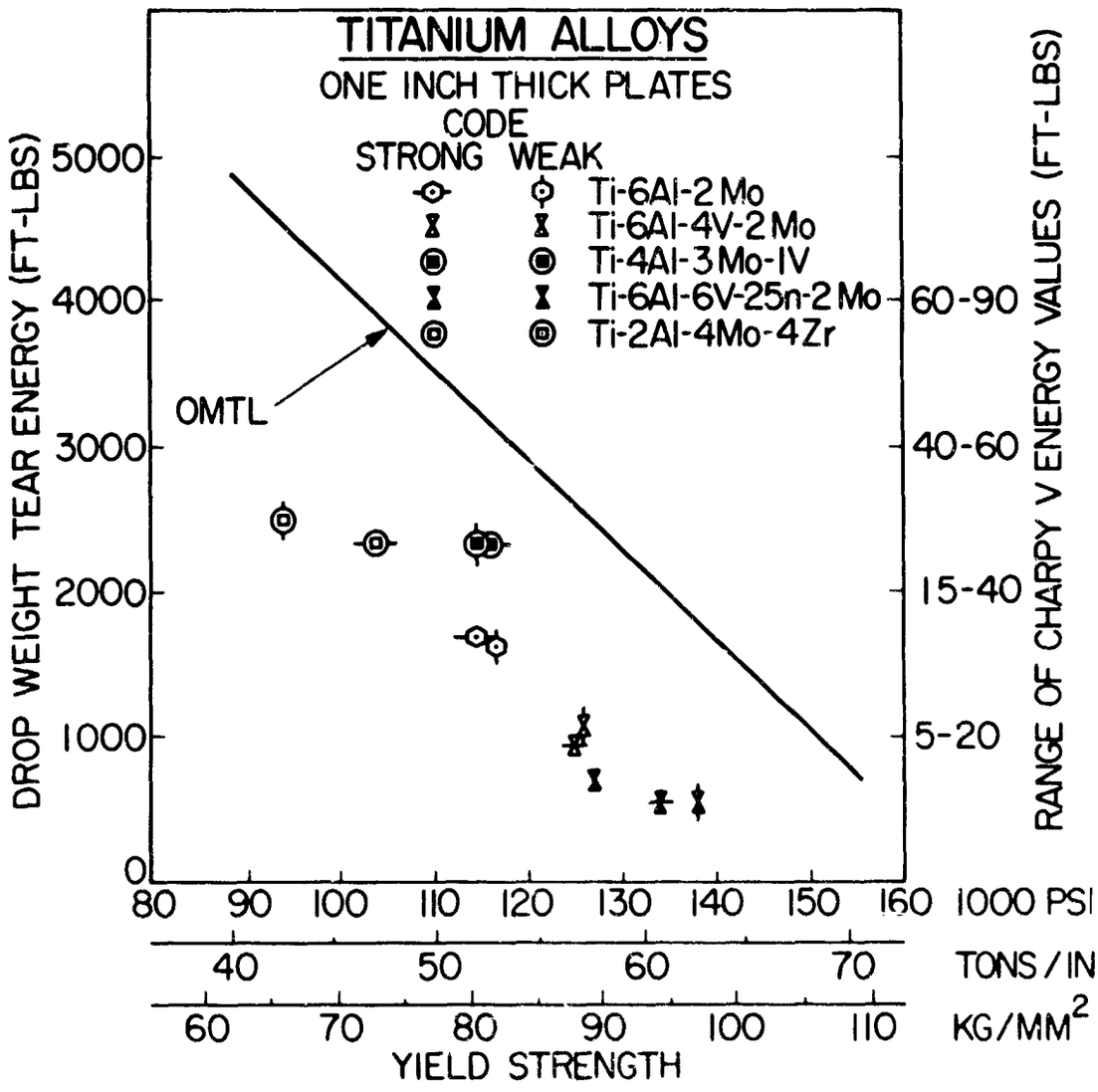

Fig. 2 - Fracture toughness characteristics of titanium alloy plates R-1 through R-5 in the as-received condition (plus vacuum 1660° F heat treatment of R-4)

and are shown in Table 2 along with the chemical analysis of the alloy and the DWTT determinations. In addition, similar data from another heat of Ti-6Al-2Cb-1Ta-0.8Mo from the same study, which contains slightly less Cb and twice as much oxygen (0.122 versus 0.058%), is contained in this table.

The DWTT energy data, plotted against the FTID features, are shown in Fig. 3 for both heats of material. The numbers by the data points correspond to the heat treatment numbers in Table 2. Several general observations can be made from this data:

1. In general, this alloy is characterized as having good fracture toughness in 1-inch thicknesses below 110 ksi yield strength.

2. High oxygen promotes lower fracture toughness (point 9 compared to point 6 - the 50°F increase in β annealing temperature wouldn't account for the large drop in DWTT energy).

3. The higher oxygen promotes greater strengthening (points 9 compared to 6, compared to 7; and 11 compared to 8 - again the 50°F β annealing temperature difference wouldn't be expected to account for the significant strength differences).

4. Aging at 1100°F for 2 hours increases the yield strength over that of the annealed material but at the same time causes a significant drop in the DWTT energy. This indicates a potential welding HAZ problem may exist for this alloy and should be investigated in the DWTT for shorter aging times and different temperatures.

5. Rapid cooling after annealing increases the strength of the material substantially; its effect on fracture toughness is not clear cut from the data, but it appears to be beneficial.

6. Charpy V energy at -80°F is not a very sensitive indicator of changes in fracture toughness in the range of strength and toughness of concern here.

Additional DWTT samples of another heat of Ti-6Al-2Cb-1Ta-0.8Mo from the same study were tested. The DWTT data are shown in Table 3 for the different heat treated conditions.

TABLE 2

HEAT TREATMENT OF Ti-6Al-2Cb-1Ta-0.8Mo 1-INCH PLATE

	Al %	Cb %	Ta %	Mo %	Fe %	C %	N %	O %	Beta Transus
Heat 292555	6.2	2.40	1.00	0.74	.06	.02	.006	.058	1845°F±5°
				R.M.I.					NRL

TENSILE AND IMPACT PROPERTIES

Heat Treatment	Test Direction	UTS[1] (ksi)	0.2%YS[1] (ksi)	Elong[1] (%)	RA[1] (%)	C_v Impact[1] -80°(ft-lb)	Drop-Weight Tear Energy +32°F(ft-lb)
As Rolled	L	119.6	101.8	10.8	23.1	23.5	2266
	T	123.0	105.0	12.5	33.6	23.0	2146
1600°F-1Hr-AC	L	118.2	99.2	12.5	28.0	29.2	2443
	T	122.4	107.4	12.5	31.9	32.2	2846
1815°F-1Hr-AC	L	118.2	97.7	12.5	31.3	32.5	2560
	T	122.2	104.0	13.0	33.0	28.2	2266
1815°F-1Hr-WQ	L	126.0	101.2	13.0	29.0	27.8	2560
	T	129.0	108.4	11.8	30.7	32.2	2443
1815°F-1Hr-WQ	L	127.0	108.9	10.5	20.8	25.5	2086
1100°F-2Hr-AC	T	135.5	118.9	10.5	22.1	29.0	1905
1900°F-1Hr-AC	L	123.2	101.4	11.8	24.6	33.0	2618
	T	123.2	103.4	12.2	27.7	28.2	1966
1900°F-1Hr-WQ	L	131.1	110.2	12.8	31.0	30.5	2265
	T	128.1	108.0	8.8	23.8	26.8	2266
1900°F-1Hr-WQ	L	135.3	117.1	9.5	24.8	24.0	1723
1100°F-2Hr-AC	T	135.4	116.2	9.5	21.2	23.2	2146

	Al %	Cb %	Ta %	Mo %	Fe %	C %	N %	O %	
Heat X-3454	6.0	1.98	0.92	0.80	.05	.03	.006	.122	
1950°F-1Hr-AC	L		127.6	105.5	12.2	27.6	24.8		1784
	T		128.5	106.3	12.5	26.4	25.5		--
1950°F-1Hr-WQ	L		135.2	115.0	11.5	27.3	22.5		--
	T		136.6	116.6	10.8	19.4	24.0		--
1950°F-1Hr-WQ	L		137.1	119.8	12.5	25.4	22.0		1173
1100°F-2Hr-AC	T		139.0	121.1	9.2	16.0	23.2		--

[1] Average of two specimens

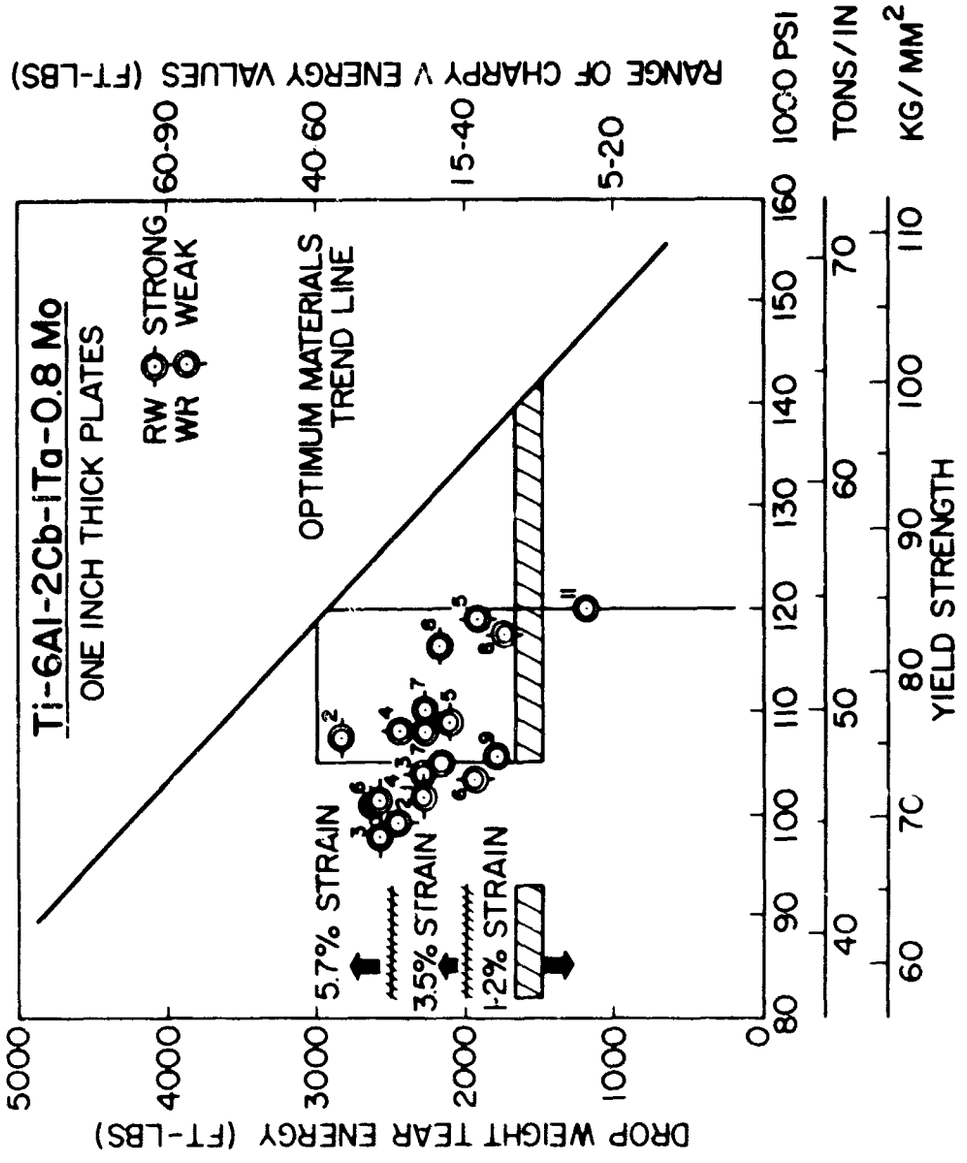

Fig. 3 - Fracture toughness characteristics of Ti-6Al-2Cb-1Ta-0.8Mo alloys from RMI heat-treating study

TABLE 3

DWTT RESULTS ON Ti-6Al-2Cb-1Ta-0.8Mo

DWTT Energy

Heat Treatment	Fracture Direction	
	RW (strong)	WR (weak)
As Rolled	2325 ft-lbs	1662 ft-lbs
1650°F-1 Hr.-AC	1996	1228
2000°F-1 Hr.-WQ	1478	1296
2000°F-1 Hr.-WQ/1000°F-4 Hr.	1478	1418
2000°F-1 Hr.-WQ/1100°F-8 Hr.		

Until the tensile data and chemical analysis is obtained not much can be said concerning this material except that the 2000°F solution anneal appears to be above the optimum annealing temperature for obtaining high fracture toughness.

FEASIBILITY STUDY ON COMPOSITE TITANIUM ALLOY PLATE

A long range study has been initiated on the crack propagation resistance and mechanical property characteristics of thick section composite titanium alloy plate. The scheme is to clad a low strength, high fracture toughness alloy on to both surfaces of a high strength, low fracture toughness core material. Some of the beneficial effects of the cladding that might be expected are:

1. Promotion of extensive plastic flow at the surfaces of the composite plate which would provide a "dragging anchor" effect on a crack moving through the core material; hopefully, this anchor effect would tend to arrest what might otherwise be a self-propagating crack in the core material.

2. Protection of the core material from stress-corrosion cracking in aqueous and other agressive environments.

3. Provide high strength plate material which is highly resistant to fatigue crack propagation from surface flaws.

The ultimate aim of this study is to provide a significant advancement in the useful strength and fracture toughness limits for titanium alloys in complex structural applications, i.e., move the OMTL in Fig. 1 to higher levels of strength and toughness.

Through the cooperation of E. I. DuPont Company test pieces of a ELI grade (0.12 oxygen minimum) Ti-6Al-4V alloy were "Deta Clad" (explosion bonded) on both sides with a 1/16-inch and a 1/4-inch thick Ti-3.5Al alloy to form a plate composite 1-inch thick. In addition, a 2-inch thick plate of the Ti-6Al-4V alloy was "Deta Clad" with 1/2-inch thick Ti-3.5Al plate on each surface and then the composite plate was hot rolled to a final thickness of 1-inch. The final cladding thickness for this plate was about 3/16-inch

Three other titanium alloy compacts (20-inches by 20-inches) were built up by welding at the edges 1/2-inch thick cover plates of the Ti-3.5Al alloy to both faces of a 2-inch thick Ti-5Al-2V-2Mo-2Sn alloy, and 1/4-inch thick cover plates of Ti-3.5Al to the faces of 2-inch thick Ti-5Al-2V-2Mo-2Sn and Ti-6Al-3V-1Mo plates. These compacts were then hot rolled by T.M.C.A. at 1700°F to a final thickness of 1-inch and air-cooled off the rolling mill.

The bonding efficiency for the deta cladding process appeared very encouraging as determined by ultrasonic inspection. Lack of bonding at one corner of the 3" explosion bonded compact was indicated. After hot rolling of this compact the whole composite was again ultrasonically examined with this same area still showing a lack of bonding-the bonding on this plate was about 85% efficient. All of the T.M.C.A. roll bonded composites showed complete bonding.

DWTT specimens were cut from all these composite plates and tested; metallographic specimens were removed from sections of the broken halves for further examination of the bonded regions. The DWTT results for the composite plates are shown in Table 4. The data indicates a decrease in toughness for the "Deta Clad" plate compared to the 811 ft-lb DWTT obtained for the 1-inch ELI Ti-6Al-4V plate material(5). This lowering of fracture toughness can be attributed to the cold working effect of the explosion shock loading in the cladding process. Vacuum annealing at 1700°F indicates that significant increases can be expected in the fracture toughness of "Deta Clad" material when the effects of cold work are removed. The DWTT energies of all the hot rolled composites are significantly higher than the corresponding values obtained for the core material alloy as 1-inch circular rolled plates(5). Although all of these composites represent initial attempts at defining the optimum cladding procedures and individual alloy characteristics in the bonding operations, the results here appear encouraging with respect to the aims of the study.

The tested DWTT specimens of the composites exhibited evidence of some delamination at the fracture surfaces; in particular with the "Deta Clad" plates. This delamination appears to be associated with plastic deformation in the region of the fracture; whether it occurred ahead of or behind the advancing crack front is not known. Preliminary

TABLE 4

FRACTURE TOUGHNESS OF 1-INCH THICK COMPOSITE TITANIUM PLATE

Alloy		As-received DWTT energy (ft-lb)	DWTT energy after Vacuum Anneal at 1700°F (ft-lb)
Deta Clad Material (DuPont)			
1. ELI Ti-6Al-4V (7-95) core material			
2. 1/16-inch cladding		455	1418
3. 1/4-inch cladding		514	1966
4. 1/2-inch deta clad on 2-inch core then hot roll to 1-inch plate; 3/16" resultant cladding thickness		2325	1844
Roll-bonded (T.M.C.A.)			
1. Ti-5Al-2V-2Mo-2Sn (T-90) core material			
a. 1/16-inch cladding	RW	2846	
	WR	2206	
b. 3/16-inch cladding	RW	2384	
	WR	2325	
2. Ti-6Al-3V-1Mo (T-93)			
a. 1/16-inch cladding	RW	2676	
	WR	1905	

metallographic examination of the bond region of the hot rolled material shows a coherent interface with little, if any, grain growth occurring across it. The bond interface of the "Deta Clad" material in general shows a wave like interface; in many regions the interface shows mechanical interlocking between the two alloys as shown in Fig. 4. This interlocking is confined to within 2 or 3 grains of the bonded interface.

Large clad plates are being processed to provide material for considerably more exhaustive study in the initial phase of this study.

*THE EFFECTS OF HEAT TREATING ENVIRONMENTAL CONDITIONS ON THE STRESS-CORROSION-CRACKING RESISTANCE OF SEVERAL TITANIUM ALLOYS

(D.G. Howe & R.J. Goode)

The effect of heat treating environmental conditions on the stress-corrosion-cracking (SCC) resistance of the very low interstitial (0.08 max oxygen and ~ 60-70 ppm hydrogen) alloys Ti-8Al-1Mo-1V, Ti-7Al-1Mo-1V, Ti-6Al-4V, and Ti-7Al-2.5Mo are being studied and the results of parts of the investigation have been reported in earlier reports (4-9).

MATERIALS AND PROCEDURES

Specimens, similar in configuration to those used by Brown and Beachem (10) were obtained from approximately 1-inch thick plate material. All specimens were machined, side-notched and fatigued until the fatigue crack had propagated approximately 1/8 inch from the root of the notch. The specimens were degreased with Methyl Ethyl Ketone, washed with acetone, and air dryed before heat treatment.

Heat treatments were conducted in either an Inconel muffle in an electric furnace or a "cold wall" vacuum furnace. The cantilever SCC test procedure (10) was used to establish the effect of heat treatment on the SCC resistance of the titanium alloys in a 3.5% NaCl solution. In this procedure the specimen is tested as a cantilever beam, with the pre-cracked zone surrounded by a plastic container holding the 3.5% NaCl solution. A moment "M" is imposed upon the pre-cracked notch by weights at the end of the lever arm which is clamped to the specimen, and the time is noted for final

*This research was supported by the Advanced Research Projects Agency as part of the ARPA Coupling Program on Stress-Corrosion Cracking.

Fig. 4 - Bond interface between Ti-3.5Al "Deta" clad to ELI grade Ti-6Al-4V (T-95) showing evidence of mechanical locking. Mag. 100X

fracture. If the specimen does not fail in the corrosive environment at the preselected load, the moment is increased until it does.

The torque "M" and specimen dimensions are then converted to the stress intensity parameter K_I through the use of equations due to J. Kies (11). The minimum value of K_I which is observed to cause SCC is designated K_{Iscc}.

EXPERIMENTAL RESULTS

The data obtained in this investigation indicate that for the alloys studied the resistance to SCC can be significantly improved if a fine grain size is maintained through processing and proper heat treatments are used. It is evident that heat treatment in vacuum, followed by helium cooling, is very beneficial as the alloys were relatively insensitive to attack by stress-corrosion-cracking under the test conditions used.

The effects of vacuum and inert atmosphere heat treatments on the SCC resistance of the alloy Ti-7Al-1Mo-1V(T-88) were studied. The results of this study are shown in Tables 5 and 6.

The solution anneals listed in Table 5 show the heat treatment given to the specimens before dividing them into three groups for aging at 1200°F for 2 hours, under various environmental conditions. The specimens were either aged in vacuum and helium cooled, aged in argon and air cooled, or aged in argon and water quenched. The environmental conditions associated with the aging treatments at 1200°F had little effect on the SCC resistance obtained as a result of the solution annealing treatment. The material solution annealed in vacuum and helium cooled showed high resistance to SCC where the material heat treated at the same temperatures and time in an inert atmosphere (argon) followed by air cooling were susceptible to SCC under identical test conditions. It should be noted that the K_I and times associated with the no-break situation in Tables 5 and 6 indicate the next to last step loading condition. In some instances, if the holding times were extended considerably, failure of the specimen might have occurred at the slightly lower K_I values. The last column in Table 5 shows variation of hydrogen content with different heat treatments. The K_{Iscc} values shown in Table 5 were plotted against the

TABLE 5

EFFECTS OF SEVERAL HEAT TREATMENTS ON THE RESISTANCE OF THE ALLOY Ti-7Al-1Mo-1V (T-88) TO STRESS-CORROSION-CRACKING IN A 3.5 PERCENT NaCl SOLUTION

Solution Heat Treatment	Aging Heat Treatment	Specimen Type	K_I (ksi/in) No Break	Time (min.)	K_{Iscc} (ksi/in)	Time (min.)	Hydrogen content (ppm by wt)
1950°F/1hr Vac/He C	1200°F/2hr Vac/He C	A	105	5	115	1/2	8
"	1200°F/2hr Argon/AC	A	104	10	109	1/2	8
"	"	B	105	5	109	1/2	8
"	1200°F/2hr Argon/WQ	A	113	5	118	1/2	7
"	"	B	100	5	105	2	7
1700°F/1hr Vac/He C	1200°F/2hr Vac/He C	A	112	15	117	1/4	
"	"	B	110	5	112	1/2	23
"	1200°F/2hr Argon/AC	A	95	5	101	1-1/2	
"	"	B	104	5	109	4	19
"	1200°F/2hr Argon/WQ	A	116	5	118	1/4	
"	"	B	111	5	114	1/2	23
1700°F/1hr Argon/AC	1200°F/2hr Vac/He C	A	65	5	68	1	38
"	1200°F/2hr Argon/AC	A	60	5	64	1/2	44
"	1200°F/2hr Argon/WQ	A	62	5	66	1-1/2	46

TABLE 6

EFFECTS OF HEAT TREATING ENVIRONMENTAL CONDITIONS ON THE RESISTANCE OF THE ALLOY Ti-7Al-1Mo-1V (T-88) TO ATTACK BY STRESS-CORROSION-CRACKING IN A 3.5% NaCl SOLUTION

Solution (Temp.)	Heat (Time)	Treatment	Aging (Temp.)	Heat (Time)	Treatment	Specimen Type	K_I (ksi$\sqrt{in}$) No Break	Time (Min.)	K_{Iscc} (ksi$\sqrt{in}$)	Time (Min.)
1700°F	1 Hr.	Vac/He C	1200°F	2 Hrs.	Vac/He C	A-WT	114	10	116	2
1700°F	1 Hr.	Vac/He C	1200°F	2 Hrs.	Vac/He C	B-WT	113	10	116	3
1700°F	1 Hr.	Vac/He C	1200°F	2 Hrs.	Vac/He C	A-WT	112	15	117	1/4
1700°F	1 Hr.	Vac/He C	1200°F	2 Hrs.	Vac/He C	B-WT	110	5	112	1/2
1700°F	1 Hr.	Vac/He C	1200°F	2 Hrs.	Vac/He C	B-RT	100	10	101	2
1700°F	1 Hr.	Vac/He C	1200°F	2 Hrs.	Vac/He C	B-RT	100	10	102	2
1700°F	1 Hr.	Helium/F.C.	1200°F	2 Hrs.	Vac/He C	B-RT	--	--	61	2-1/2
1700°F	1 Hr.	Helium/F.C.	1200°F	2 Hrs.	Vac/He C	B-RT	--	--	92	1/2
1700°F	1 Hr.	Helium/F.C.	1200°F	2 Hrs.	Vac/He C	B-RT	50	15	51	4
1700°F	1 Hr.	Helium/F.C.	1200°F	2 Hrs.	Vac/He C	B-WT	--	--	60	19
1700°F	1 Hr.	Helium/F.C.	1200°F	2 Hrs.	Vac/He C	B-WT	55	15	58	8
1700°F	1 Hr.	Helium/F.C.	1200°F	2 Hrs.	Vac/He C	B-WT	57	5	62	18
1700°F	1 Hr.	Argon/F.C.	1200°F	2 Hrs.	Vac/He C	B-RT	--	--	52	10
1700°F	1 Hr.	Argon/F.C.	1200°F	2 Hrs.	Vac/He C	B-RT	44	15	45	14
1700°F	1 Hr.	Vacuum/Vacuum Cool	----No Age----			B-RT	90	5	100	2
1700°F	1 Hr.	Vacuum/Vacuum Cool	----No Age----			B-RT	103	15	105	1
1700°F	1 Hr.	Vacuum/Vacuum Cool	----No Age----			B-WT	--	--	119	1
1700°F	1 Hr.	Vacuum/Vacuum Cool	----No Age----			B-WT	111	10	114	1

interstitial hydrogen content present in the material after heat treatment. This observed relationship is shown in Fig. 5. It can be seen that the specimens which were susceptible to SCC had a larger hydrogen content present in the structure.

The effects of different environmental conditions associated with 1 hour - 1700°F solution anneals are shown in Table 6. Four environmental conditions during and after solution annealing treatments were studied. All specimens listed in Table 6 as being aged were heat treated together in vacuum at 1200°F for 2 hours and helium cooled. The cooling rates as a result of these environmental conditions were also determined and are illustrated in Figs. 6 and 7.

The SCC resistance of the Ti-7Al-1Mo-1V alloy (T-88) resulting from different environmental conditions during a 1 hour - 1700°F solution anneal is illustrated in Fig. 8. The specimens solution annealed in vacuum followed by helium cooling were highly resistant to attack by SCC. The specimens that were solution annealed in an argon or helium atmosphere at the same temperature and time exhibited some susceptibility to attack by SCC.

Tests conducted two months after the vacuum solution annealing of SCC specimens taken from Ti-6Al-4V(T-27) and Ti-7Al-2.5Mo(T-94) material showed both alloys to be highly resistant to SCC. Recent tests to determine whether under laboratory atmospheric environment the beneficial condition developed through vacuum solution annealing was a permanent effect have shown that nine months after the heat treatments the Ti-6Al-4V and Ti-7Al-2.5Mo alloys are still essentially immune to attack by stress-corrosion-cracking. The results of these tests are given in Table 7.

A preliminary summary of the K_{Iscc} values obtained as a result of various heat treatments compared to the residual interstitial hydrogen contents for all four of the alloys investigated is shown in Fig. 9. It is interesting to note that for these alloys where the hydrogen contents were at very low values the material was non-susceptible to stress-corrosion-cracking. Where hydrogen contents were greater it can be seen that the alloys displayed varying degrees of susceptiblity to SCC. This would appear to indicate that the interstitial hydrogen present in the alloy plays a role in the stress-corrosion-cracking reaction mechanism.

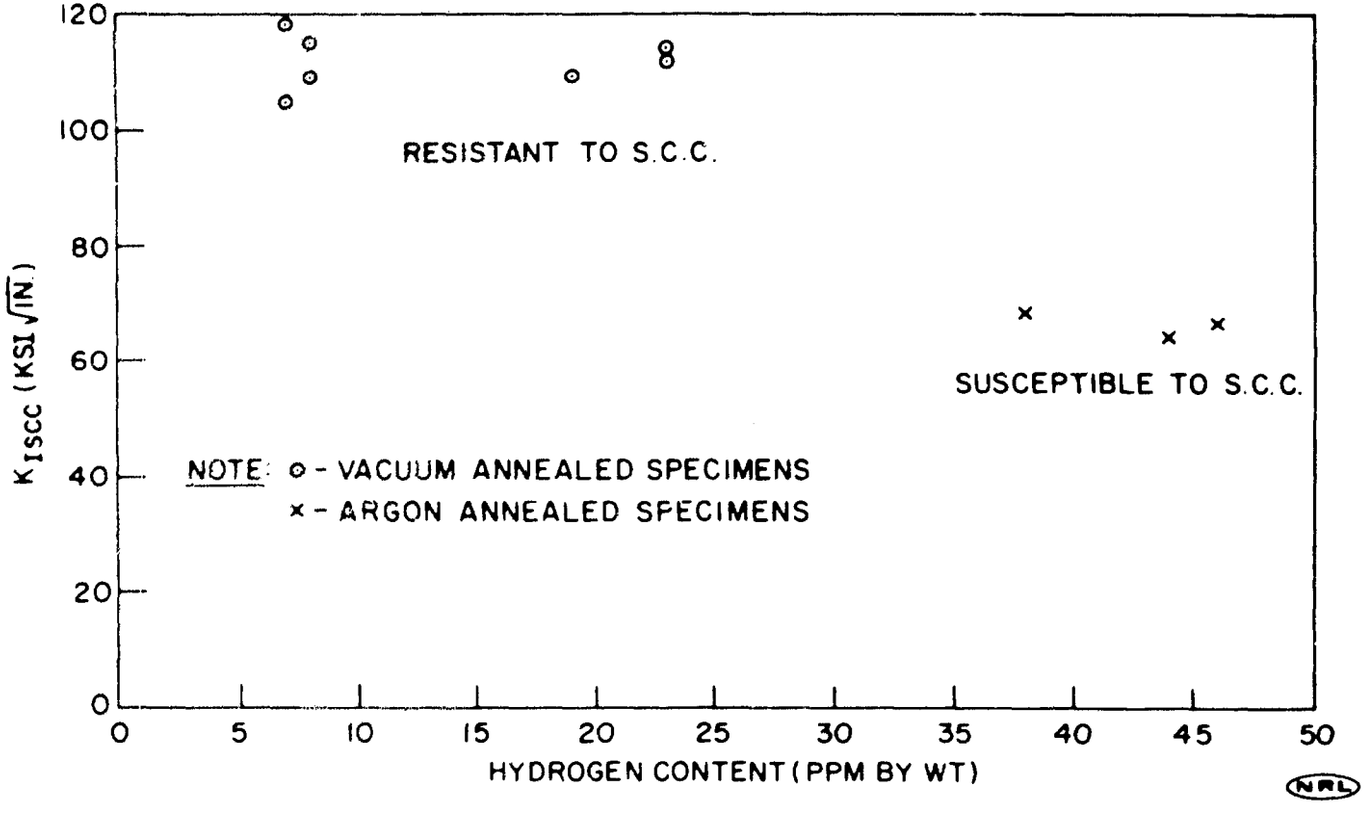

Fig. 5 - Stress corrosion cracking resistance of the Ti-7Al-1Mo-1V alloy (T-88)

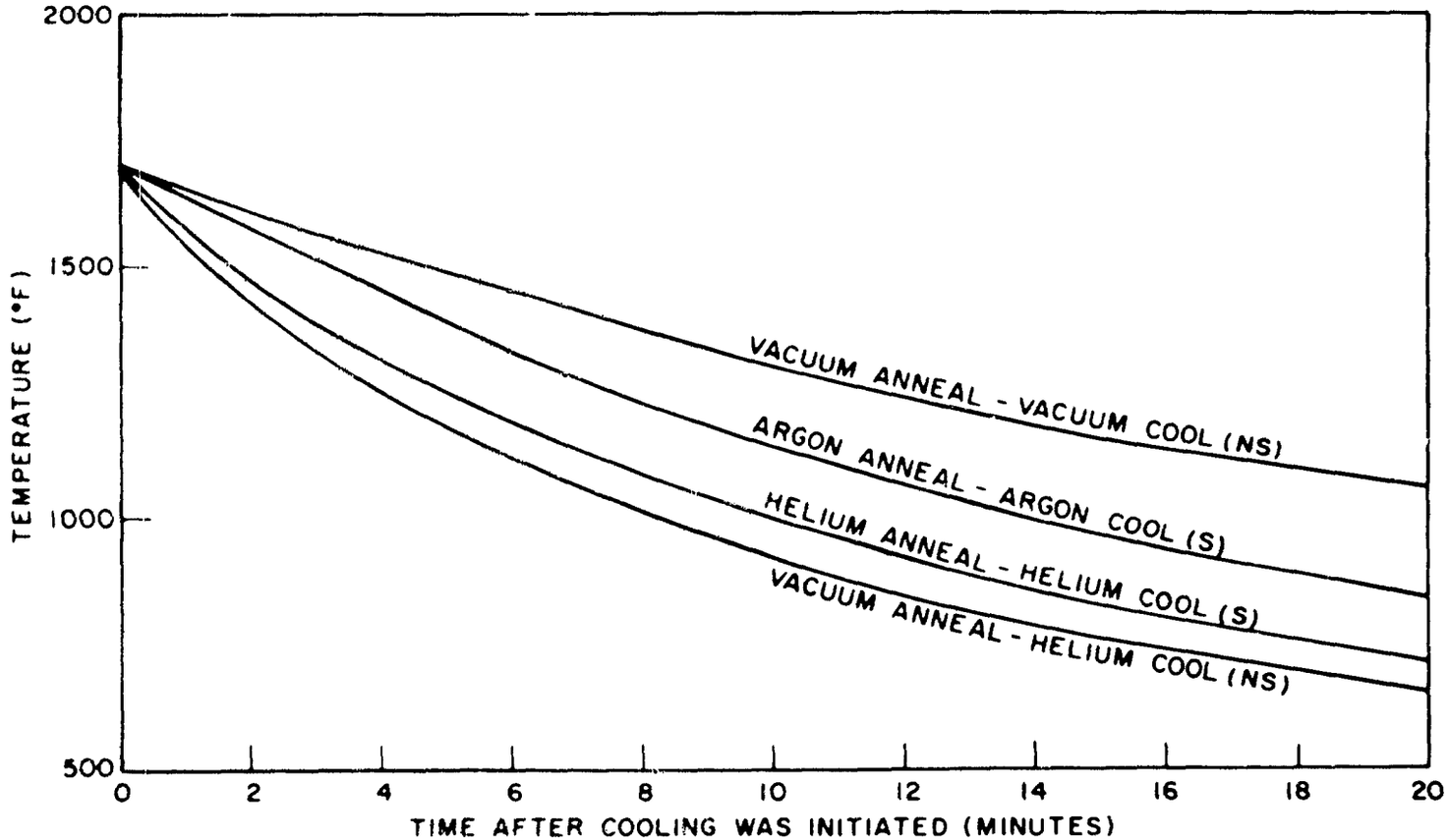

Fig. 6 - Cooling curves for the Ti-7Al-1Mo-1V alloy (T-88) under several different environmental conditions after a 1700° F solution anneal

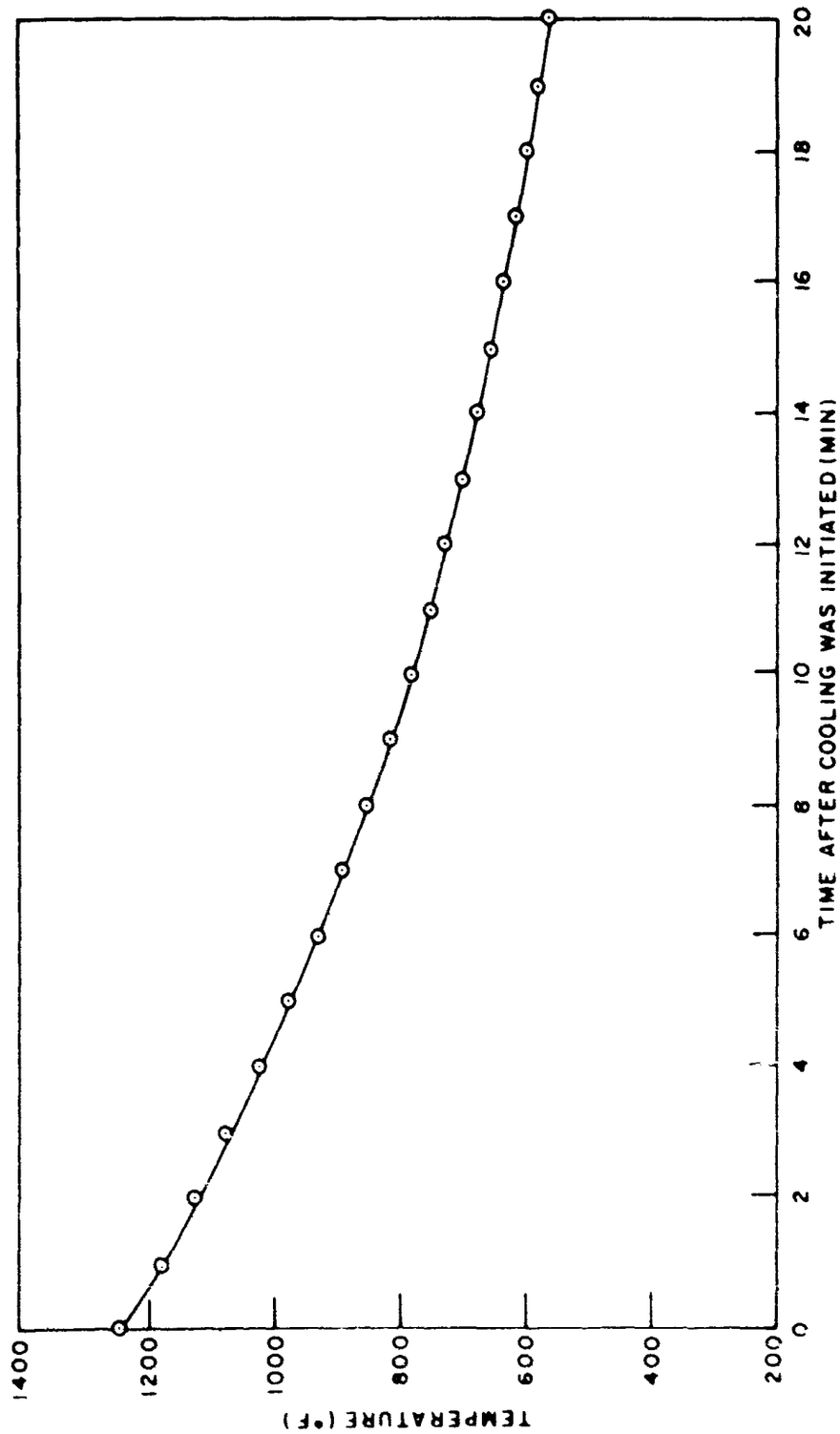

Fig. 7 - Ti-7Al-1Mo-1V alloy (T-88) cooling curve after 1200°F aging treatment in vacuum for 2 hours - helium cool

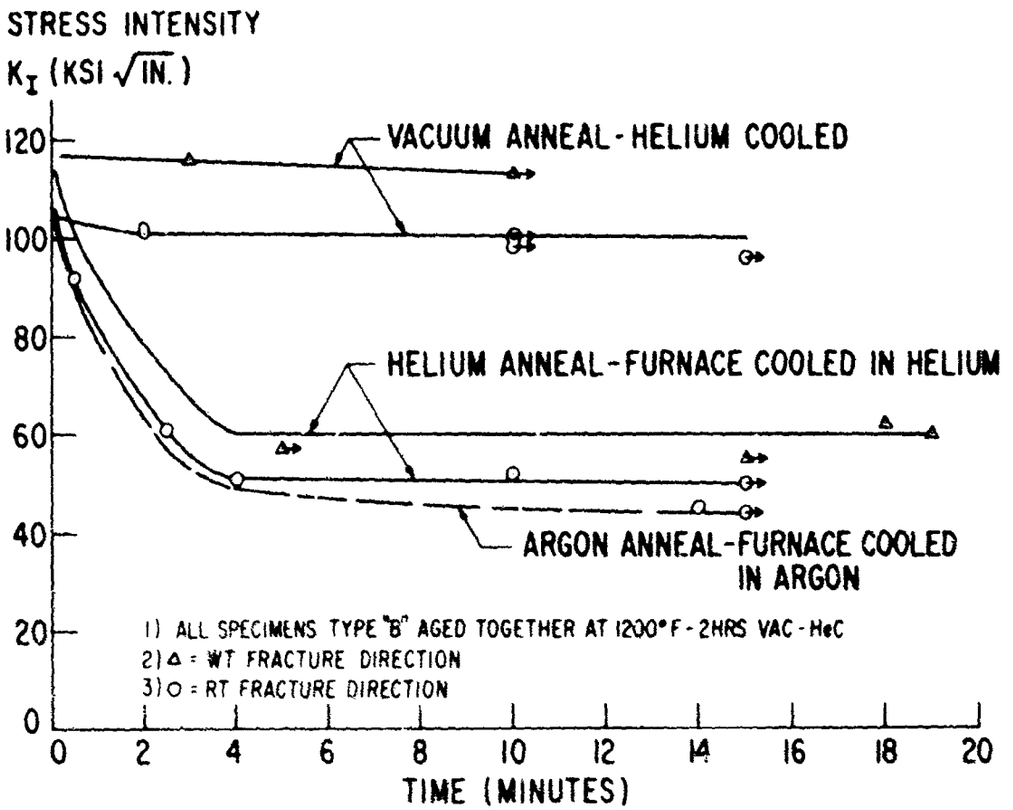

Fig. 8 - Plot of K_{Iscc} and hydrogen content for some titanium alloys

TABLE 7

STRESS-CORROSION-CRACKING RESISTANCE OF VACUUM ANNEALED Ti-6Al-4V (T-27) and Ti-7Al-2.5Mo (T-94) NINE MONTHS AFTER HEAT TREATMENT

Alloy	Vacuum Solution Anneal	K_{Iscc} (ksi/in.)	Time (min.)	Visual Observations
Ti-6Al-4V	As Received	72	10	Susceptible
Ti-6Al-4V	1700°F/1 hr Vac He C	98	11	Non-Susceptible
Ti-7Al-2.5Mo	As Received	81	1	Susceptible
Ti-7Al-2.5Mo	1700°F/1 hr Vac He C	100	4	No -Susceptible

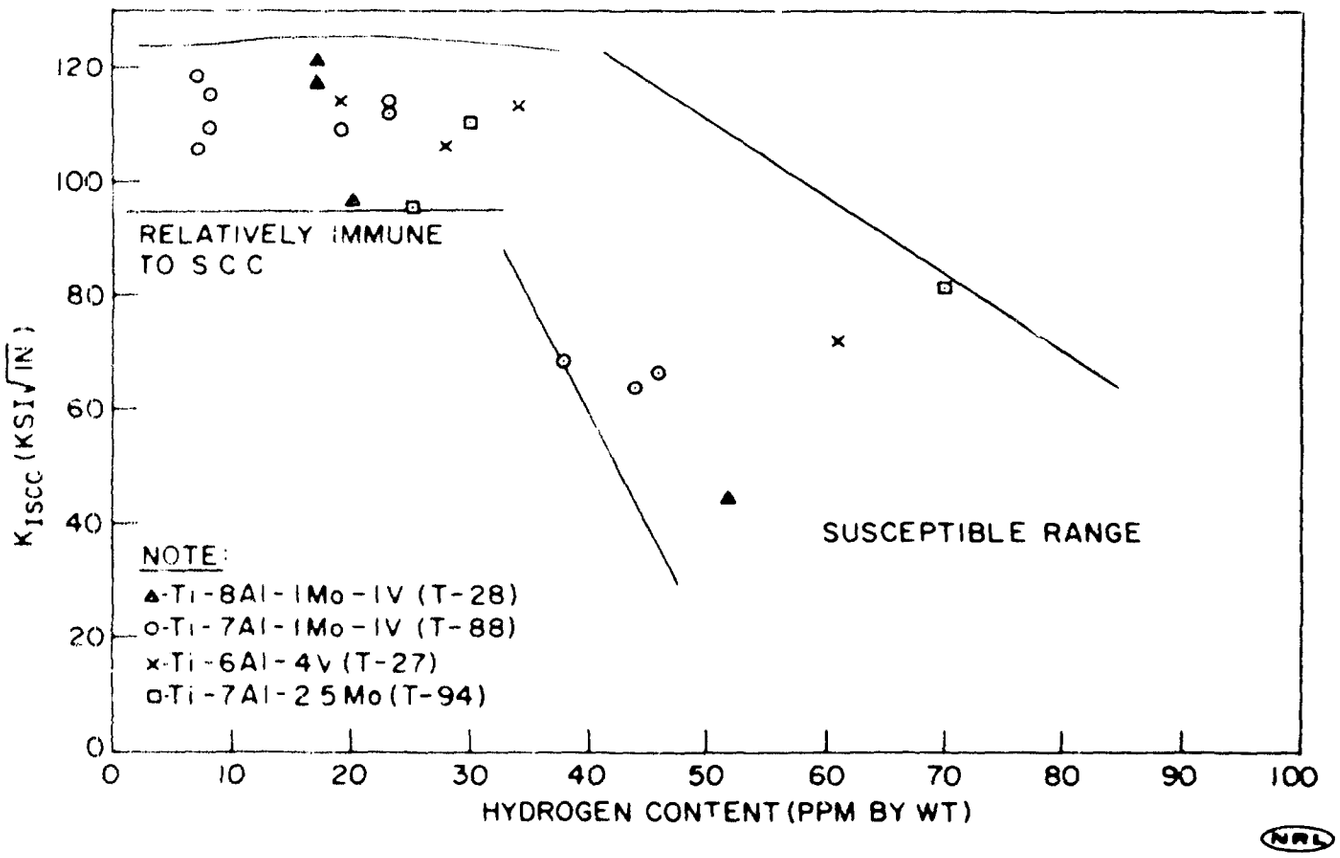

Fig. 9 - S.C.C. resistance of several titanium alloys

The data obtained to date in this investigation, indicate that a significant reduction of interstitial hydrogen content promotes high resistance to SCC. Indicated also is a possible threshold level of hydrogen content below which the alloys are highly resistant to SCC and above which increased sensitivity to SCC develops. The hydrogen level of this threshold may be alloy dependent and may well fall at a level below the solubility limit of the alloy.

A permanent resistance to salt SCC would be dependent upon not having additional hydrogen absorbed into the structure during actual service conditions.

*STRESS CORROSION CRACKING OF SOME TITANIUM ALLOYS

(R. W. Judy, Jr. and R. J. Goode)

Stress-corrosion-cracking (SCC) studies have been conducted on a wide variety of commercial and experimental titanium alloy plates. The tests were conducted by the cantilever method introduced by B.F. Brown (12).

The SCC resistance of a metal can be determined only when certain conditions are met simultaneously; these conditions are a sufficient stress level and flaw size together with an active environment. For a number of titanium alloys, an aqueous (salt water, distilled water, etc.) environment is sufficiently active. The stress level and flaw size necessary to cause SCC to occur are very conveniently combined and expressed in terms of the stress intensity factor K_I. A threshold level of stress intensity above which SCC will definitely occur has been shown to exist for a number of titanium alloys (13). This stress intensity level is denoted by K_{Iscc}. Comparison of K_{Iscc} with K_{Ix}, the stress intensity required for fracture in air (designated "dry"), gives an indication of the relative resistance of an alloy to environmental cracking. The formula used to calculate K values was the cantilever equation:

$$K_I = \frac{4.12M\sqrt{\frac{1}{\alpha^3} - \alpha^3}}{BD^{3/2}}$$

*This research was supported by the Advanced Research Projects Agency as part of the ARPA Coupling Program on Stress-Corrosion Cracking.

where M = moment at test section
B = specimen width
D = specimen thickness
α = 1 - a/D
a = depth of flaw (notch and fatigue crack).

The specimens tested were 1/2 x 1 x 7 in. long with a machined notch and fatigue crack flaw located at its center in the WT or LT fracture direction (14). The specimens had shallow side grooves to insure plane strain conditions. A 3.5-wt-%-salt-water solution was used as the aqueous environment.

CURRENT RESULTS OF SCC STUDY

The SCC resistance and mechanical properties (where available) of several titanium alloys as one-inch-thick plate are shown in Table 8 and Figs. 11 through 27. Except as noted all the plates were in as-received (mill-annealed) condition and were low interstitial content (below 0.08% O_2). Included in this set of data are characterization curves for several alloys in the as-received condition, a variety of heat treatments for a Ti-7Al-1Mo-1V alloy, and base plate data for material taken from heat-treated MIG weldments (weldment data shown in Table 9).

A summary chart showing the relative SCC sensitivities of a wide variety of titanium alloys in different plate thicknesses and in a variety of heat-treated conditions is shown in Fig. 10. The chart is a plot of yield strength (YS) versus K_{Iscc} and is referenced by lines of constant critical flaw depths. These reference lines represent the flaw depth necessary to initiate SCC at yield strength loading for the case of the 10:1 flaw (flaw width = 10 times flaw depth) - considered to be the most critical condition. The flaw depth is calculated by

$$a = 0.2 \left(\frac{K_{Iscc}}{YS}\right)^2$$

where a is the critical crack depth (1).

Samples of Ti-7Al-1Mo-1V taken from DWTT specimens in the as-received condition and solution heat treated at 1750°F

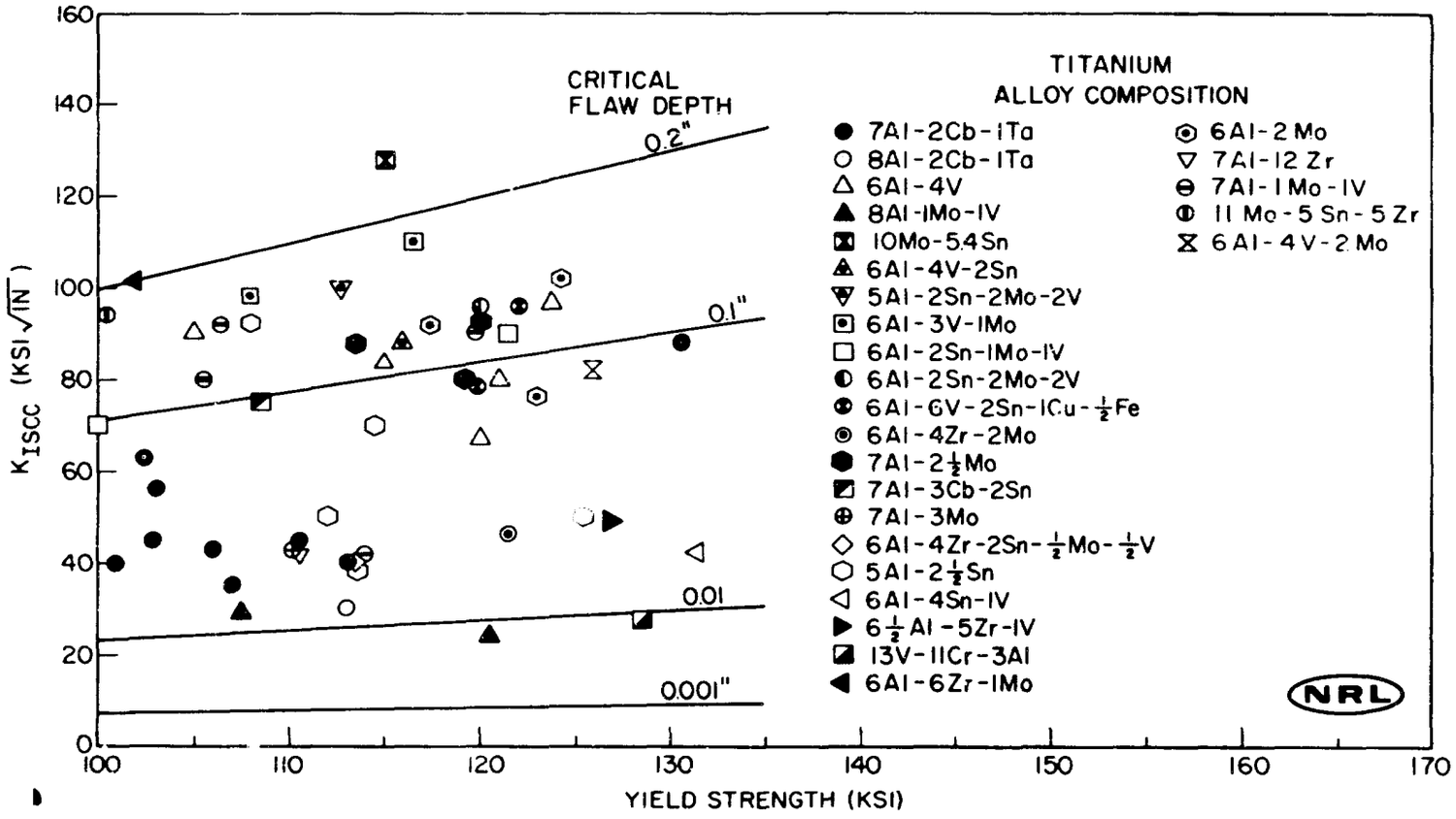

Fig. 10 - Summary stress corrosion cracking resistance index for titanium alloys in 3.5% salt water

TABLE 8

STRESS-CORROSION-CRACKING DATA ON SOME TITANIUM ALLOYS

Titanium Alloy	Code	YS (ksi)	DWTT (ft-lb)	K_{Ix} (ksi$\sqrt{in}$)	K_{Iscc} (ksi$\sqrt{in}$)	Specimen Dimensions: Depth (in)	Width (in)	Side Groove Depth (in)	Remarks
Unalloyed	T17	83	500	69	40	1	3/4	1/32	High Interstitial
7Al-1Mo-1V	T88C	105.6	2443	111	80	1	1/2	1/32	
7Al-1Mo-1V	T88D	106.4	2026	122	92	1	1/2	1/32	1850°F/1 Hr/He Cool
7Al-1Mo-1V	T88E	119.8	1228	117	90	1	1/2	1/32	1750°F/1 Hr/He Cool
6Al-6V-2Sn-1Cu-.5Fe	T88	114.2	--	118	42	1	3/4	1/32	Plate from HT MIG Weld 1800°F/1 Hr/He Cool
6Al-3V-1Mo	T92	120.1	--	102	78	1	3/4	1/32	Plate from HT MIG Weld 1850°F/1 Hr/He Cool
7Al-2.5Mo	T93	107.9	--	112	98	1	3/4	1/32	Plate from HT MIG Weld 1850°F/1 Hr/He Cool
6Al-4V (ELI)	T94	108	--	123	92	1	3/4	1/32	Plate from HT MIG Weld 1850°F/1 Hr/He Cool
11Mo-5Sn-5Zr	T95	115.2	--	112	84	1	3/4	1/32	Plate from HT MIG Weld 1800°F/1 Hr/He Cool
.5Al	T97	100.5	1021	117	94	1	1/2	1/32	Plate from HT MIG Weld 1850°F/1 Hr/He Cool
.5Al	T98	74.0	397	90	80	1	1/2	1/32	
Al-4V	T98	70.9	4724	101	80	1	1/2	1/32	
6Al-2Mo	T100E	--	1052	107	100	1	1/2	1/32	1660°F/1 Hr/He Cool
6Al-4V-2Mo	R1	117.6	1601	107	94	1	1/2	1/32	
6Al-6V-2Mo-2Sn	R2	126.0	1052	96	82	1	3/4	1/32	
6Al-6V-2Mo-2Sn	R4	138.2	514	71	65	1	3/4	1/32	
	R4	126.8	681	91	82	1	3/4	1/32	
						1	3/4	1/32	1660°F/2 Hr/He Cool

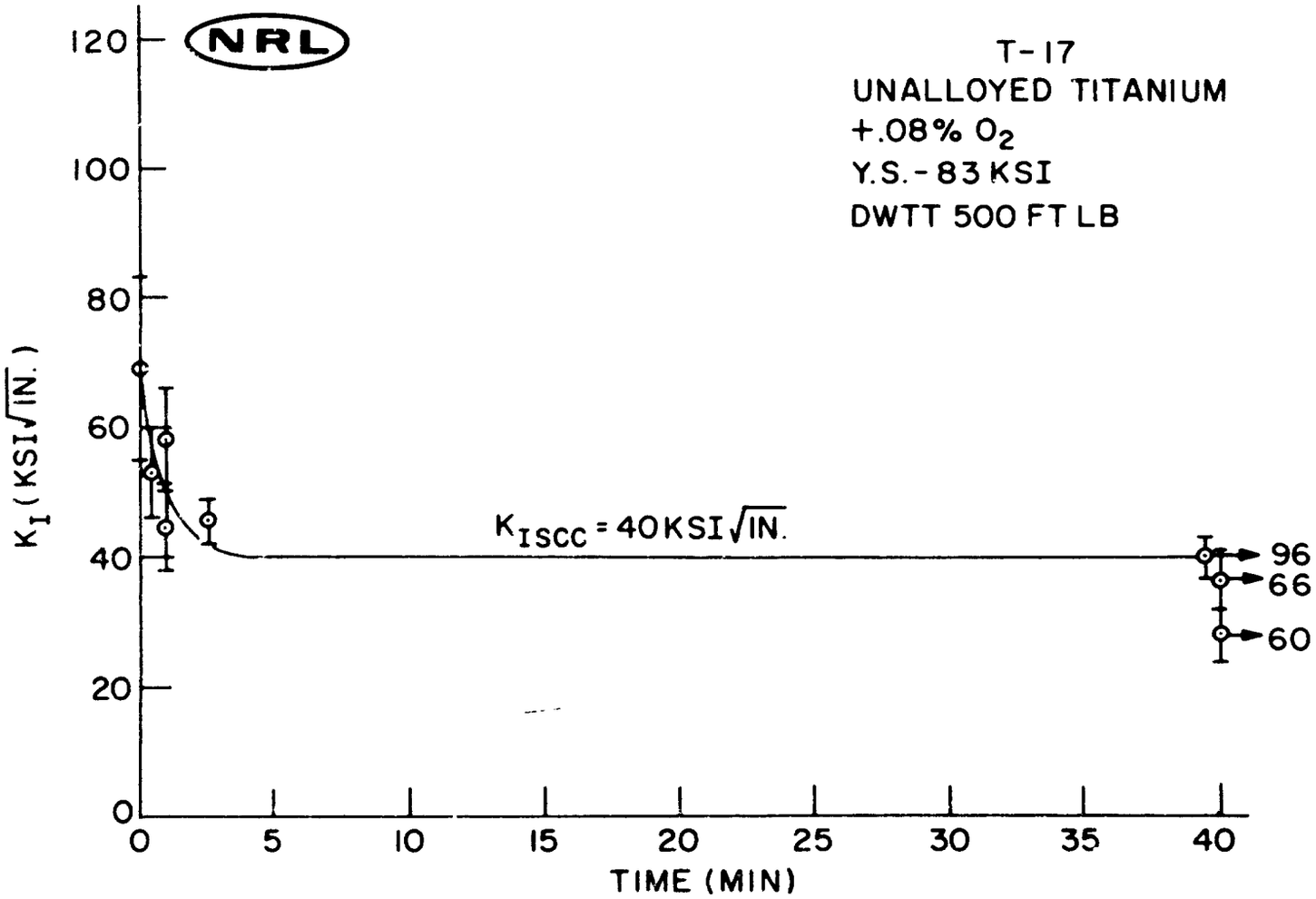

Fig. 11 - Salt water SCC characteristics of unalloyed titanium, T-17

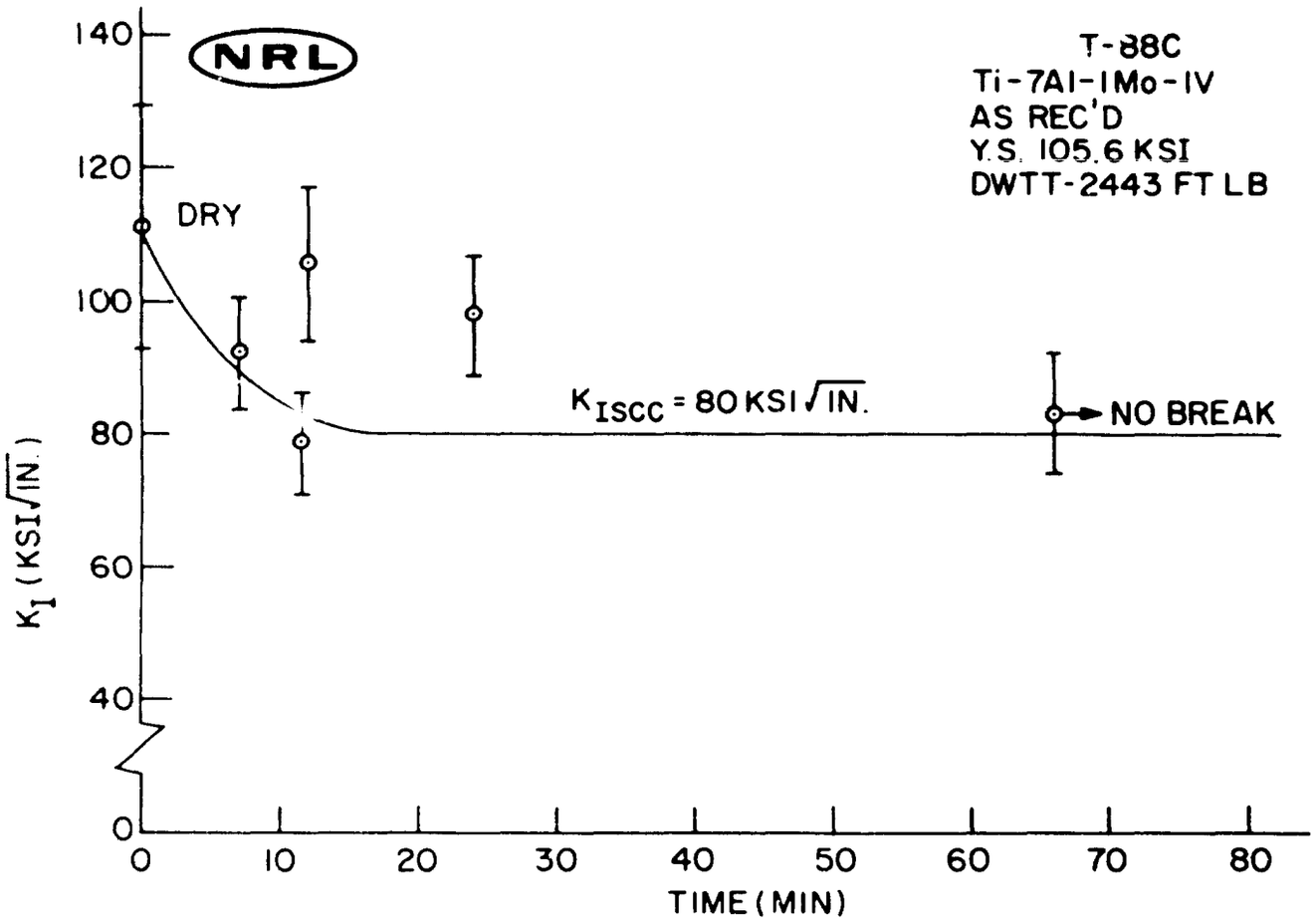

Fig. 12 - Salt water SCC characteristics of Ti-7Al-1Mo-1V alloy, T-88

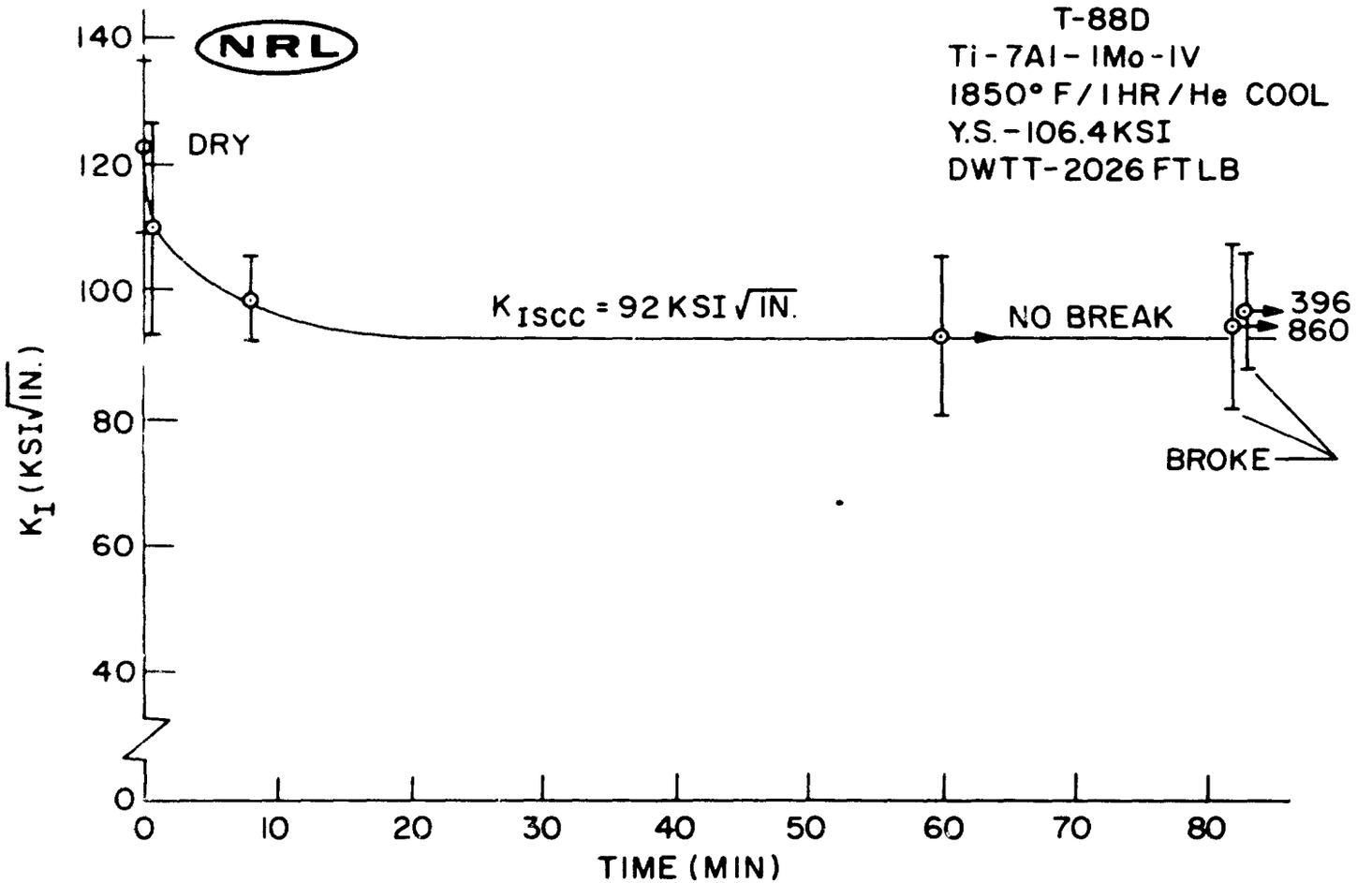

Fig. 13 - Salt water SCC characteristics of Ti-7Al-1Mo-1V alloy, T-88

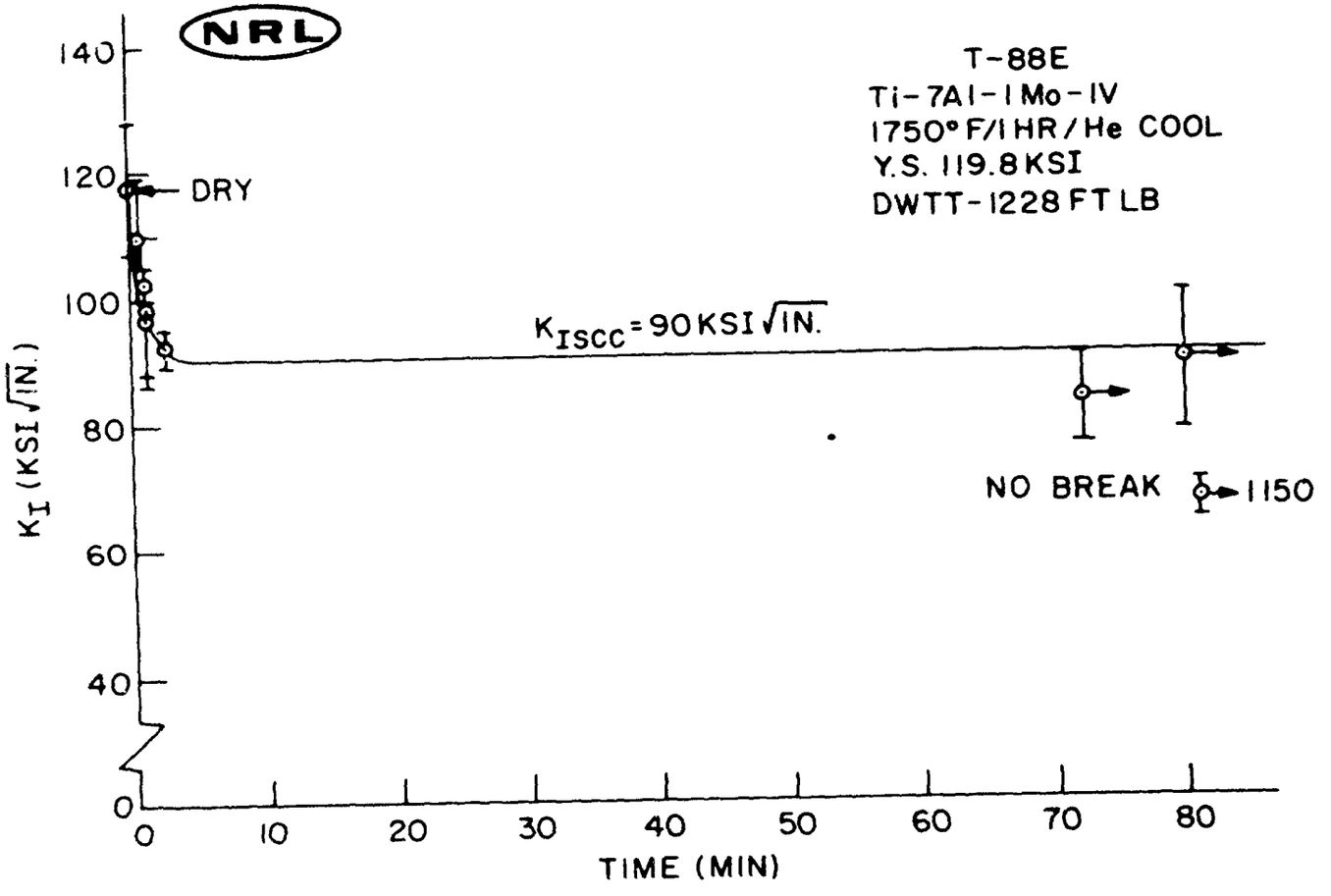

Fig. 14 - Salt water SCC characteristics of Ti-7Al-1Mo-1V alloy, T-88

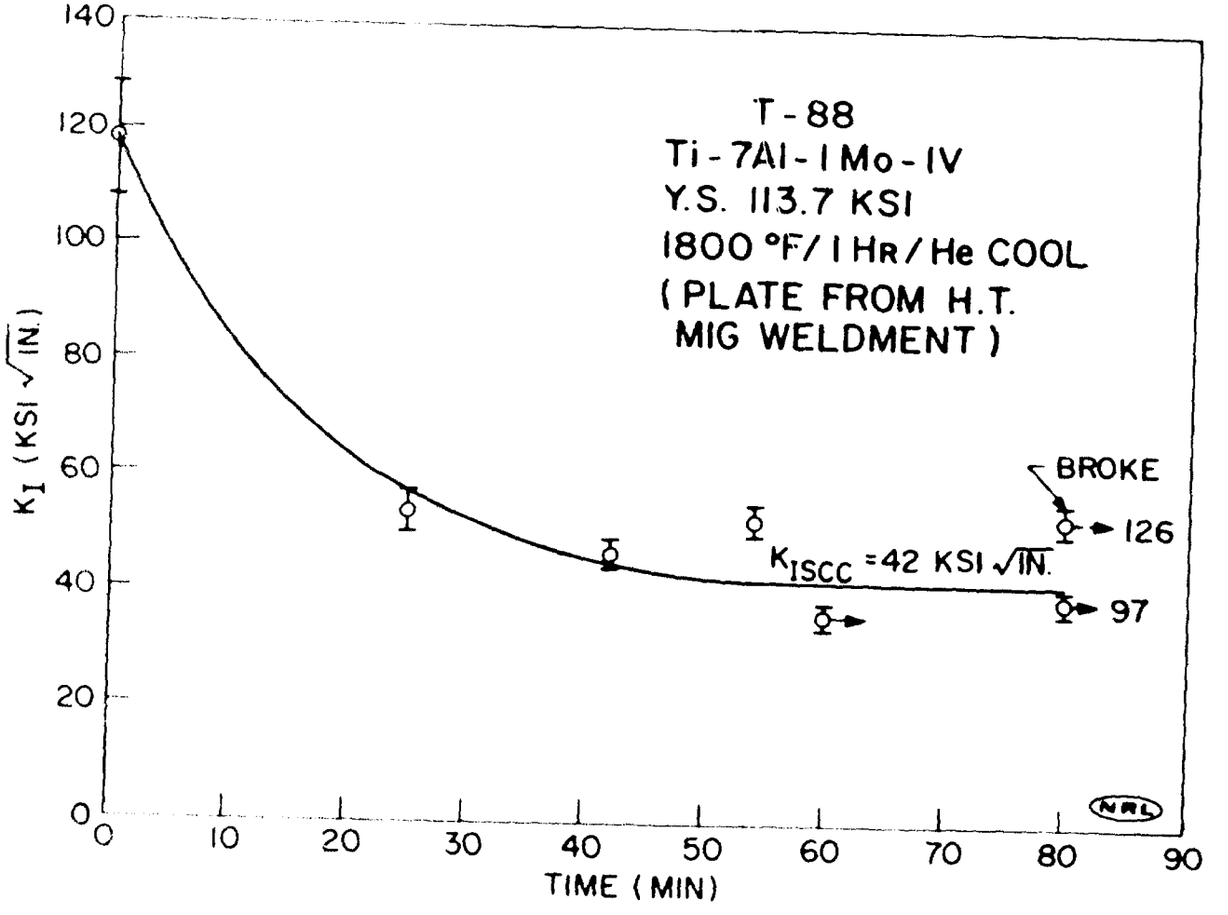

Fig. 15 - Salt water SCC characteristics of Ti-7Al-1Mo-1V alloy, T-88

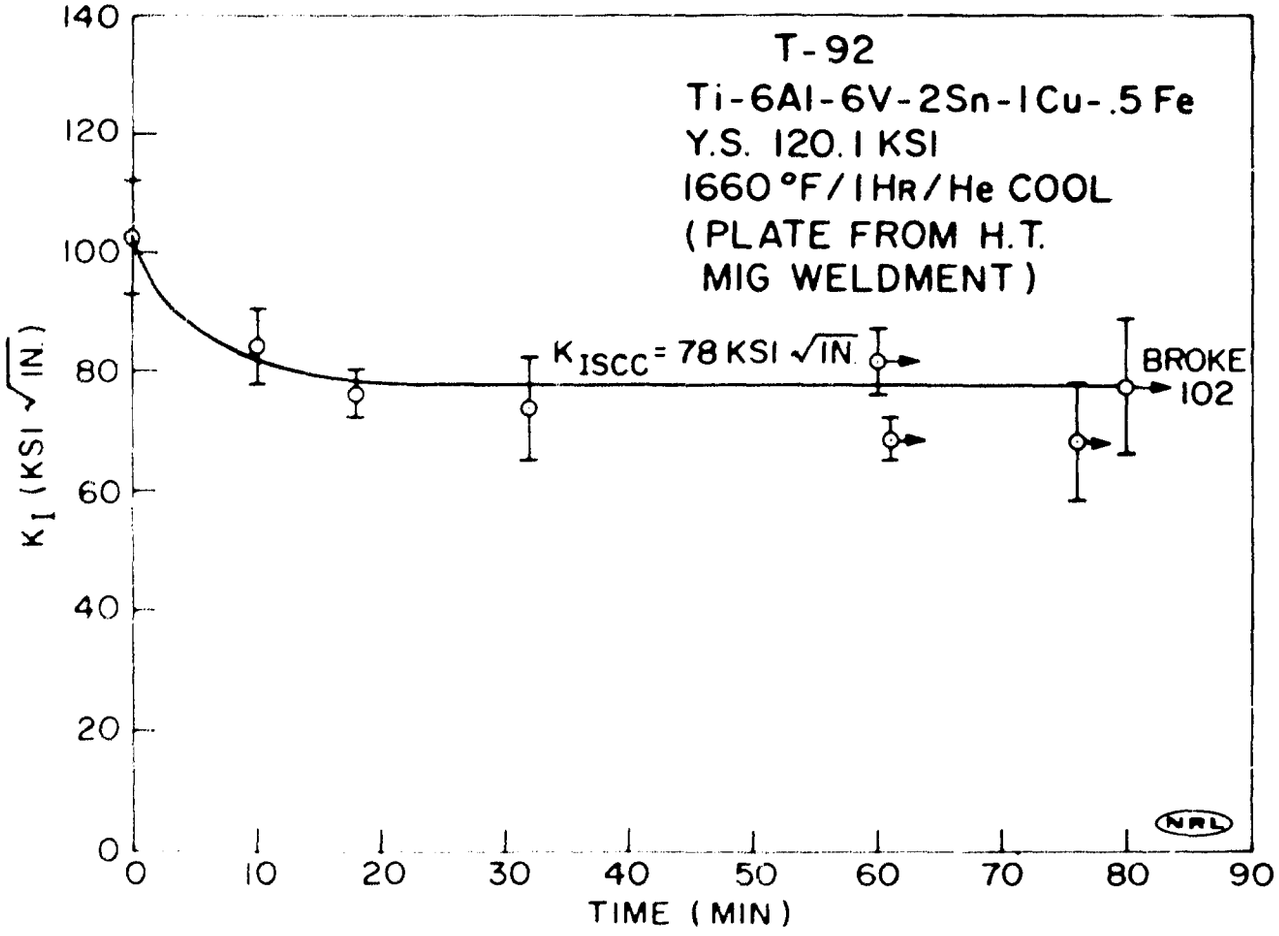

Fig. 16 - Salt water SCC characteristics of Ti-6Al-6V-2Sn-1Cu-.5Fe alloy, T-92

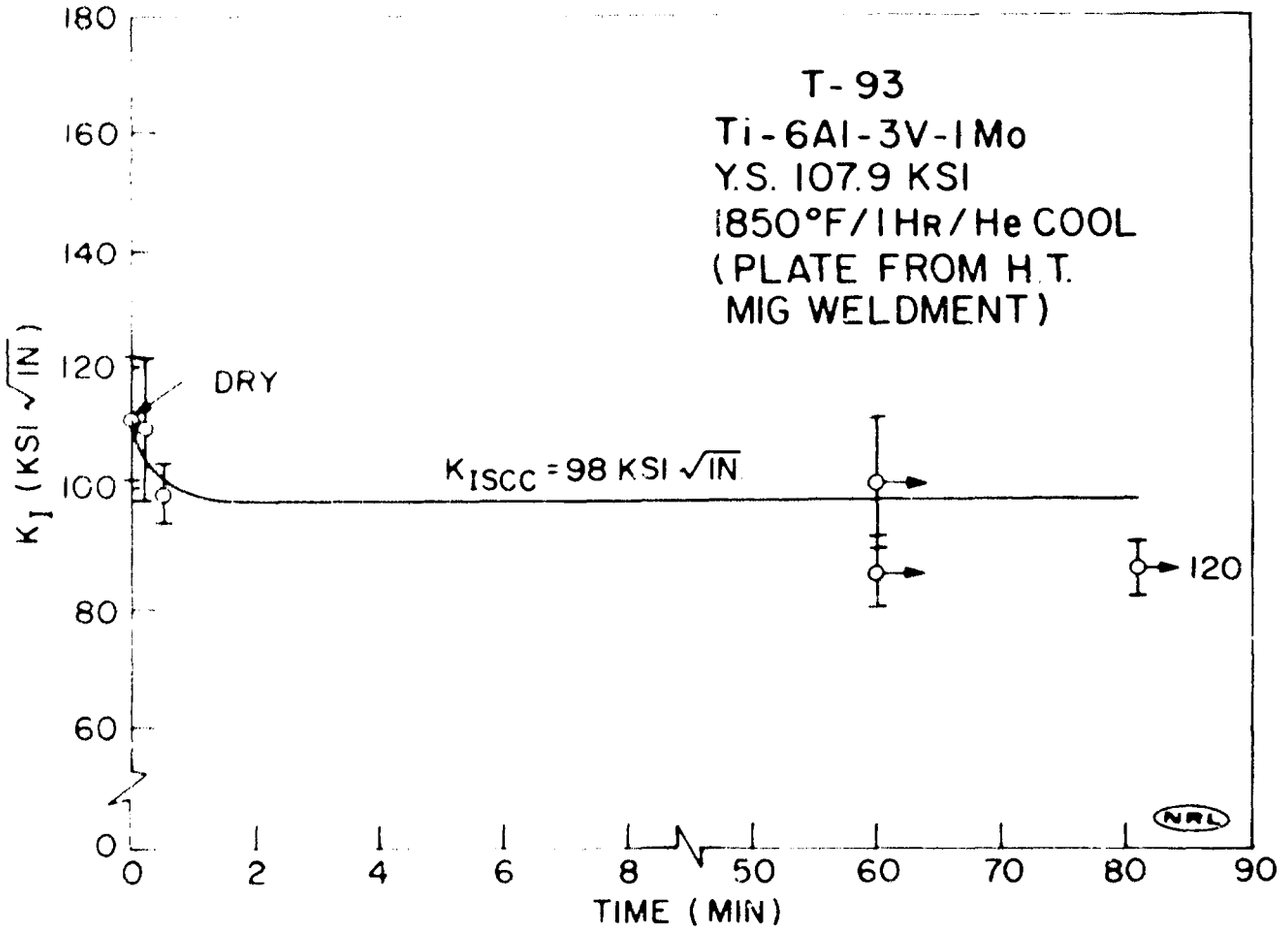

Fig. 17 - Salt water SCC characteristics of Ti-6Al-3V-1Mo alloy, T-93

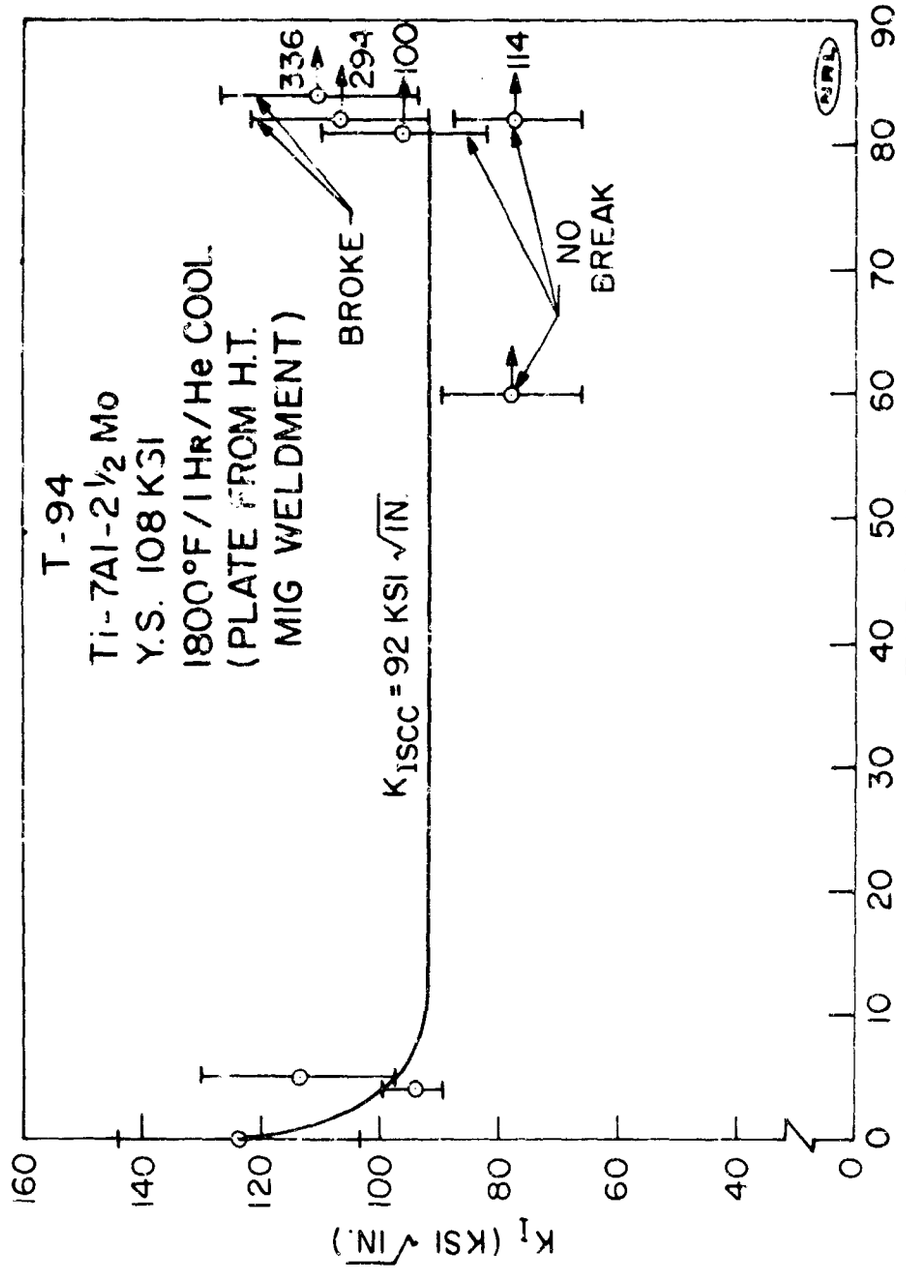

Fig. 18 - Salt water SCC characteristics of Ti-7Al-2.5Mo alloy, T-94

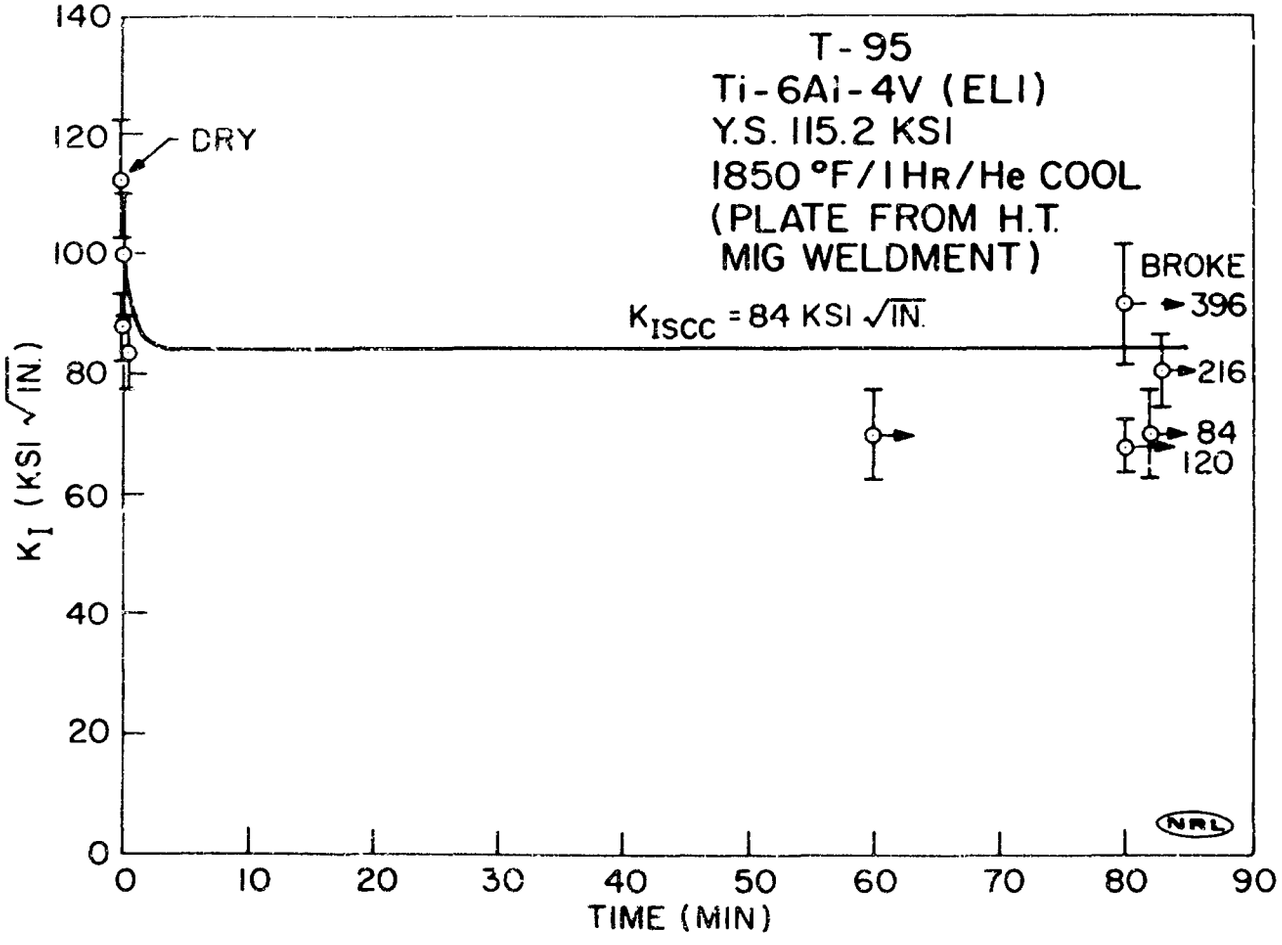

Fig. 19 - Salt water SCC characteristics of Ti-6Al-4V (ELI) alloy, T-95

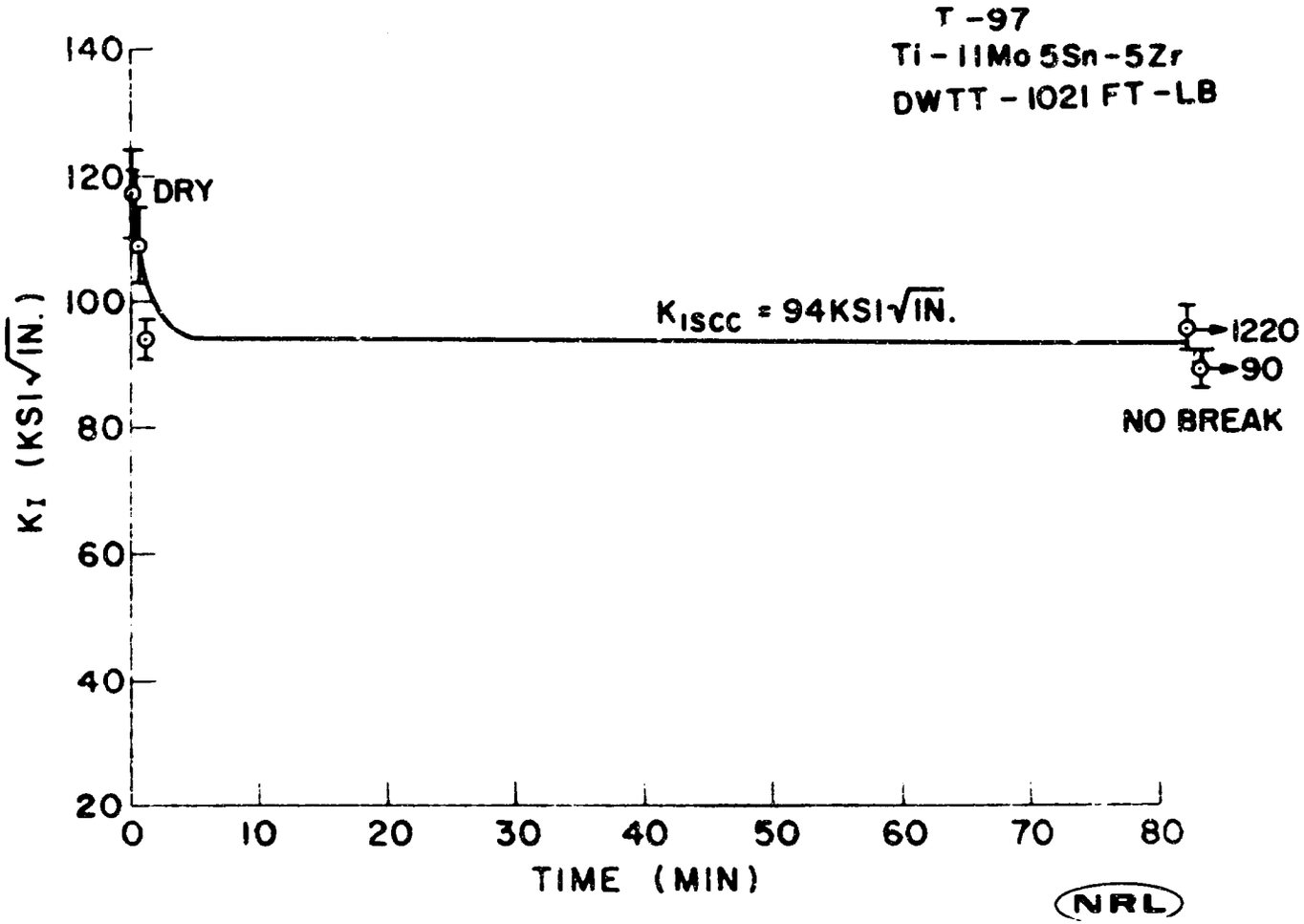

Fig. 20 - Salt water SCC characteristics of Ti-11Mo-5Sn-5Zr alloy, T-97

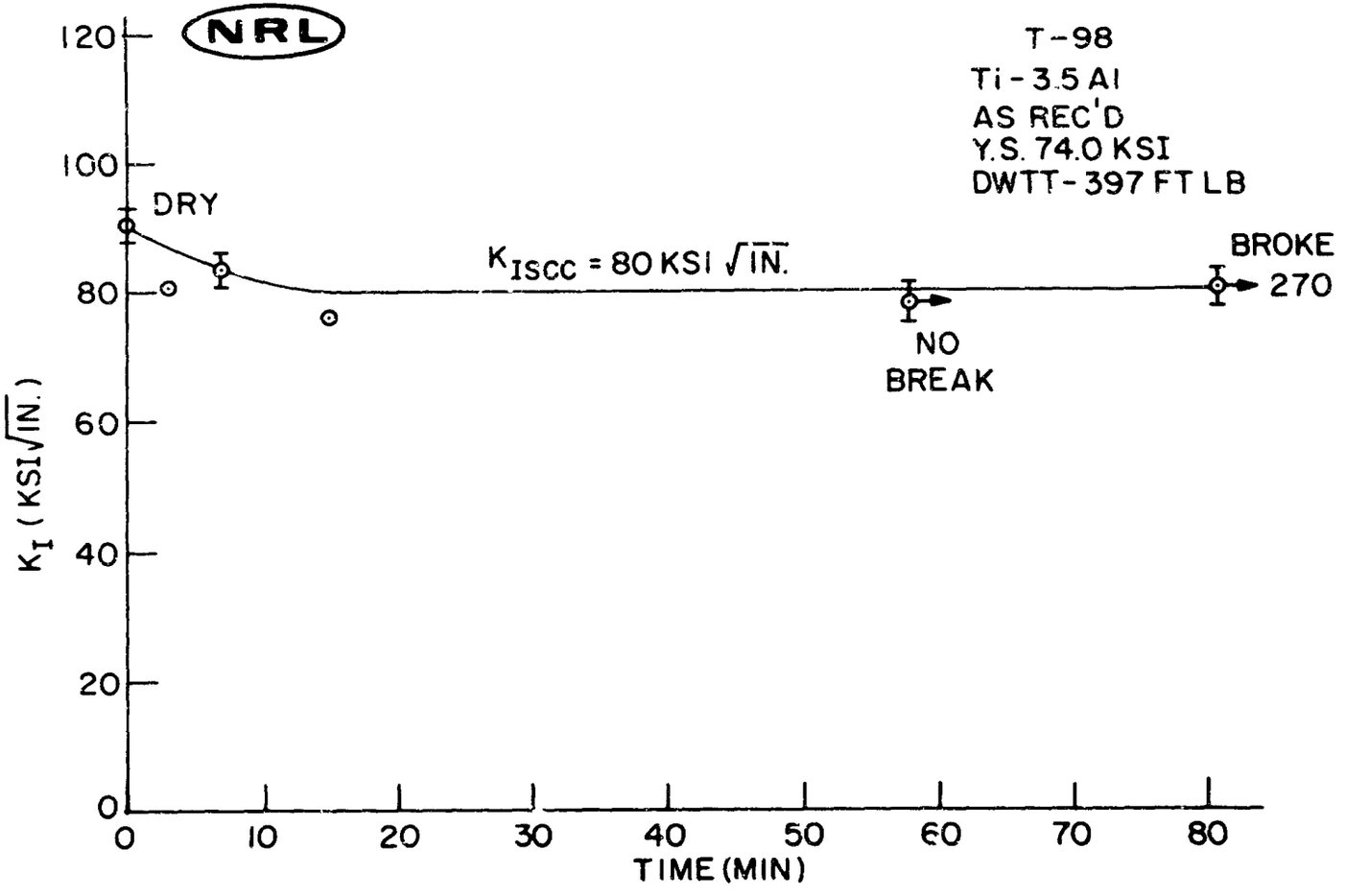

Fig. 21 - Salt water SCC characteristics of Ti-3.5Al alloy, T-98

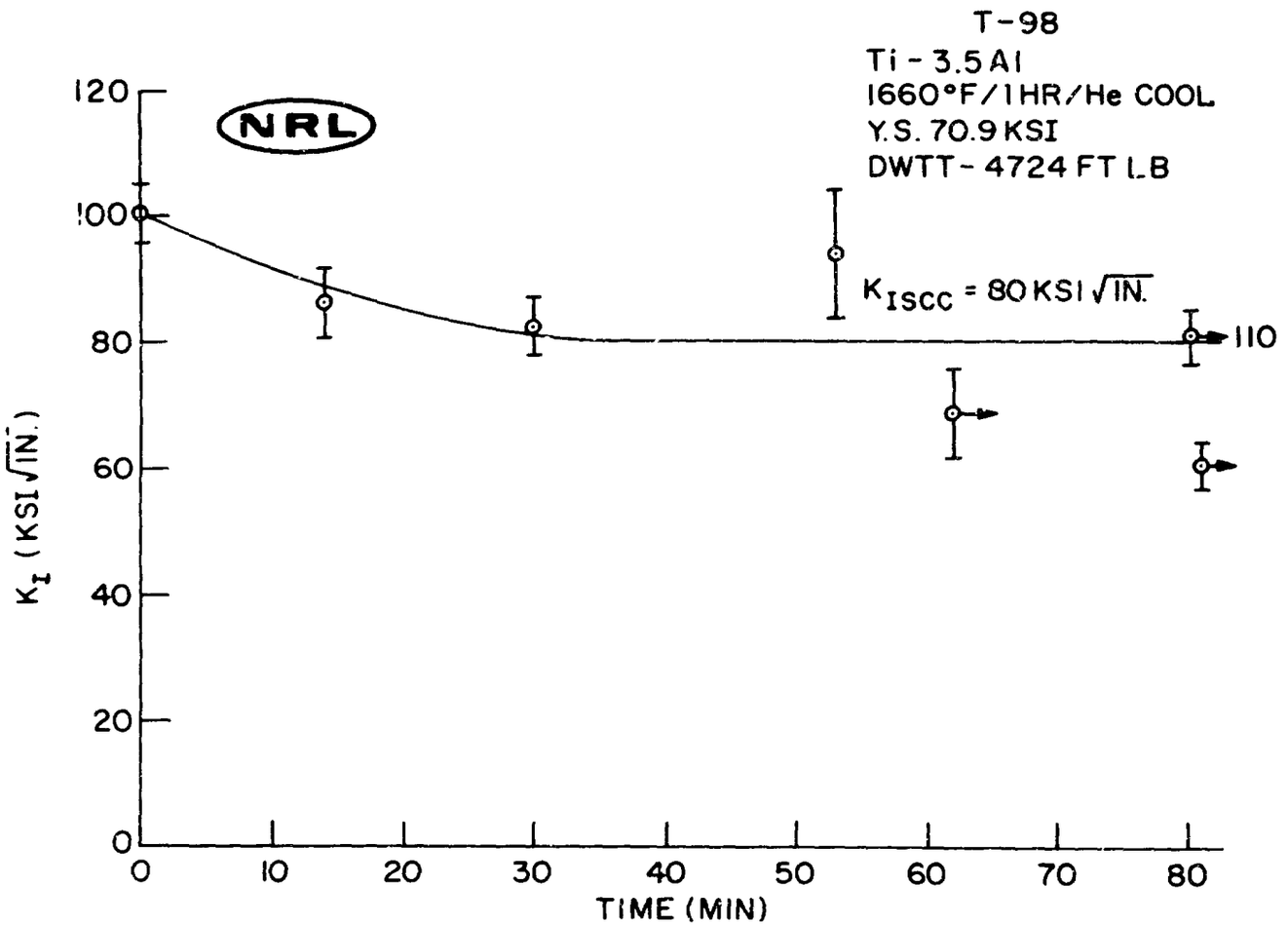

Fig. 22 - Salt water SCC characteristics of Ti-3.5Al alloy, T-98

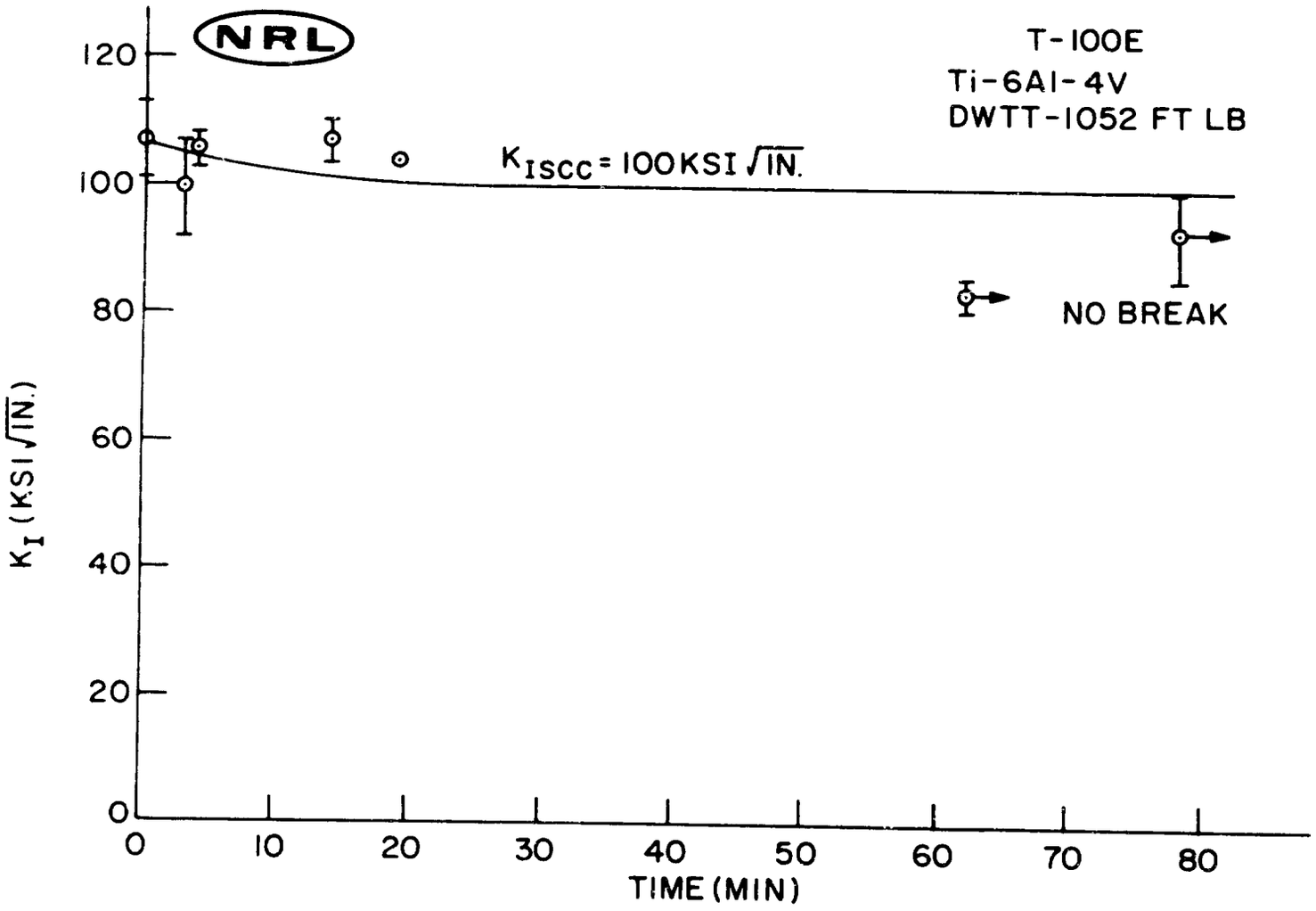

Fig. 23 - Salt water SCC characteristics of Ti-6Al-4V alloy, T-100E

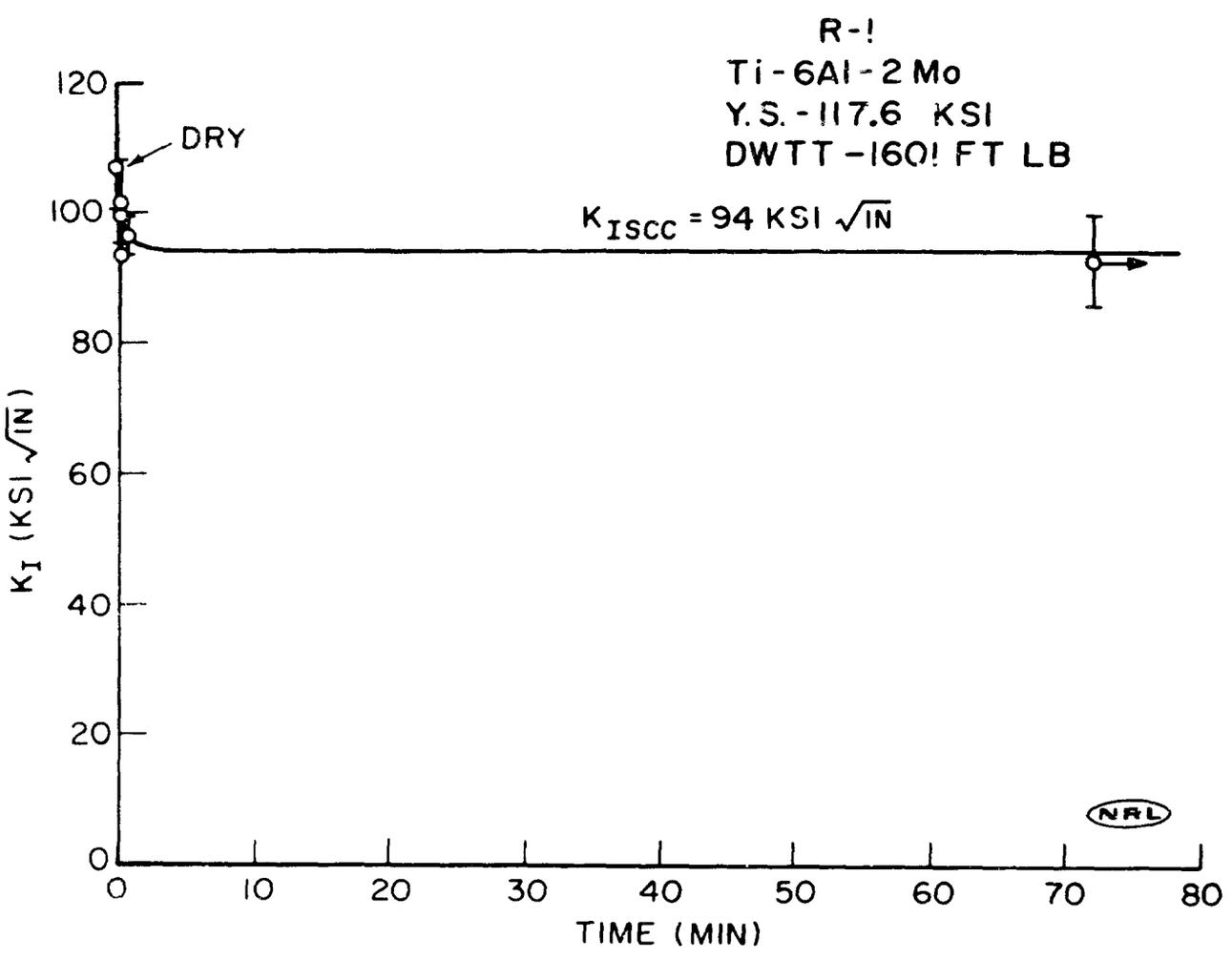

Fig. 24 - Salt water SCC characteristics of Ti-6Al-2Mo alloy, R-1

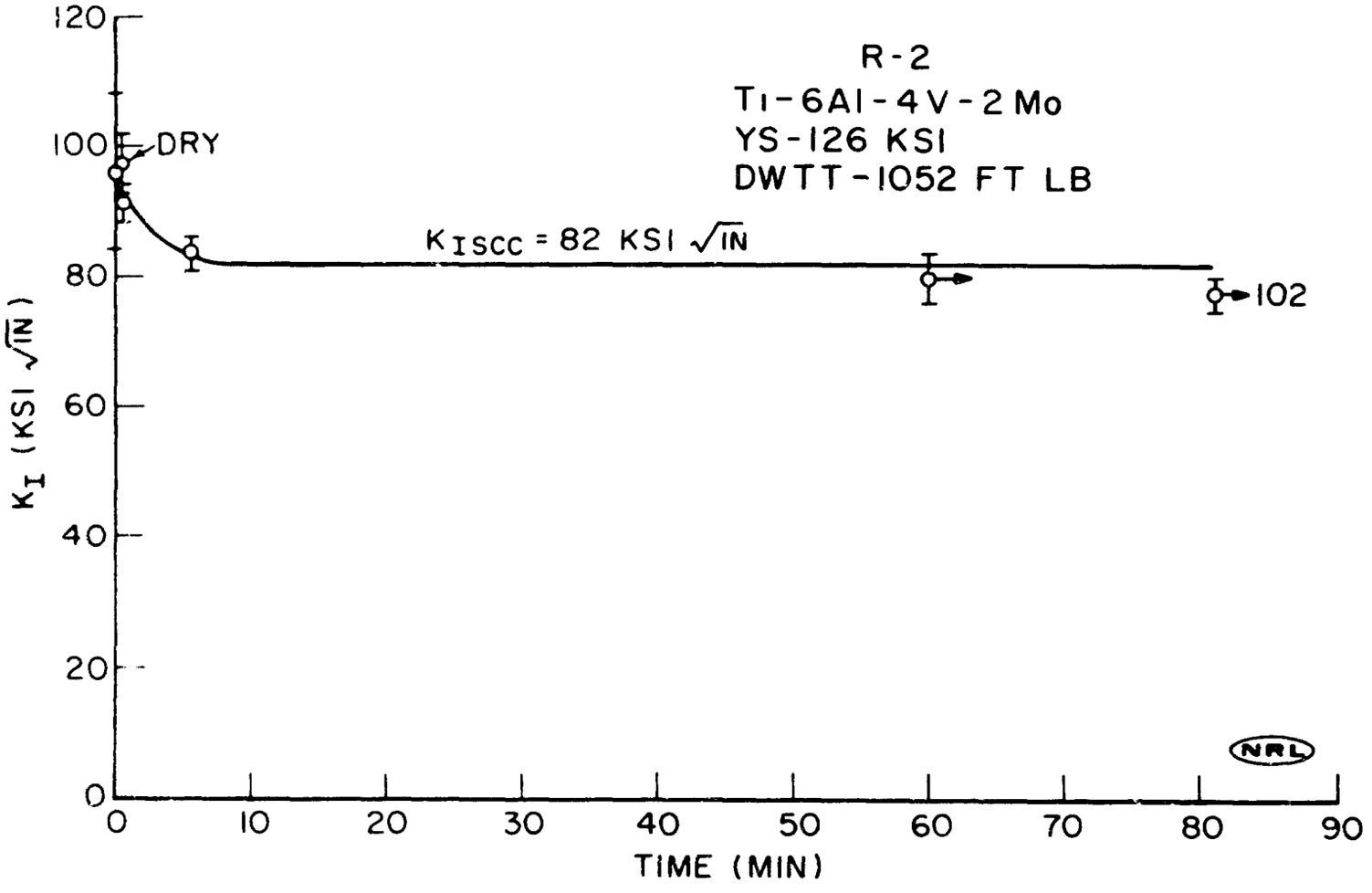

Fig. 25 - Salt water SCC characteristics of Ti-6Al-4V-2Mo alloy, R-2

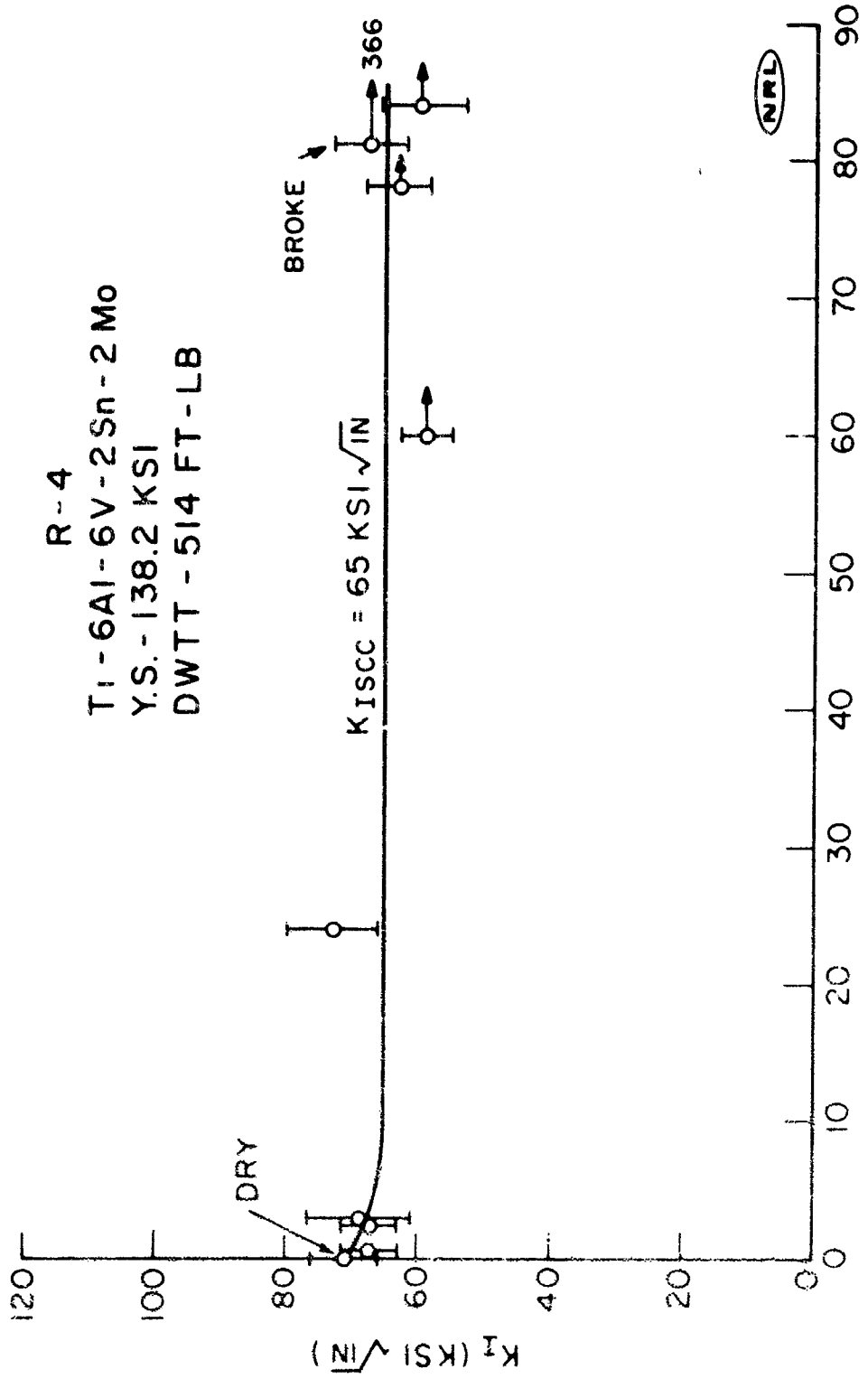

Fig. 26 - Salt water SCC characteristics of Ti-6Al-6V-2Mo-2Sn alloy, R-4

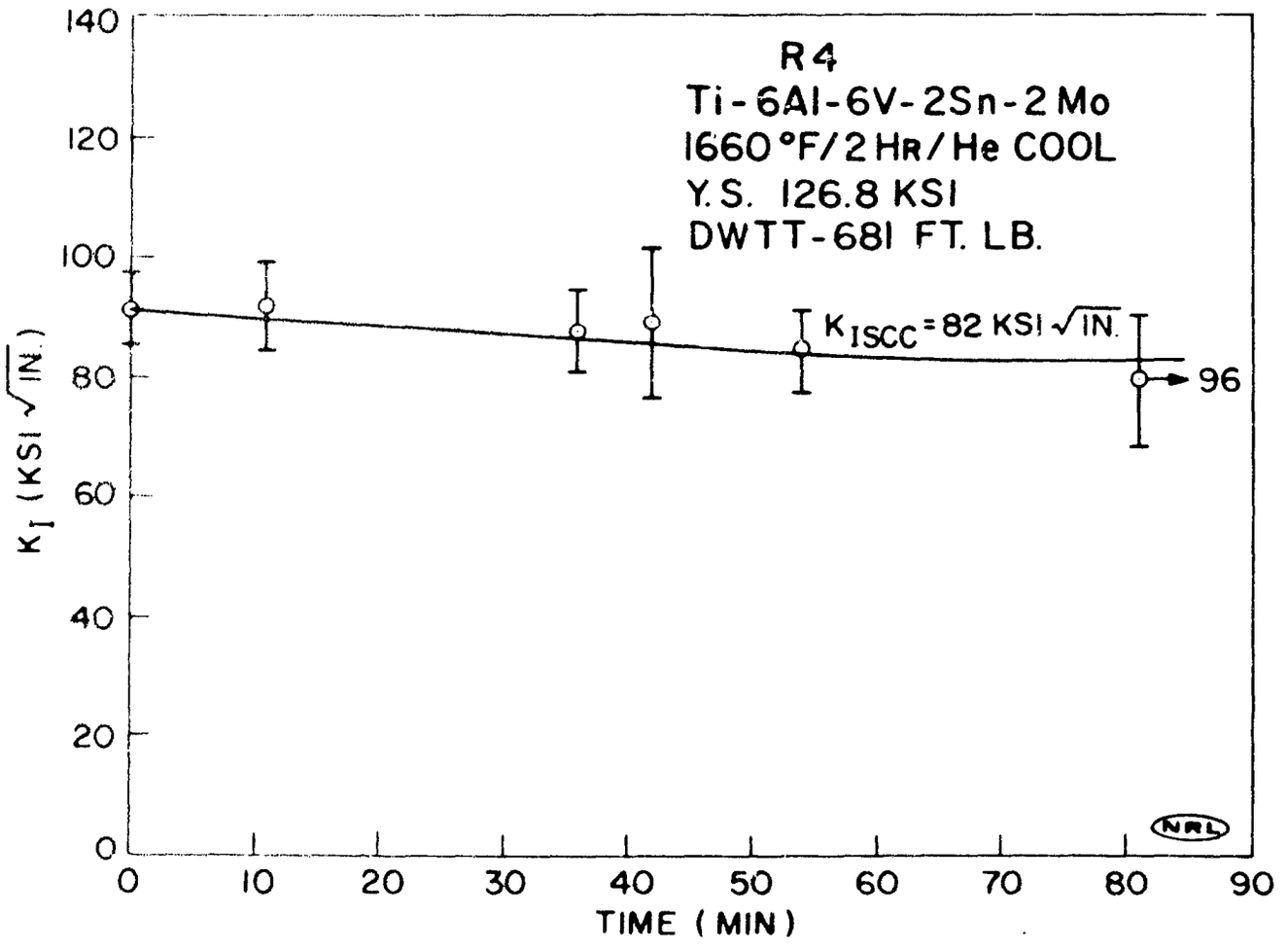

Fig. 27 - Salt water SCC characteristics of Ti-6Al-6V-2Mo-2Sn alloy, R-4

TABLE 9

SCC CHARACTERISTICS OF TITANIUM ALLOY PLATES AND WELDMENTS

Composition	Code	Weld ℄		HAZ Weld ℄ +3/16 in.		Plate		Remarks
		K_{Ix} (ksi/in)	K_{Iscc} (ksi/in)	K_{Ix} (ksi/in)	K_{Iscc} (ksi/in)	K_{Ix} (ksi/in)	K_{Iscc} (ksi/in)	
7Al-1Mo-1V	T-88	76	66	72	61	--	--	
5Al-2V-2Mo-2Sn	T-90	80	75	66	47	x108	100	
6Al-4V	T-91	83	74	115	94	x118	90	
6Al-6V-2Sn-1Cu-1/2Fe	T-92	52	49	68	48	x111	96	
6Al-3V-1Mo	T-93	102	98	106	90	x116	110	
7Al-2 1/2Mo	T-94	66	59	92	75	101	80	
6Al-4V (ELI)	T-95	86	75	78	76	94	68	
7Al-1Mo-1V	T-88	100	82	97	92	118	42	1800°F/1 Hr/He Cool
5Al-2V-2Mo-2Sn	T-90	103	87	120	95	--	--	1660°F/1 Hr/He Cool
6Al-6V-2Sn-1Cu-1/2Fe	T-92	80	66	106	74	,102	78	1660°F/1 Hr/He Cool
6Al-3V-1Mo	T-93	104	84	110	92	,112	68	1850°F/1 Hr/He Cool
7Al-2 1/2Mo	T-94	*90	*74	99	81	,123	92	1800°F/1 Hr/He Cool
6Al-4V (ELI)	T-95	106	90	110	94	112	84	1850°F/1 Hr/He Cool

*Flaws in weldment

3/4" specimen width, 1/32 in side groove depth

x 3/4" specimen width, 1/10 in side groove depth

All other specimens 1/2 in wide, 1/32 in side groove depth

and at 1850°F for one hour and then cooled in helium, were tested in the cantilever test; K_{Iscc}:K_{Ix} values for these were 80:111, 92:122, and 90:117, respectively (Figs. These values indicated neither an appreciable sensitivity to SCC nor an obvious effect of heat treatment in this case. However, specimens of base plate material cut from a MIG weldment of the same material heat treated at 1850°F/1 hr/ He cooled indicated a pronounced sensitivity to SCC, K_{Iscc}:K_{Ix} being 42:118 (Fig. 15). The obvious differences in the tests were the difference in specimen width (1/2-inch wide for the specimens from DWTT specimens, 3/4-inch wide for specimens from the MIG weldment) and the difference in the section size being heat treated (1 in x 5 in x 17 in for DWTT specimens versus 1 in x 10 in x 20 in for MIG weldments). Tests of base plate material from other heat treated MIG weldments (Figs. 16 through 19) did not show the same discrepancy compared to as-received base plate values (5) or to MIG weldment values (Table 9), the relation between specimen sizes being the same.

In other base-plate tests, high interstitial unalloyed titanium was shown to be sensitive to SCC (K_{Iscc}/K_{Ix} = 40/69) while all other alloys tested were relatively unaffected by the salt water environments.

The results of tests conducted on MIG weldments both as-welded and solution heat treated are shown in Table 9 and in Figs. 28 through 34. Base plate values for both conditions are shown for comparison. The procedures used in fabricating the weldments and the mechanical properties of the weldments are described in detail in reference 7. The procedure in SCC testing the weldments has been described in the same reference. As indicated in Table 9, specimens for tests at weld centerline (℄), at the heat affected zone (HAZ) (℄ + 3/16-in), and in the as-received base plate for alloys T94 and T95 were 1/2-in. wide with 1/32-in. deep side-grooves. Specimen dimensions for other plates are indicated in the table.

The values of K_{Iscc} for as-received base plate material were higher than those for the weld deposit and HAZ, both as-welded and heat treated. Also the K_{Iscc} values for heat treated plate material generally exceeded the K_{Iscc} values for the heat treated weld metal deposits and HAZ. Values of K_{Iscc} were generally higher at weld centerline

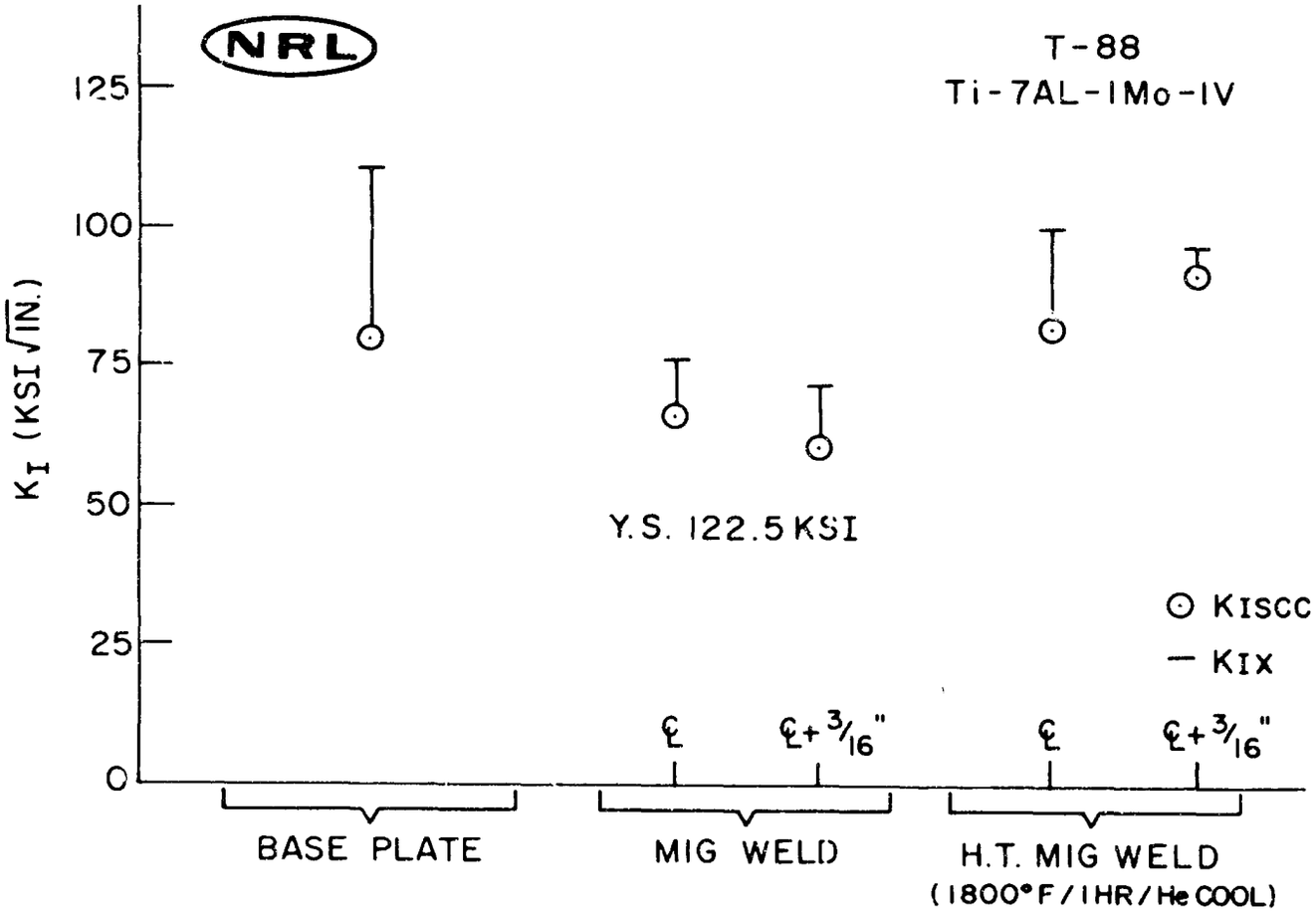

Fig. 28 - Salt water SCC characteristics of a MIG weldment of Ti-7Al-1Mo-1V alloy (T-88) at weld centerline and HAZ in as-welded and heat treated conditions

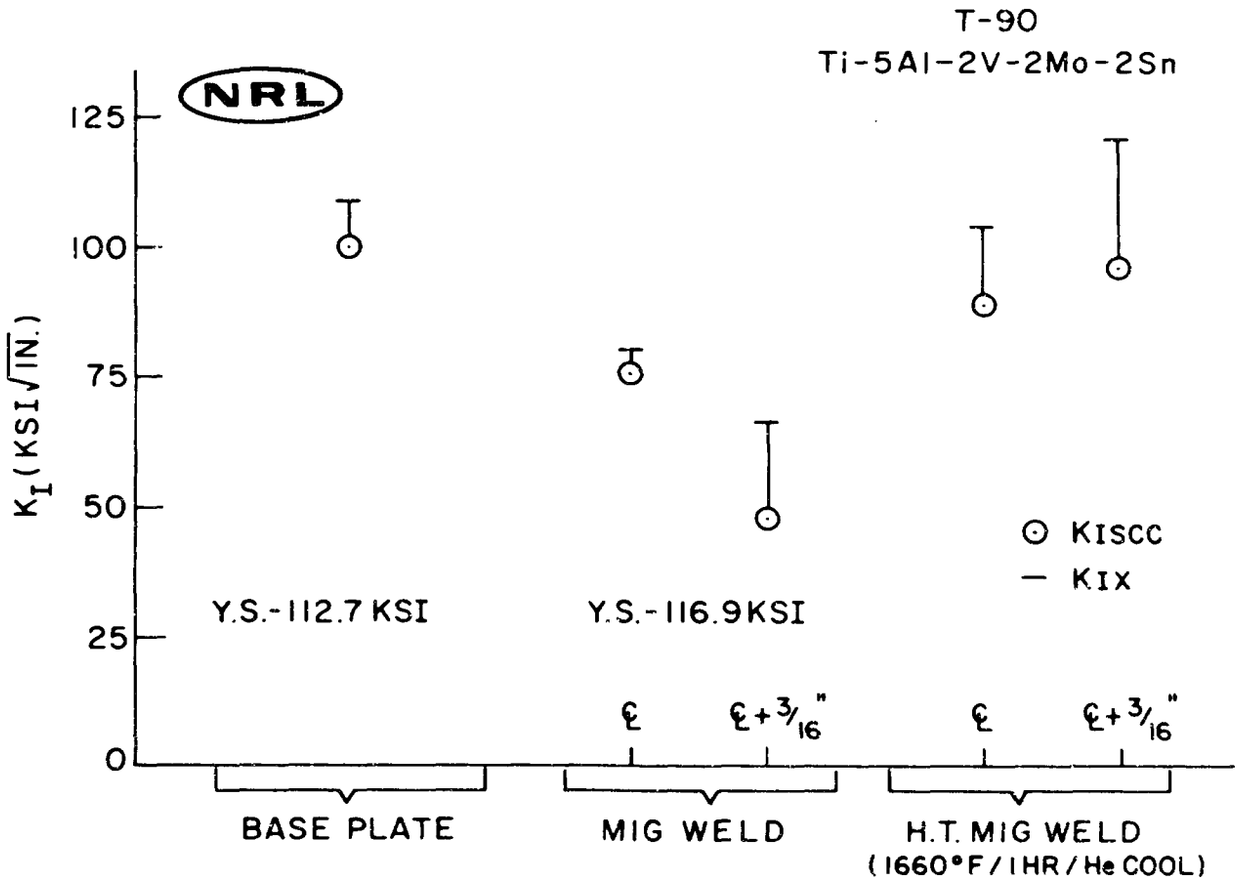

Fig. 29 - Salt water SCC characteristics of a MIG weldment of Ti-5Al-2V-2Mo-2Sn alloy (T-90) at weld centerline and HAZ in as-welded and heat treated conditions

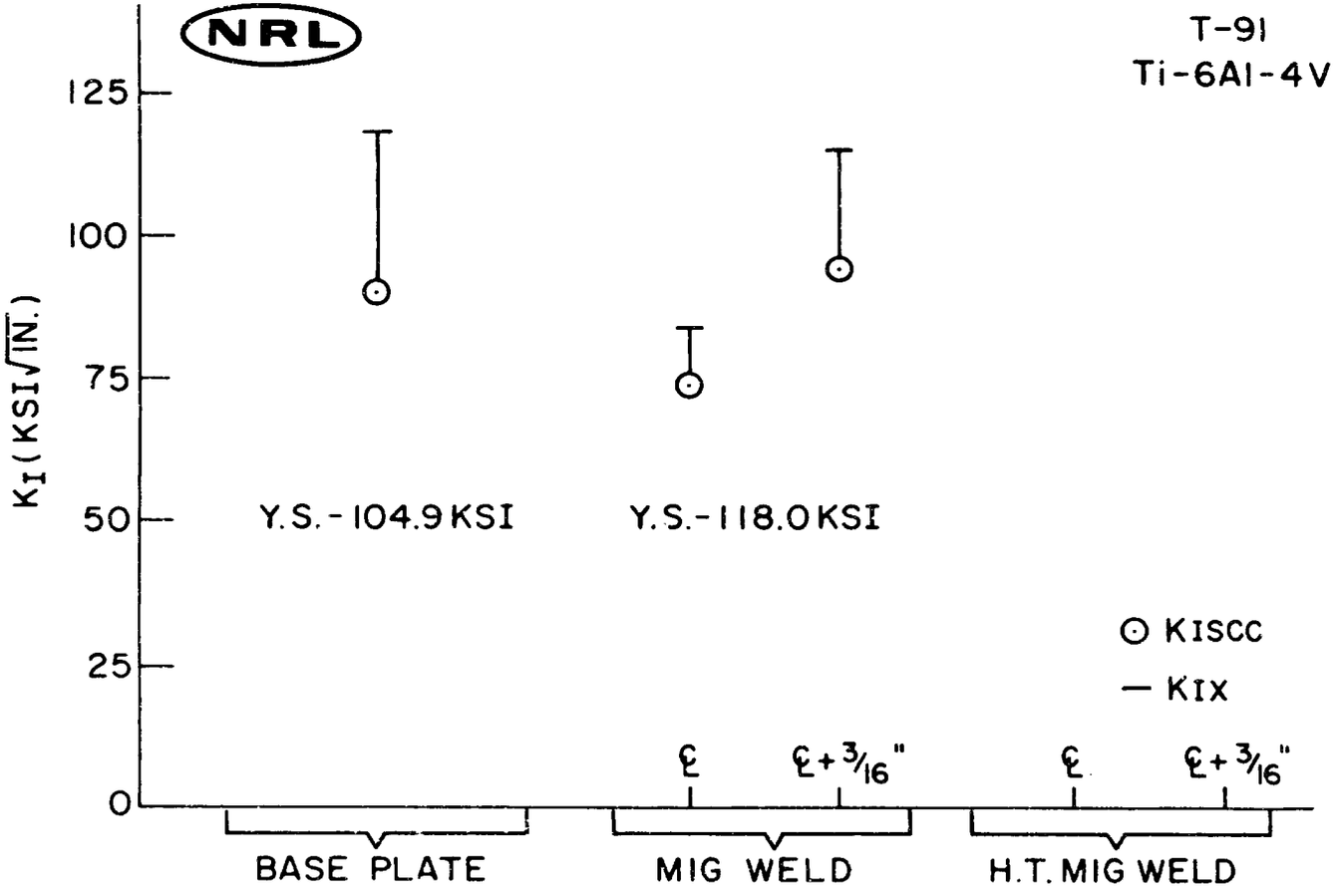

Fig. 30 - Salt water SCC characteristics of a MIG weldment of Ti-6Al-4V alloy (T-91) at weld centerline and HAZ in as-welded condition

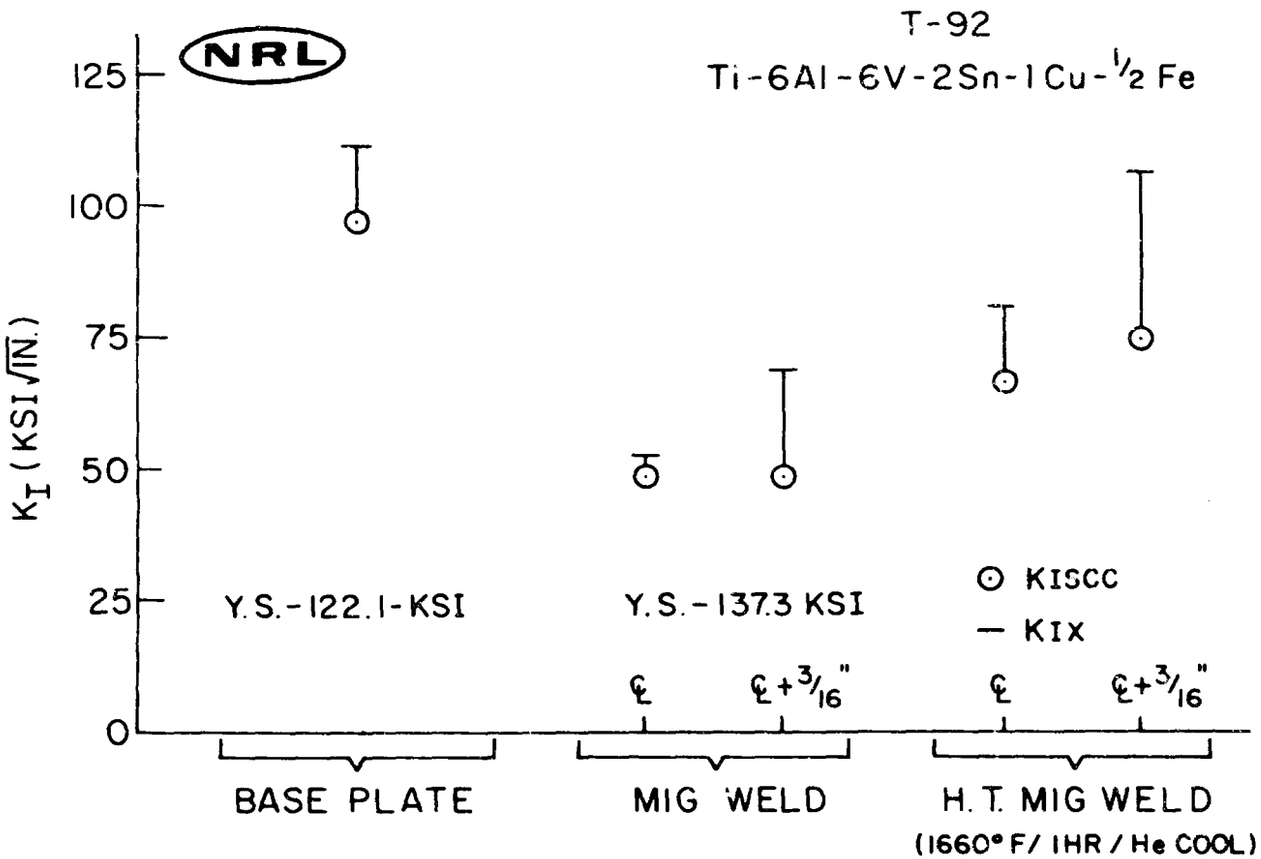

Fig. 31 - Salt water SCC characteristics of a MIG weldment of Ti-6Al-6V-2Sn-1Cu-.5Fe alloy (T-92) at weld centerline and HAZ in as-welded and heat treated conditions

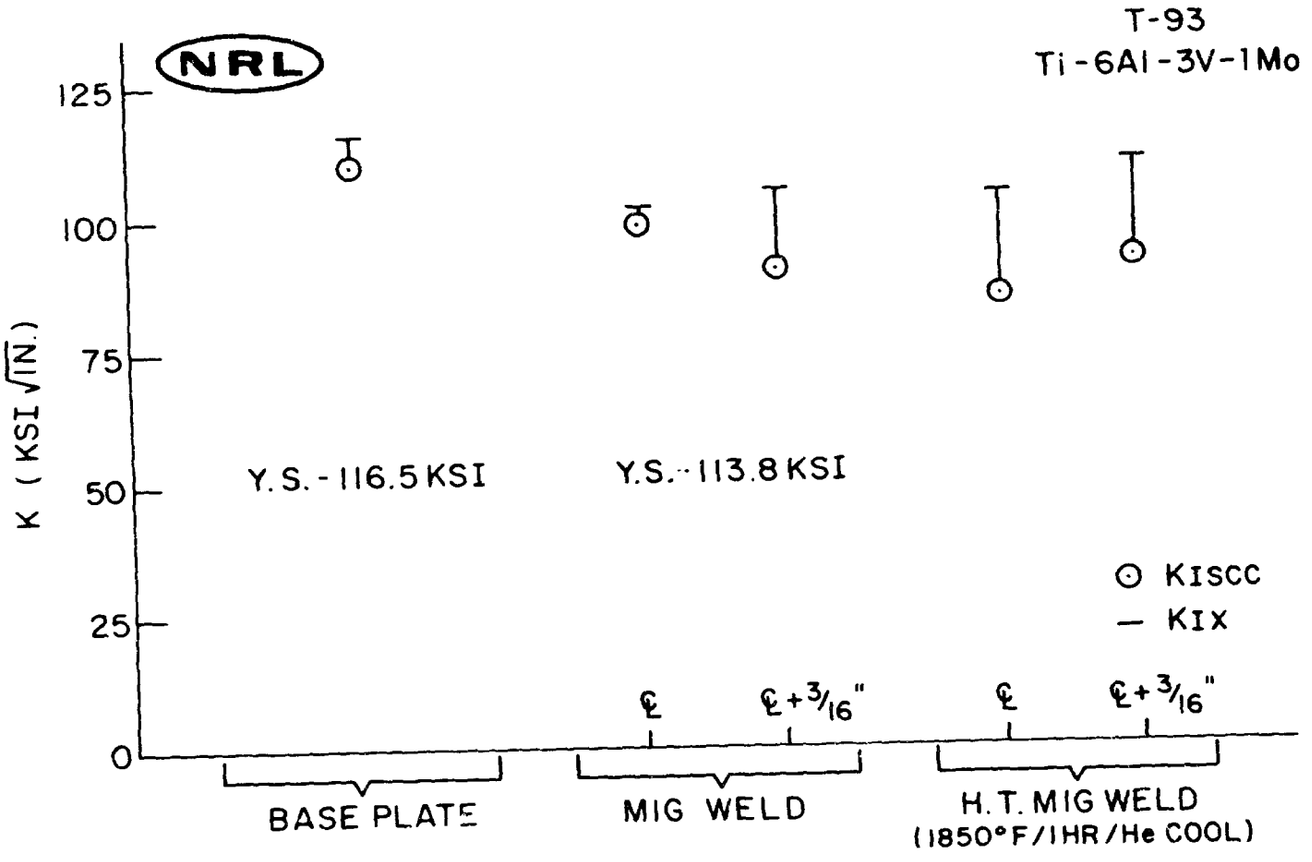

Fig. 32 - Salt water SCC characteristics of a MIG weldment of Ti-6Al-3V-1Mo alloy (T-93) at weld centerline and HAZ in as-welded and heat treated conditions

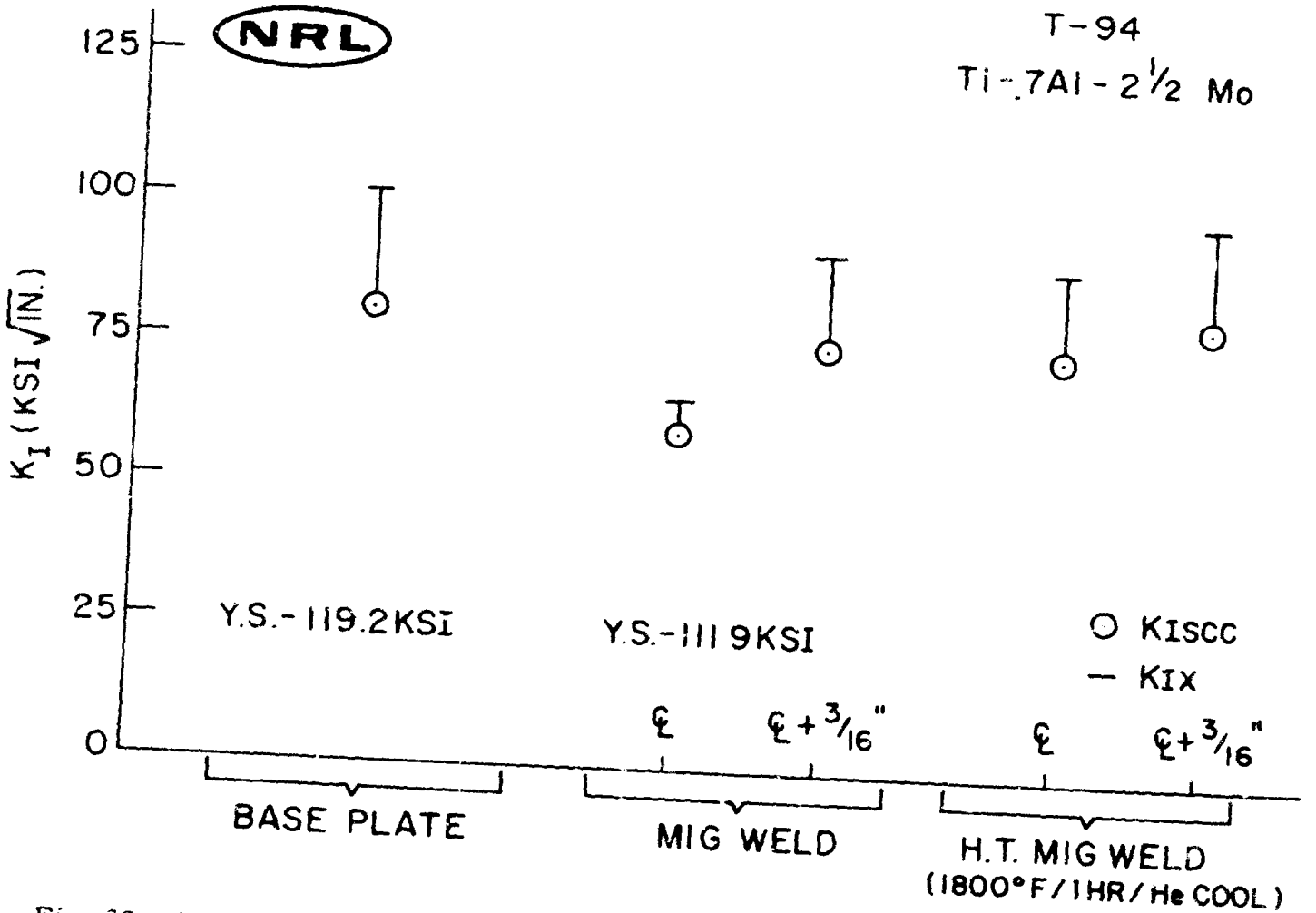

Fig. 33 - Salt water SCC characteristics of a MIG weldment of Ti-7Al-2.5Mo alloy (T-94) at weld centerline and HAZ in as-welded and heat treated conditions

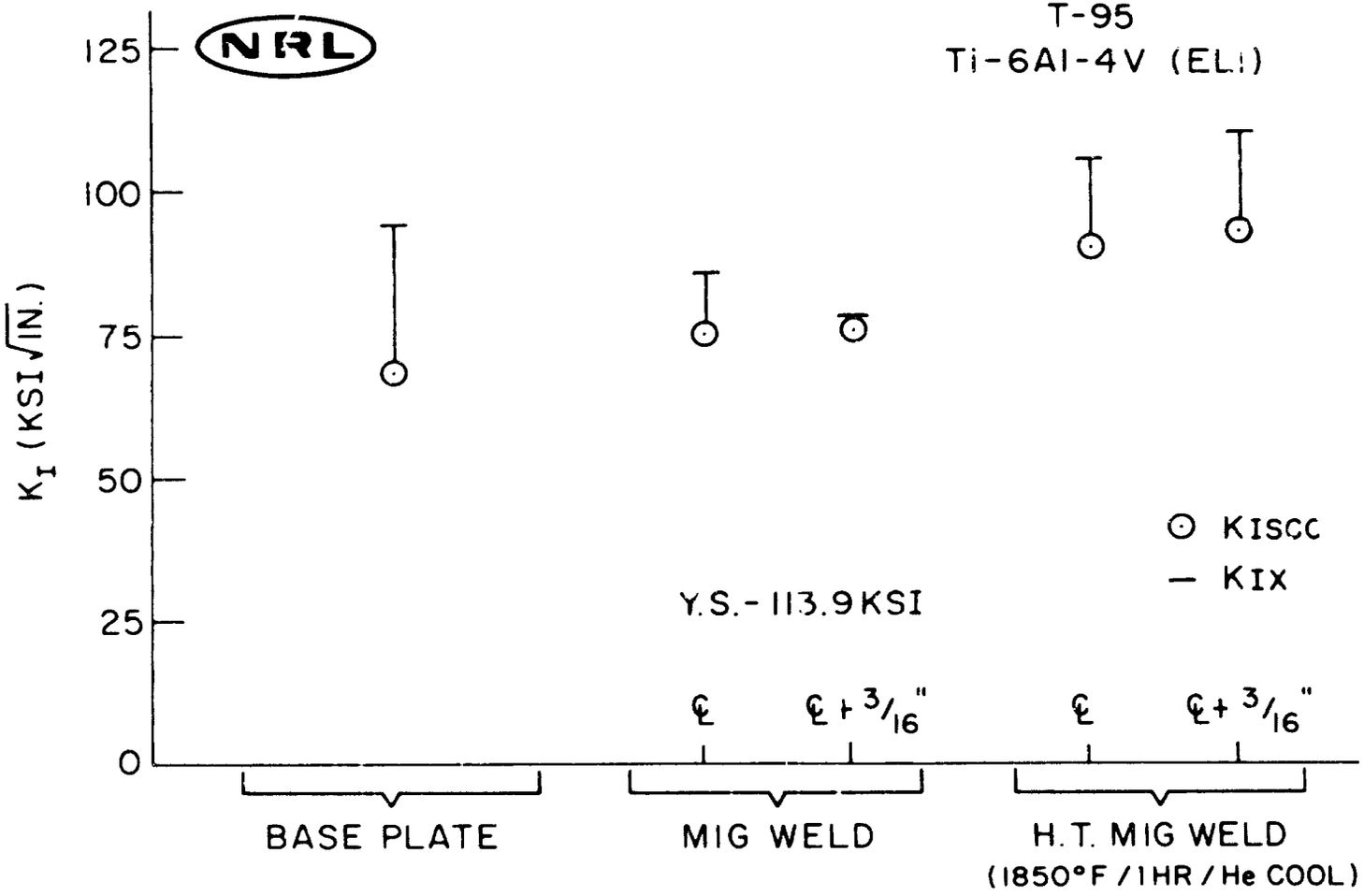

Fig. 34 - Salt water SCC characteristics of a MIG weldment of Ti-6Al-4V (ELI) alloy (T-95) at weld centerline and HAZ in as-welded and heat treated conditions

than at the HAZ for as welded plate, while the opposite was true for the heat treated weldment. Heat treated weldments had generally higher K_{Iscc} values for both weld centerline and HAZ compared to as deposited weldments.

FRACTOGRAPHIC STUDY OF FATIGUE FRACTURES

In a recent low cycle fatigue study of Ti-7Al-2Cb-1Ta in air and in salt water environments, electron fractography methods revealed the presence of quasi-cleavage fracture on the fracture surfaces of the specimens tested in salt water (15). Quasi-cleavage fracture, which indicates SCC was also observed at the fatigue-fast fracture interface on a specimen tested entirely in air. Since a high likelihood exists that such fractures can be caused by moist air in alloys which are highly sensitive to SCC, a number of single-edge-notch (SEN) fracture mechanics specimens of titanium alloys were examined for evidence of quasi-cleavage fracture in the fatigue cracked portion of the fracture surface and at the fatigue crack-fast fracture interface.

The eight specimens examined by electron fractographic methods were selected to represent the variety of K_{IC}, yield strength (YS), and drop-weight tear energy levels available. Preparation of the SEN specimens had included fatiguing them in three point bending at approximately 30% of YS to generate a fatigue crack before they were fractured in tension. Table 10 shows the composition and K_{IC} values for these alloys alone, with SCC test parameters (K_{Ix} and K_{Iscc}). The SEN specimens were tested in the heat treated condition shown, while SCC values were taken from mill-annealed material, with the exception of T21, which was SCC tested in the heat-treated condition shown.

The fractographic method used was the standard two step method of replication described in reference (15), with examination of the replica in the electron microscope at relatively low levels of magnification (3000X-6000X). Cleavage or quasi-cleavage was observed on some of the specimens, while others showed none (See Table 10). The presence of this low energy fracture mode indicated that some crack growth, especially in the fatigued region, was due to SCC. In the specimens where cleavage or quasi-cleavage was evident the fatigue-fast fracture interface could not be clearly defined, therefore, whether this mode of fracture extended into the region of the fracture surface associated

TABLE 10

FRACTURE MECHANICS AND SCC DATA FOR TITANIUM ALLOYS

Composition	Code	K_{Ic} (ksi $\sqrt{in}$)	K_{Ix} (ksi $\sqrt{in}$)	K_{Iscc} (ksi $\sqrt{in}$)	Condition*	Remarks
Unalloyed	T17	99	--	--	As received	Quasi cleavage fracture noted
Ti-8Al-1Mo-1V	T19	69	113	28	1800°F/1 Hr/WQ 1100°F/2 Hr/AC	Large amounts of cleavage fracture noted
Ti-6Al-6V-2.5Sn	T21	31.8	55	21	1550°F/1 Hr/WQ 900°F/4 Hr/AC	Very small amount of low energy fracture noted
Ti-6Al-4V	T27	106	88	67	1700°F/1 Hr/WQ 900°F/2 Hr/AC	No low energy fracture noted
Ti-6Al-4Zr-2Mo	T55	113	147	46	1750°F/1 Hr/WQ 1100°F/2 Hr/AC	Some low energy fracture noted
Ti-6Al-4V-2Sn	T67	82	97	88	1775°F/1 Hr/WQ 1000°F/2 Hr/AC	No low energy fracture noted
Ti-6Al-4Zr	T68A	119	124	40	1800°F/1 Hr/WQ 1100°F/2 Hr/AC	Some low energy fracture noted
2Sn-.5Mo-.5V	T68B	110	124	40	1750°F/1 Hr/WQ 1100°F/2 Hr/AC	Some low energy fracture noted

*Applies only to fracture mechanics specimen (K_{Ic}) not to SCC specimen (K_{Ix} and K_{Iscc}) except applies to both for T-21.

with "pop-in" in the fracture mechanics test is not known. Since yielding is associated with the crack tip in both the fatigue and pop-in portions of the fracture surface such an extension could be considered possible. Typical fractographs of the low energy fracture are shown in Figs. 35 through 37.

LOW CYCLE FATIGUE CRACK PROPAGATION IN A201B, A302B, and A517F PRESSURE VESSEL STEELS

(T. W. Crooker and E. A. Lange)

This report describes the results of an investigation of low cycle fatigue crack propagation in three structural steels widely used in welded pressure vessels: A201B, A302B, and A517F. The purpose of such a study stems from the fact that the occurrence of small sharp defects in large welded structures cannot be totally eliminated. Careful fabrication and nondestructive testing procedures are not sufficient to completely guarantee the absence of small fabrication defects. Therefore, low cycle (i.e., failure in less than 100,000 cycles) fatigue crack propagation is a potential failure mode for large welded structures which undergo repeated loading excursions.

The crack propagation phase of fatigue failure is a relatively new area of study. It departs from the traditional design approach to fatigue which combines crack initiation plus crack propagation into an arbitrary definition of fatigue failure. However, fatigue crack propagation studies are a promising means of providing a more rational approach to structural fatigue situations where experience suggests a very high probability of pre-existing flaws.

Attention is currently limited to plate materials for two reasons: the inherent simplicity of plate materials rather than weldments for an initial research program and the fact that, although welded joints are a prime source of defects, the propagation of defects in fatigue is controlled by the stress pattern and is by no means limited to weld metal.

The steels chosen for this investigation are important because of their broad application, but are of particular significance in this study because the fatigue test specimens employed were taken from the shell materials of full-size pressure vessels. The pressure vessels themselves had first undergone fatigue testing as part of the Welding Research Council's Pressure Vessel Research Committee (PVRC) program of testing full-size pressure vessels. The final failure analyses conducted on the six PVRC vessels are published in references 16-19. The subsequent laboratory

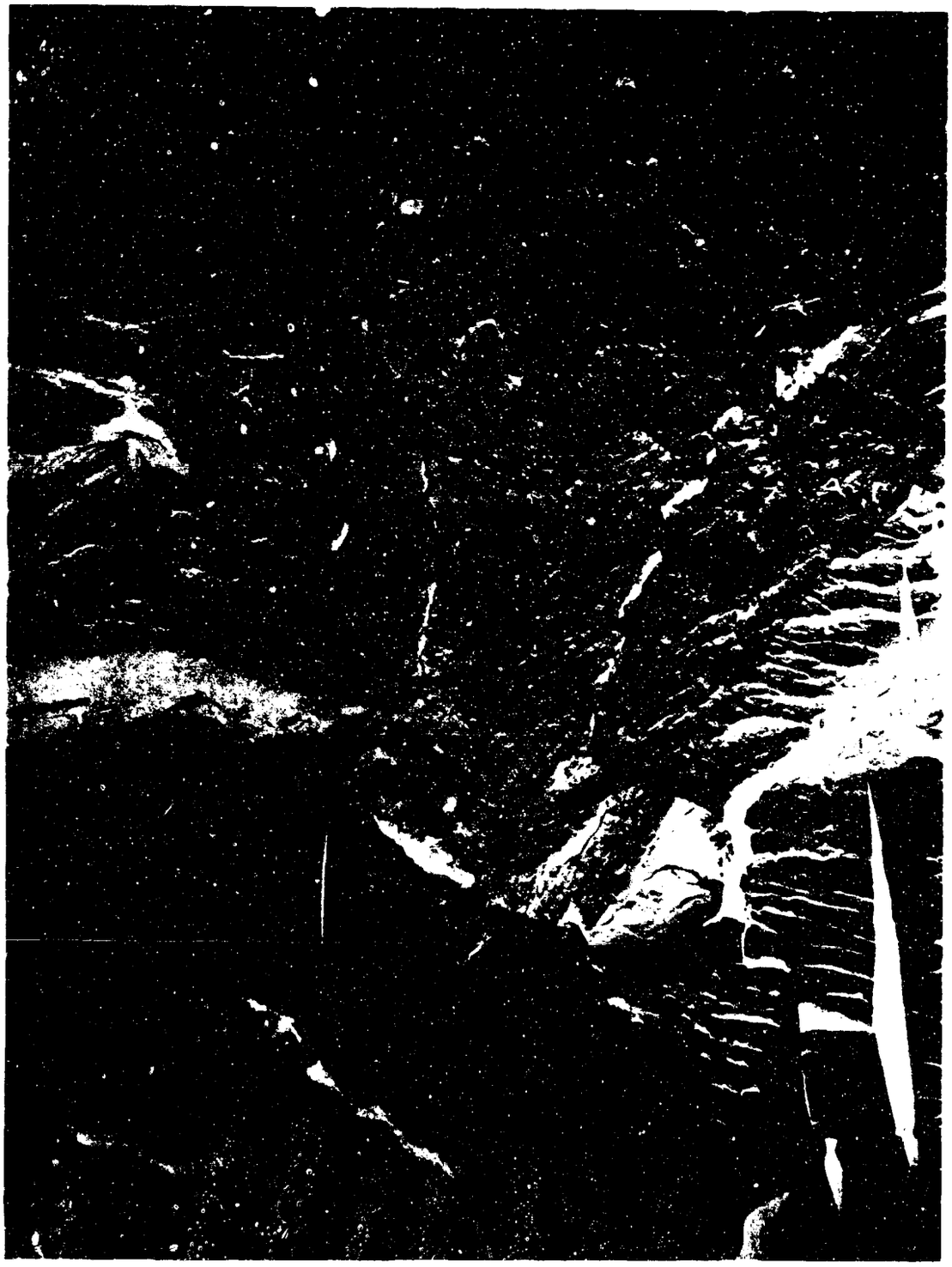

Fig. 35 - Quasi-cleavage facets in fatigued zone of unalloyed titanium (T-17) SEN specimen. Note fatigue striations almost completely surrounding facets. 3000X

Fig. 36 - Cleavage fracture in Ti-8Al-1Mo-1V alloy (T-19) SEN specimen. 3000X

Fig. 37 - Low energy fracture in Ti-6Al-4Zr-2Mo alloy (T-55) SEN specimen. 3000X

investigation discussed in this report describes the low cycle fatigue crack propagation characteristics of these steels in air and in two aqueous environments, simulated boiler water and 3.5% salt water. In addition, approximate correlations between the results of these laboratory tests and the actual vessel fatigue lives are shown.

EXPERIMENTAL

(a) TEST SPECIMEN AND MATERIALS

Plate bend fatigue specimens, Figure 38, were machined from 2-inch thick vessel shell materials of A201B, A302B, and A517F steels. The A201B and A302B steels were normalized and the A517F steel was quenched and tempered. Chemical compositions and tensile properties of these steels are given in Tables 11 and 12, respectively.

(b) APPARATUS AND PROCEDURE

The experimental data reported herein are based on the optically observed macroscopic growth of fatigue cracks across the surface of center-notched plate bend specimens. The specimens are cantilever loaded in full-reverse (tension-to-compression) strain cycling. These procedures are treated in detail in reference 20 and their development and prior application are contained in previous reports in this series.

An engraved center surface notch is placed at the minimum thickness of the test section to assure rapid fatigue crack initiation at relatively low cyclic strain levels. A foil-type resistance strain gage is placed on the test section well ahead of the advancing fatigue crack to monitor nominal surface strains, which are recorded as total strain range values. The progress of the fatigue crack across the test section is observed from directly above through a slide mounted optical micrometer. Extensions at both ends of the crack are monitored and the sum is reported. Automatic deflection control of the test is obtained through micrometer adjusted microswitches which contact the specimen arm at the maximum and minimum points in the loading cycle. Specimens are cycled at a rate of approximately five cycles per minute in a sinusoidal loading pattern.

Based on extensive experience with this test method, it has been found that, in the plate bend specimen, constant total strain range cycling results in a constant value of

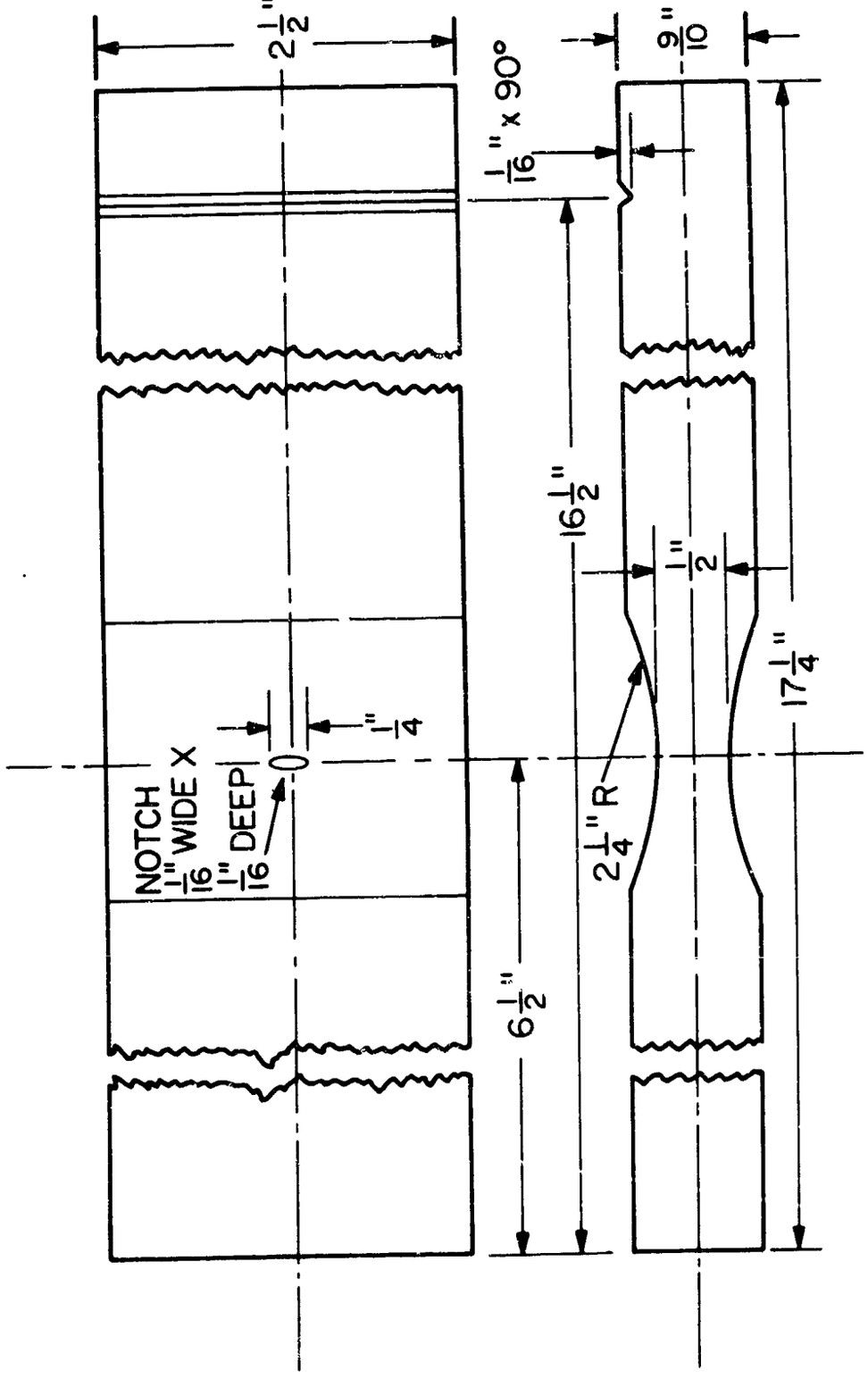

Fig. 38 - Detail of plate bend fatigue specimen

TABLE 11

CHEMICAL COMPOSITIONS OF PRESSURE VESSEL STEELS

Material	Composition (Wt-%)							
	C	Mn	Si	P	S	Ni	Cr	Mo
A201B	0.18	0.65	0.21	0.010	0.024	--	--	--
A302B	0.20	1.42	0.19	0.018	0.022	--	--	0.52
A517F	0.14	0.72	0.22	0.010	0.007	0.78	0.51	0.45

TABLE 12

TENSILE PROPERTIES OF PRESSURE VESSEL STEELS

Material	Yield Strength (ksi)	Tensile Strength (ksi)	Elongation (%)	Reduction in Area (%)
A201B	48.0[1]	67.9[1]	40.0[1]	54.6[1]
A302B	58.1[3]	79.5[3]	26.0[3]	54.5[3]
A517F	107.0[2]	118.0[2]	20.0[2]	64.4[2]

[1] Ref. 16
[2] Ref. 17
[3] Ref. 18

fatigue crack growth rate. For this reason, all tests reported in this paper were conducted under constant total strain range loading. Such loading is obtained by gradually reducing the deflection control limits as the fatigue crack increases in size.

Cycling is begun at the lowest desired strain range and is continued until a fatigue crack is initiated, propagates away from the mechanical notch, and establishes a constant rate of growth. Then the specimen is loaded to the next higher strain range level desired and cycled until the new, higher rate of growth is established. Using this procedure, one specimen can be used to generate several successive datum points. As a general practice, data on a material are first taken in air and then the test procedures are repeated with fresh specimens under the aqueous environments.

The corrosion cell employed in the aqueous environment tests is placed over the portion of the test section containing the fatigue crack. It is made of molded polyurethane which is relatively soft and flexes with the specimen. The aqueous solution is constantly circulated through the corrosion cell from a reservoir by a small electric pump. The solution undergoes filtering and periodic monitoring of its pH value and salt content. A glass cover at the top of the corrosion cell permits optical observation of the fatigue crack. Periodic removal of tarnish or rust from the test surface is required to maintain good visibility of the crack.

Wet fatigue studies were conducted with two environments, simulated boiler water and 3.5% salt water. The simulated boiler water is the same composition used for internal pressurization of the PVRC full-size pressure vessels during fatigue testing. Therefore, its effect on the fatigue performance of the three pressure vessel materials discussed in this paper is of special interest.

The chemical composition and preparation procedure of the simulated boiler water is as follows: 4.0 grams of sodium hydroxide (NaOH), 7.6 grams of sodium sulfite (Na_2SO_3), and 0.09 grams of copper sulfate ($CuSO_4$ $5H_20$) were each dissolved separately into two liters of distilled water, forming three solutions. Fifty ml from each of these three solutions was then added to one liter of distilled water to produce the final mixture. A pH value of 10.5 to 11.0 is obtained from this mixture. Tannin was included in the PVRC simulated

boiler water but was eliminated from the NRL solution because it interfered with optical observation of the fatigue crack.

RESULTS AND DISCUSSION

(a) FATIGUE CRACK PROPAGATION IN AIR

Fatigue crack growth rate data from the air environment tests are plotted versus total strain range on log-log coordinates in Fig. 39. The data for A201B and A302B steels fall on a common third power (3:1) curve and the data for A517F steel fall on a fourth power (4:1) curve. The equations between fatigue crack growth rate and total strain range which are established by these plots have the form

$$\frac{d(2a)}{dN} = c(\epsilon_T)^m$$

where $\frac{d(2a)}{dN}$ is the fatigue crack growth rate, ϵ_T is the total strain range, m is a numerical exponent (slope), and c is a numerical constant (intercept). These fatigue crack growth rate versus total strain range plots provide baseline relationships that illustrate the intrinsic resistance of these materials to the growth of fatigue cracks. This information is used for comparing the fatigue crack propagation characteristics of materials, determining the effects of aqueous environments on fatigue crack propagation and estimating structural fatigue life.

Consider first the sensitivity of the three steels to cyclic strain. The data in Fig. 39 indicate that, on a strain range basis for load intensity, the two normalized steels A201B and A302B display very similar low cycle fatigue crack propagation characteristics. The quenched and tempered A517F steel displays distinctly different characteristics. Previous testing experience suggests that the locus of the data on Fig. 39 for the normalized steels is not shared by any other material, i.e., no relationships with slopes as low as three have been observed among a wide variety of ferrous and nonferrous metals previously tested by these methods. However, the locus of the data for the quenched and tempered steel is very close to that of other high strength, quenched and tempered steels such as HY-80 and 5Ni-Cr-Mo-V (20-24).

A second comparative perspective is shown in Fig. 40. This is a summary log-log plot of the air environment fatigue

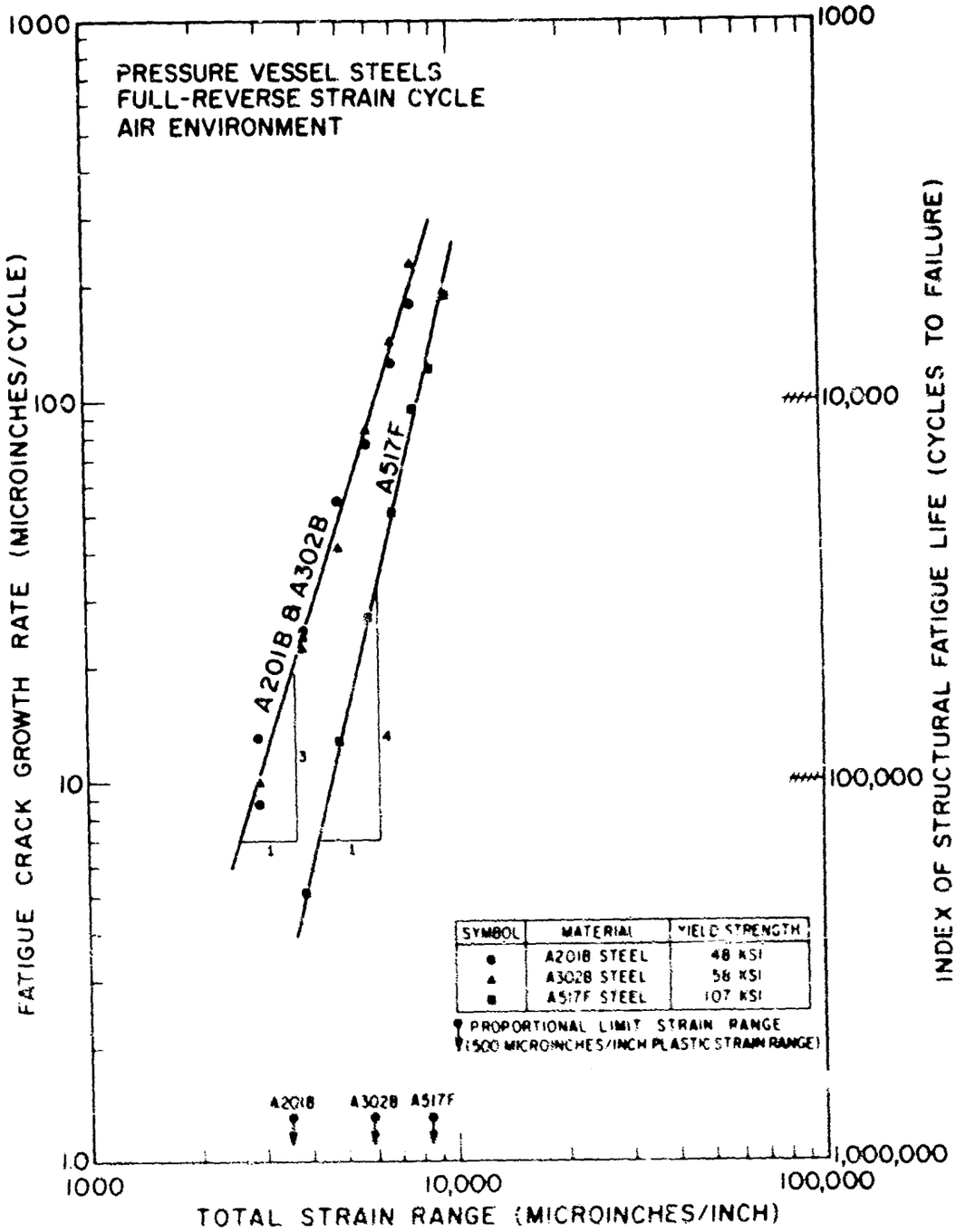

Fig. 39 - Log-log plot of fatigue crack growth rate versus total strain range for A201B, A302B, and A517F steels in an ambient air environment. The Index of Structural Fatigue Life is indicated along the right-hand ordinate.

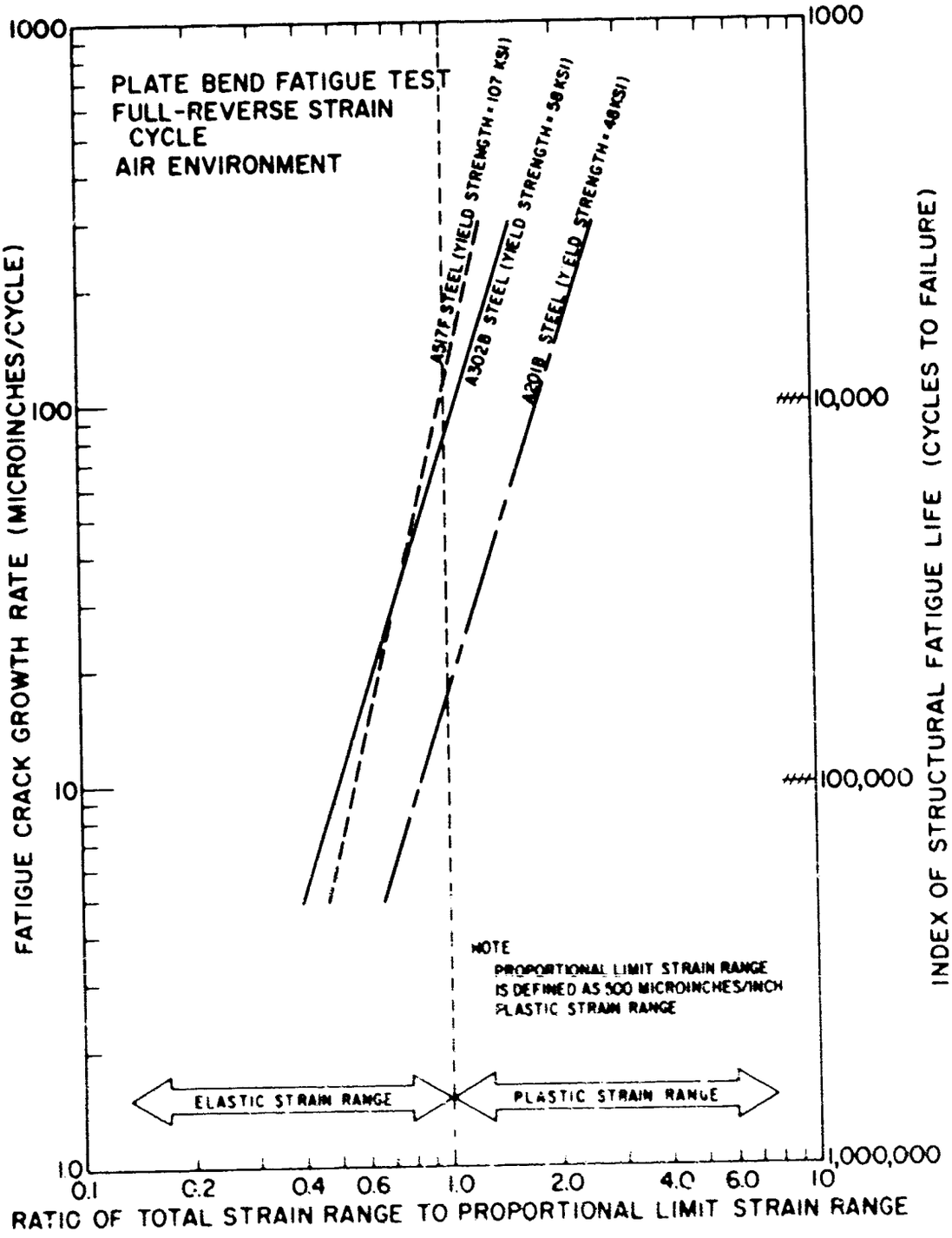

Fig. 40 - Air environment low cycle fatigue crack propagation characteristics of A201B, A302B, and A517F steels on a normalized load intensity basis

crack growth rate versus the ratio of total strain range to proportional limit strain range for the three steels considered in this report. The proportional limit of each steel in the plate bend specimen configuration is indicated on the total strain range axis of Fig. 39. Using this reference point, a normalized load intensity factor is obtained on Fig. 40 which is comparable to yield strength loading at a factor value of unity.

Looking at Fig. 40. it can be seen that when fatigue crack growth rates for the three steels are compared on this normalized load intensity basis, a different order appears than what is suggested by the curves in Fig. 39.

Significant differences exist among these materials with regard to the rate of fatigue crack propagation at total strain range levels which are in fixed relation to the proportional limit strain range. On this basis, it can be seen that A201B propagates fatigue cracks less rapidly than either A302B or A517F, which display similar characteristics in this respect By the same reasoning it can be shown that A201B possesses a greater tolerance for plastic strain under cyclic loading than either A302B or A517F. For example, Fig. 40 shows that at a total strain range equal to the proportional limit in each material, fatigue cracks propagate approximately four times faster in A302B than in A201B and five times faster in A517F. The higher fatigue crack growth rate in the steels with higher yield strength are more largely due to increased loading (strain range) rather than to a decrease in the intrinsic resistance to the growth of fatigue cracks.

This discussion should not be interpreted as a condemnation of higher strength materials. On the contrary, it merely points out little understood but important differences in the fatigue crack propagation characteristics of metals at various strength levels and provides a guide for their safe use in high performance structures. Since structural design and fabrication processes can alter the relative merit of a specific material, these aspects, as perceived from the PVRC full-size pressure vessel tests, will receive further consideration in a later section of this report.

(b) FATIGUE CRACK PROPAGATION IN AQUEOUS ENVIRONMENTS

The results of the fatigue crack propagation tests conducted in the two aqueous environments, simulated boiler water

and 3.5% salt water, are shown in Figs. 41 through 44. These figures are log-log plots of fatigue crack growth rate versus total strain range. In each case the air environment plot for the corresponding material is indicated by the dashed line. The effect of the aqueous environment is illustrated by the vertical displacement of the aqueous environment data to higher crack growth rates than were observed in air environment tests at corresponding values of total strain range. For convenience, data for the A201B and A302B steels are plotted on common curves, Figs. 41 and 42, and the A517F data are plotted separately, Figs. 43 and 44.

As might be expected, fatigue crack propagation in each of the three steels was generally adversely affected by the presence of an aqueous environment. Exceptions to this trend occurred at low total strain range levels in the A201B and A302B steels, where the environment appeared to have little or no effect. All three steels were affected more severely by the 3.5% salt water than by the simulated boiler water.

Generally, the effect of the aqueous environments increased in proportion to the total strain range level. The salt water environment data for all three steels show such abrupt transitions as to suggest the existence of a threshold level of cyclic strain below which the materials are relatively insensitive to the environment, in a manner similar to the K_{Iscc} concept for stress-corrosion-cracking (12). Also the salt water environment data for each of the three steels appeared to indicate a maximum environmental affect in the mid-range of total strain range values, with the environmental effects diminishing somewhat at peak total strain range levels. However, these tests were conducted under 5 cycle per minute sinusoidal loading with no hold period at maximum load. Therefore, loading rate effects may be reflected in these data and this must be considered when the information is applied to full-size structural situations involving slower rates of cycling.

inally, experience suggests that an order of magnitude increase in fatigue crack growth rates due to the introduction of an aqueous environment provides a first-order benchmark for judging the performance of structural materials. Most high strength structural steels exceed this benchmark and some ultrahigh strength steels grossly exceed it (21). Looking again at Figs. 41 through 44, it can be seen that the maximum

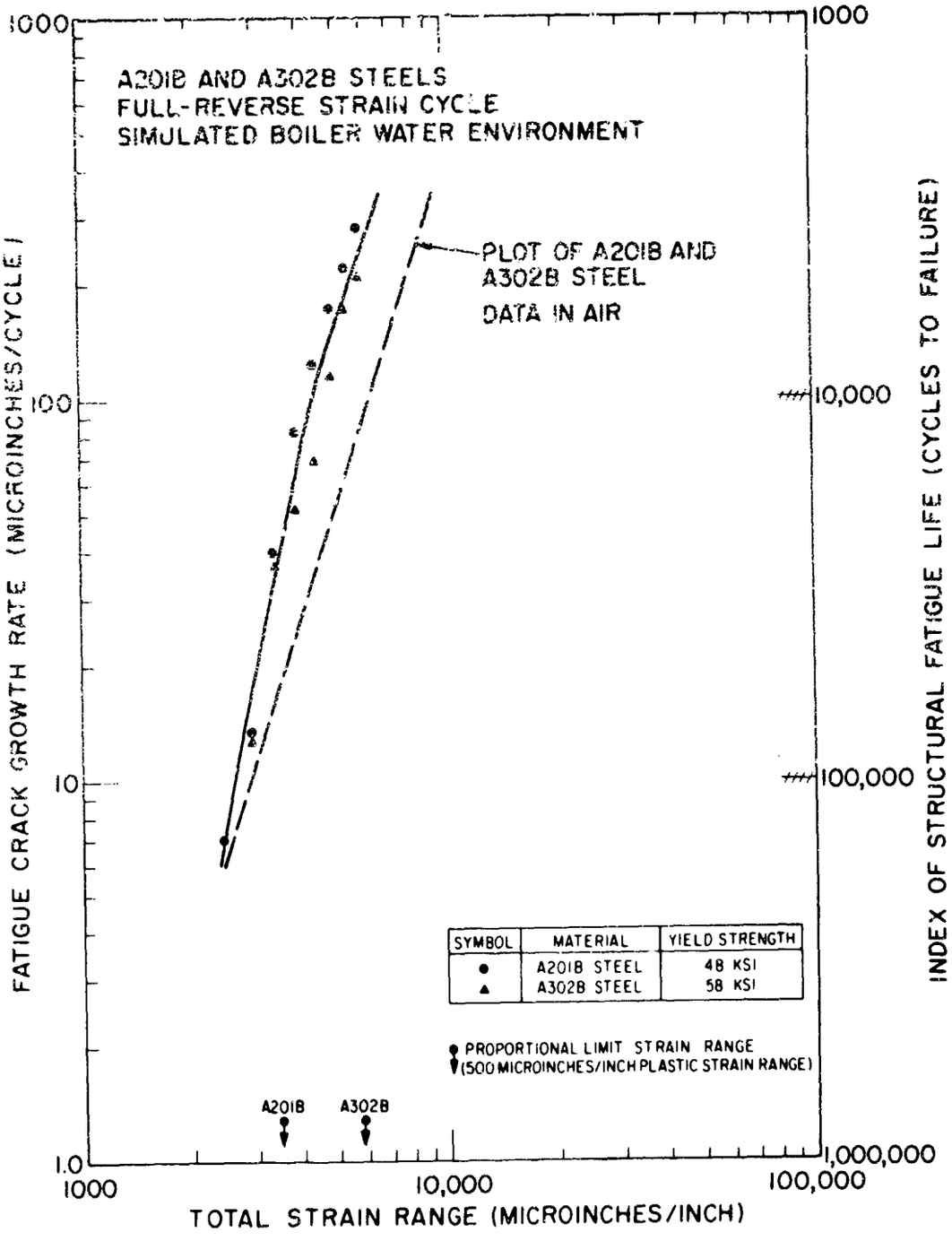

Fig. 41 - Log-log plot of fatigue crack growth rate versus total strain range for A201B and A302B steels in a simulated boiler water environment

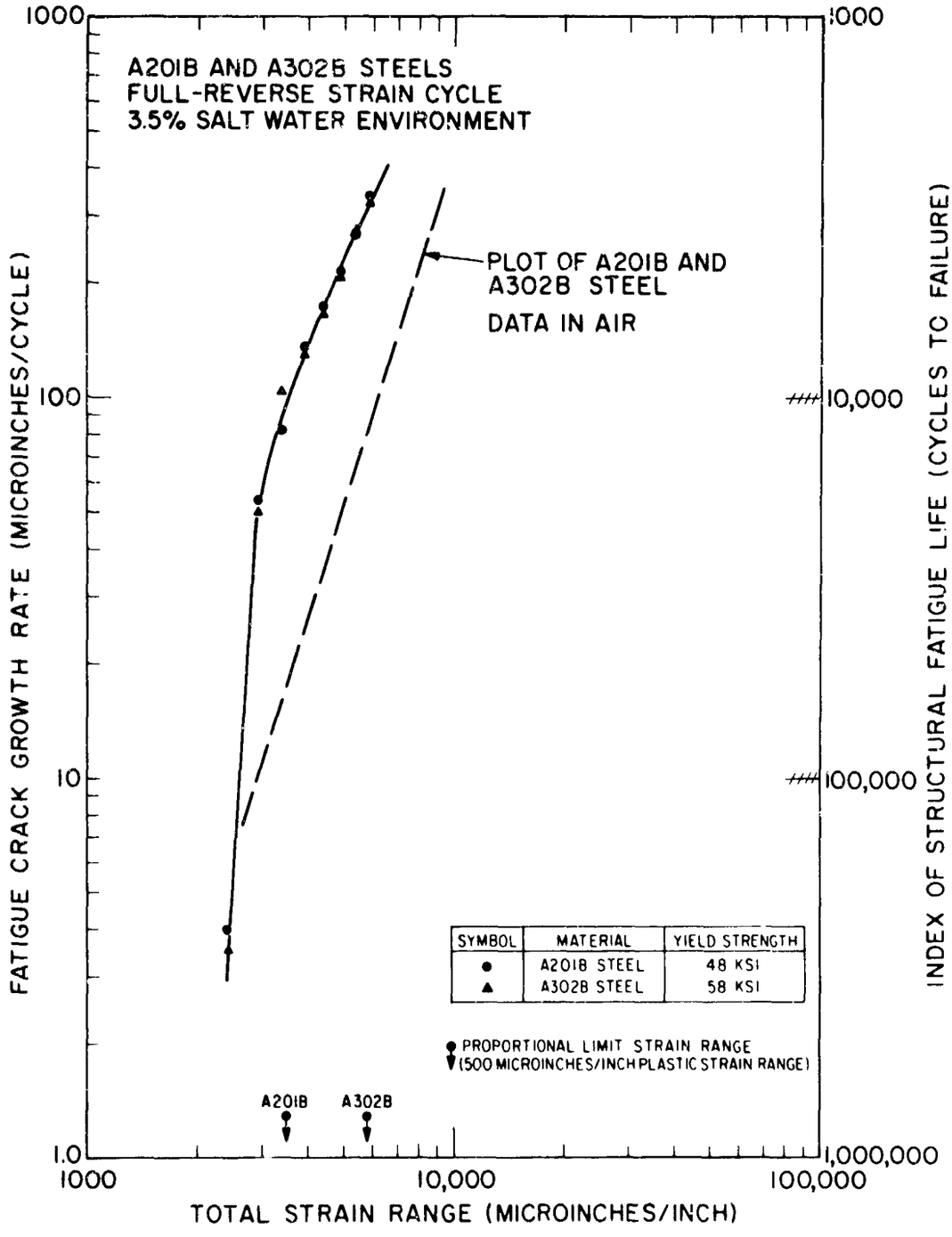

Fig. 42 - Log-log plot of fatigue crack growth rate versus total strain range for A201B and A302B steels in a 3.5% salt water environment

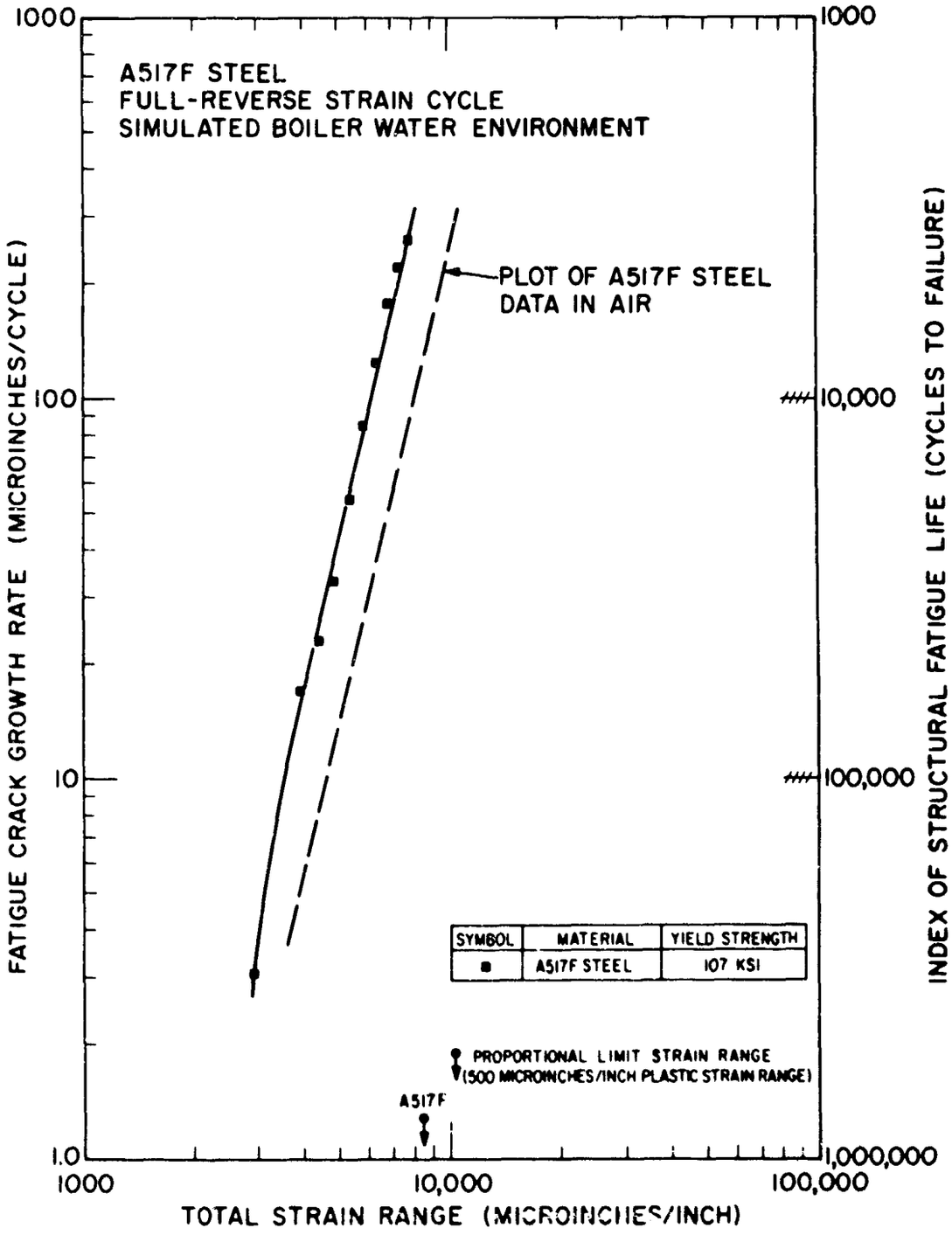

Fig. 43 - Log-log plot of fatigue crack growth rate versus total strain range for A517F steel in simulated boiler water environment

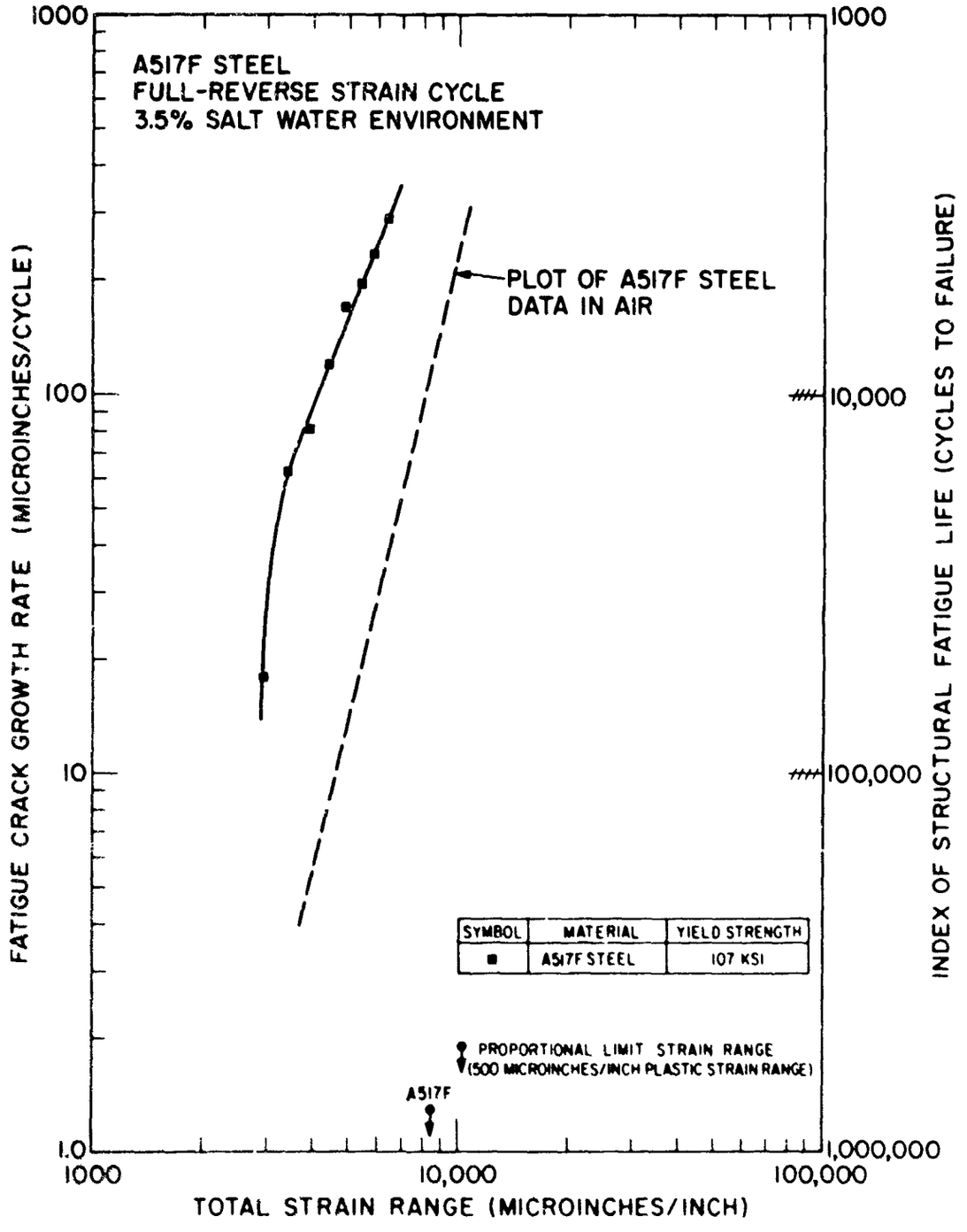

Fig. 44 - Log-log plot of fatigue crack growth rate versus total strain range for A517F steel in a 3.5% salt water environment

increase in fatigue crack growth rates due to the aqueous environments in the A201B and A302B steels lie well within an order of magnitude for the simulated boiler water and the 3.5% salt water environments. The A517F steel data exceed an order of magnitude increase in the salt water environment but fall well below this increase in the simulated boiler water environment.

(c) COMPARISONS WITH FULL-SIZE VESSEL TEST RESULTS

The results of this investigation present a rare opportunity to compare laboratory fatigue crack propagation data with full-size structural tests. Low cycle fatigue crack propagation is gaining recognition as a critical failure mode in cyclically-loaded large welded structures. In particular, there is general agreement that fatigue crack propagation was the dominant fatigue failure mode in the PVRC vessels. However, scant data are available to enable the establishment of proper criteria for designing against this mode of failure. As a first step toward this goal, the authors have proposed the Index of Structural Fatigue Life as an initial attempt to correlate the effects of cyclic strain, mean strain, and aqueous environments with the fatigue life of structures (20).

The Index of Structural Fatigue Life is defined as the number of cycles of repeated load required to propagate a small subcritical flaw to 1-inch length at a given intensity of loading, as measured by the total strain range, in the plate bend fatigue test. This Index is shown along the right hand ordinate of each data plot, Figs. 39 through 44. Although it is an arbitrary failure criterion, it serves as a helpful means of translating crack growth rate data into a more commonly recognized form of fatigue data.

Figure 45 shows a log-log plot of total strain range versus cycles to failure for the PVRC vessels (19). Three data symbols are indicated for each of the six vessels: the actual vessel failure based on the measured or estimated total strain range at the failure location, a predicted failure point based on the Index of Structural Fatigue Life for the vessel shell material in a simulated boiler water environment, and a predicted failure point based on the Index of Structural Fatigue Life for the vessel shell material in an air environment with a correction for the effect of mean strain. The mean strain correction consisted simply of taking the fatigue crack growth rate for full-reverse strain cycling, Fig. 39, and multiplying it by a

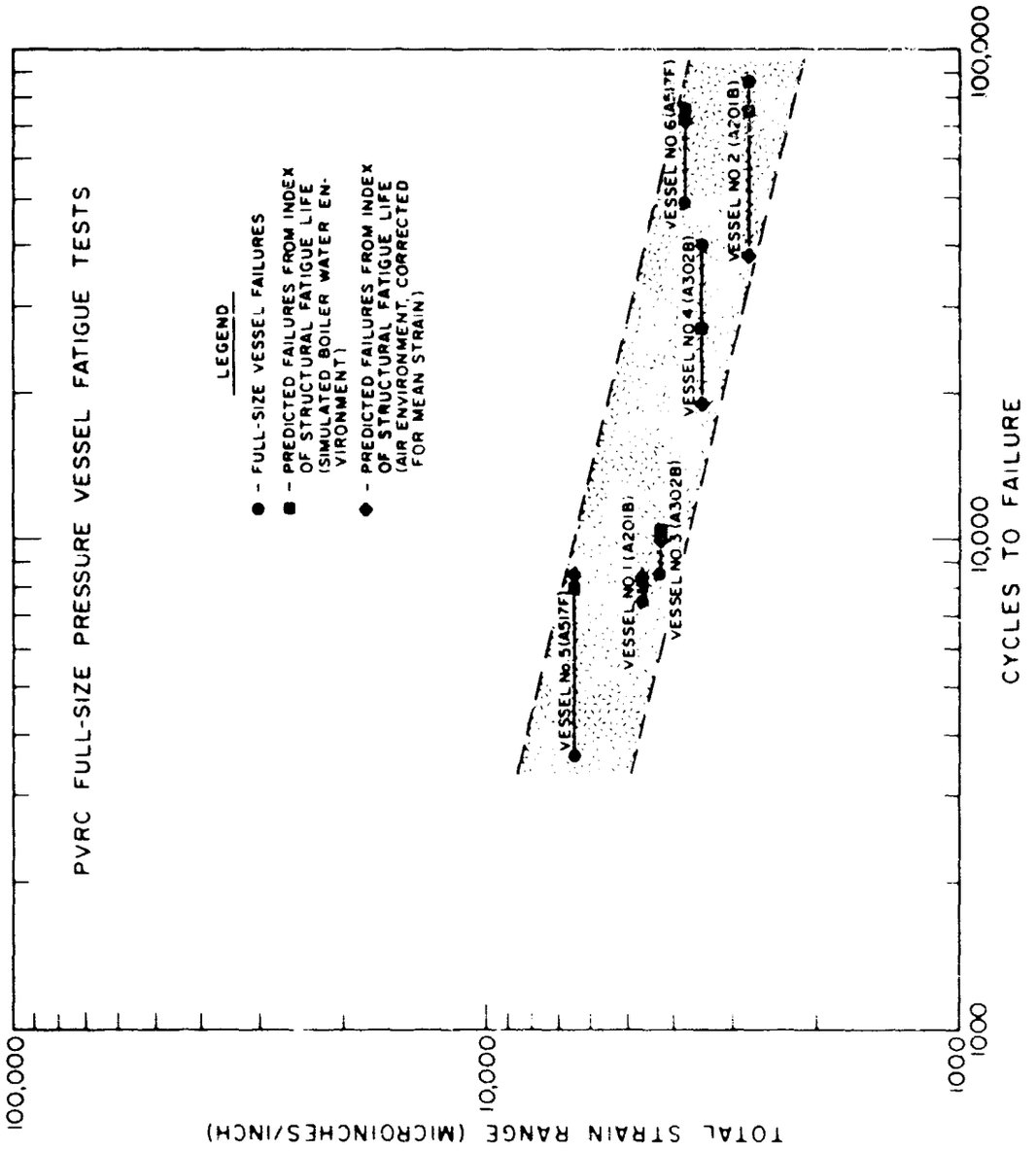

Fig. 45 - Log-log plot of total strain range versus cycles to failure for the PVRC full-size pressure vessel test results. Actual failure points plus failure predictions based on the Index of Structural Fatigue Life are indicated.

factor of three to obtain the approximate Index of Structural Fatigue Life value. Laboratory investigations have shown that a threefold increase in fatigue crack growth rates is the minimum affect of mean strain on structural steels cycled to strain amplitudes near or into the plastic strain range (20, 22).

The comparison of actual failures versus laboratory predictions is rather encouraging for an initial effort. The predictions for vessels 1 (A201B) and 3 (A302), which failed in the cyclic life span between 7000 and 9000 cycles, agreed very closely with the actual life to failure. For vessels 2 (A201B) and 4 (A302B), which failed in the life span between 40,000 and 90,000 cycles, the predictions were conservative. The closest agreement for vessels 2 and 4 came from predictions based on the simulated boiler water environment.

The opposite relationship between predicted and actual failure points was seen for vessels 5 and 6 which were made of A517F steel. Actual cyclic life to failure in these vessels fell well below the predicted failure points. For the A517F steel, the predicted fatigue lives for each of the two criteria considered, simulated boiler water environment or air environment corrected for mean strain were identical.

Based on fatigue life at a specific total strain range, the largest factor separating actual and predicted failures was 2.4. Considering the inexactness of fatigue testing in general and specifically the fatigue testing of large welded structures, this represents a good first approximation. Further experimentation and refinements upon the crack propagation approach to fatigue failure would seem to offer a more realistic method of predicting failures for the "worst case," i.e., the case of the large welded structure which contains undetected sharp flaws which preclude a structural life period for crack initiation.

An additional aspect of the fatigue life data in fig. 45 illustrates a potential advantage in the use of higher strength materials. Vessels 1, 3, and 6 were constructed to identical dimensions and cycled at the same maximum internal pressurization (4400 psig). However, vessel 1 was made of A201B steel, vessel 3 was made of A302B steel, and vessel 6 was made of A517F steel having yield strengths of 48, 58, and 107 ksi respectively. Referring back to Fig. 45, we see that with

higher yield strength, plastic strains were minimized. Consequently, a smaller total strain range existed at the constant value of internal pressure, resulting in longer fatigue life. Specific life values were 7,516; 8,500 and 19,272 cycles for the A201B, A302B and the A517F vessels respectively. This series of experiments serves to illustrate one manner in which the potential advantages of higher strength materials can be exploited while minimizing the potential disadvantages of such materials. The interaction of the material, structural, and environmental parameters are highly complex. Additional precise structural tests are required to develop a comprehensive fatigue life model incorporating all of the parameters affecting the growth rate of fatigue cracks including mean strain, stress state, and effect of flaw size on strain range.

SUMMARY AND CONCLUSIONS

Low cycle fatigue crack propagation studies were conducted on A201B, A302B, and A517F pressure vessel steels in ambient air and in two aqueous environments, simulated boiler water and 3.5% salt water. The study employed plate bend fatigue specimens which had been machined from the shell materials of full-size pressure vessels. The vessels had previously undergone fatigue testing under the auspices of the Pressure Vessel Research Committee. Empirical correlations were made between the fatigue crack growth rate and total strain range. These data were then compared to the fatigue life of the six PVRC vessels.

The following conclusions have been reached from this study:

1. Fatigue crack growth rates in A201B and A302B steels in an air environment follow a common third power relationship with total strain range. For A517F steel in an air environment a fourth power relationship with total strain range was observed. The locus of the relationship for A201B and A302B is unique among structural steels tested to date; whereas the relationship for A517F is very similar to that observed for other high strength, quenched and tempered steels such as HY-80 and 5Ni-Cr-Mo-V.

2. Comparisons of fatigue crack propagation characteristics among the three steels tested, based on total strain range units normalized with respect to the respective proportional

limits, indicate that A201B possesses the greatest tolerance for cyclic plastic strain. A302B and A517F exhibit similar behavior in this regard. At a total strain range equal to the proportional limit in each material, fatigue cracks propagate approximately four times faster in A302B than in A201B and five times faster in A517F.

3. Fatigue crack propagation in all three steels was adversely affected by the presence of an aqueous environment. The 3.5% salt water environment proved to be more severe than the simulated boiler water environment. Generally A517F was more sensitive to environment than A201B or A302B, although none of the three steels exhibited a gross degradation in fatigue properties due to an aqueous environment.

4. Comparisons between an Index of Structural Fatigue Life based on these fatigue crack propagation data and results of the PVRC full-size vessel tests are reasonably close for the A201B and A302B steels. Less satisfactory agreement was found for the A517F steel in that the predicted values were not conservative.

CORRELATION OF TWO FRACTURE TOUGHNESS TESTS FOR HIGH-STRENGTH STEELS

(C. N. Freed)

Linear elastic fracture mechanics allows measurement of the rate at which strain energy is released upon crack extension from a sharp flaw or fatigue crack. The stress intensity factor, K_{Ic}, which may be calculated is a property of the material. As the test is based upon the assumption that plane strain exists in the center of the specimen, the material to be tested can not possess high toughness, i.e., it must fracture under conditions of elastic loading. The chief advantage of this fracture toughness is that K_{Ic} is a function of the length of the crack and of the stress acting upon the crack; thus, if any two of these values are known, the third may be calculated.

A preliminary correlation has been developed between the two fracture toughness parameters, K_{Ic} and DWTT, for a variety of steel alloys. This correlation permits predictions to be made of the expected range of K_{Ic} from drop-weight tear test (DWTT) energy values and reasonable estimates of flaw size and stress level for steels in which a crack will propagate without gross plastic deformation.

MATERIALS AND PROCEDURE

The steel alloys which were investigated include 12- and 18-Ni maraging steels, 9-4-0.25 (Ni-Co-C) quenched-and-tempered, 4140, D6-AC, and 5Ni-Cr-Mo-V steel. (Table I) About one-half of the specimens were tested in the "as-received" mill condition while the remainder were heat treated at NRL as part of a program headed by Dr. P. Puzak. The specific mill processing and NRL heat-treatments have been reported in previous Quarterly Reports (5, 24, 25) The mechanical properties presented in Table 13 are also due to Dr. Puzak.

The single-edge-notched specimen (SEN) was used to determine the K_{Ic} values reported in Table 14. The dimensions of this specimen are similar to those reported in the Seventh Quarterly Report (25). In both the DWTT and the K_{Ic} investigations, the specimens were approximately one-inch thick (except J-79); this usually represented the full-plate thickness although in several cases the specimens were cut from 2-in.-thick plate. Many of the K_{Ic} specimens were side-grooved to a depth of 5 percent of the thickness on each side. A fatigue crack of 0.10 in. was formed at the tip of the edge notch.

Load-displacement graphs for each K_{Ic} specimen were drawn by an X-Y recorder. When initial deviation from linearity occurred at or very near maximum load, this value was used to calculate K_{Ic}; otherwise, the load at the lowest, distinct instability was chosen for the calculation. The detection of the load instability was made with a beam displacement gage instrumented with a strain gage circuit. A plastic zone correction (one iteration) was included in the determination of K_{Ic}; however, Table 14 also indicates the K_{Ic} value before inclusion of the plastic zone correction.

ANALYSIS OF DATA

In Fig. 46, K_{Ic} is plotted against yield strength (YS). The graph indicates that an inverse relationship exists between K_{Ic} fracture toughness and YS for high strength steels. It is evident that a wide range of K_{Ic} values can exist at a given YS for various alloy steels and heat treatments. The fracture direction is indicated as RW (horizontal lines) and WR (vertical lines) according to ref. 14. Each point represents an average

TABLE 13

MECHANICAL PROPERTIES OF HIGH-STRENGTH STEELS

Alloy Designation	Fracture Direction	Material Type	Tension Test Data 0.2%YS (ksi)	UTS (ksi)	Elong. in 2 in. (%)	RA (%)	Charpy V at 30°F (ft-lb)	Drop Weight Tear Energy at 30°F (ft-lb)
J-14	RW	9-4-0 25C	180.0	198.2	61.0	16.8	38	1644
J-14	WR	Mill heat treated straight rolled	180.3	196.4	48.0	15.0	30	1295
J-15	RW	9-4-0 25C	--	--	--	--	38	1996
J-15	WR	Mill heat treated 1 x 1 cross roll	183.2	195.0	61.0	17.0	40	2000
J-66	RW	12-Ni Mill heat treated	--	--	--	--	29	--
J-66	WR	12-Ni Mill heat treated	185.3	188.0	56.7	13.8	32	--
J-66	WR	12-Ni NRL heat treated	176.3	179.9	52.1	13.5	28	--
J-67	RW	12-Ni Mill Heat treated	178.6	182.3	57.2	15.0	34	--
J-67	WR	12-Ni Mill Heat treated	--	--	--	--	31	--
J-67	WR	12-Ni NRL Heat treated	178.0	181.9	54.9	14.0	40	--
J-68	WR	12-Ni Mill Heat treated	171.2	177.2	49.1	14.0	21	744
J-68	WR	12-Ni NRL Heat treated	180.7	183.5	51.9	12.0	36	1630
J-70	WR	9-4-0 25 Mill Heat treated	176.3	186.6	55.2	16.0	40	2112
J-70	WR	9-4-0 25 NRL Heat treated	186.1	198.0	55.2	18.0	36	1280
J-71	WR	12-Ni Mill Heat treated	176.8	183.2	59.6	14.5	42	--
J-71	WR	12-Ni NRL Heat treated	174.9	179.2	64.1	15.0	74	4340
J-72	WR	12-Ni Mill Heat treated	177.3	183.3	59.2	14.5	47	3251
J-72	WR	12-Ni NRL Heat treated	177.1	180.2	63.4	16.0	65	3538
J-78	WR	12-Ni Mill Heat treated	185.5	188.7	59.7	14.0	41	2271
J-78	WR	12-Ni NRL Heat treated	189.4	192.2	54.6	12.5	44	2176
J-87	WR	9-4-0 25 Mill Heat treated	179.2	189.4	64.5	17.0	39	1996
J-87	WR	9-4-0 25 NRL Heat treated	169.7	178.5	51.4	16.5	42	2026
J-88	WR	9-4-0 25 Mill Heat treated	180.2	191.3	54.1	16.0	42	1692
J-88	WR	9-4-0 25 NRL Heat treated	186.3	178.6	61.4	18.0	62	2.
H-57	WR	4140 NRL Heat treated	176.6	194.8	32.6	9.5	4	493
D-63A	RW	18 Ni Mill Heat treated	229.5	240.3	9.0	45.9	24	400-500
D-63B	RW	18 Ni Mill Heat treated	214.5	245.7*	7.0*	29.2*	--	400-500
D-63C		NRL Heat treated	212	229	12.0	44.6	20	--
J-79 .2 (Ni-Al)	WR	5 Ni Mill Heat treated	144	150	65.0	19.0	92	--

These values are for the RW fracture direction.

These values represent the WR fracture direction.

TABLE 14

PLANE-STRAIN FRACTURE TOUGHNESS DATA FOR HIGH-STRENGTH STEELS

Alloy Designation	Fracture Direction	YS (ksi)	DWTT Energy at 30°F (ft-lb)	No. Specimens	K_{Ic} [1] Range (ksi$\sqrt{in}$)	Avg. K_{Ic} (ksi$\sqrt{in}$)	Avg.[1] β_{Ic}	Young's Modulus (ksi)	Avg.[1] G_{Ic} (in-lb/in^2)	Nominal Stress to Yield Stress σ_n/σ_y	Avg.* K_{Ic} (ksi$\sqrt{in}$)
J 14	RW	180.0	1844	2	158-165	162	0.80	28.6	919	0.76	158
J 14	WR	180.3	1295	2	137-138	138	0.56	28.6	657	0.65	135
J-15	RW	--	1996	2	155-156	156	0.73	28.6	854	0.72	151
J-15	WR	183.2	2000	2	152-155	154	0.69	28.6	832	0.72	149
J-66	RW	--	--	1	166	166	0.80	27.5	1000	0.87	161
J-66	WR	185.3	--	2	116-124	120	0.40	27.5	524	0.58	118
J-66	WR	176.3	--	3	131-143	137	0.57	27.5	684	0.67	134
J-67	RW	178.6	--	1	153	153	0.71	27.5	852	0.74	148
J-67	WR	--	--	2	119-130	125	0.46	27.5	568	0.57	124
J-67	WR	178.0	--	3	131-137	135	0.55	27.5	666	0.68	132
J-68	WR	171.2	744	2	100	100	0.36	27.5	364	0.54	98
J-68	WR	180.7	1630	2	125-126	126	0.50	27.5	580	0.64	123
J-70	WR	176.3	2112	3	163-166	164	0.80	28.6	945	0.83	160
J-70	WR	186.1	1200	4	150-156	153	0.69	28.6	822	0.77	149
J-71	WR	176.8	--	3	198-206	203	1.22	27.5	1503	1.0	192
J-71	WR	174.9	4340	1	(252)	(252)	(1.93)	27.5	(2310)	1.2	(235)
J-72	WR	177.3	3251	3	201-213	208	1.33	27.5	1580	1.0	197
J-72	WR	177.1	3538	1	211	211	1.35	27.5	1620	1.0	200
J-78	WR	185.5	2271	1	155	155	0.70	27.5	873	0.72	150
J-78	WR	189.4	2176	2	184-192	188	1.00	27.5	1285	0.89	182
J-87	WR	179.2	1996	2	158-169	163	0.83	28.6	930	0.63	158
J-87	WR	169.7	2026	3	167-175	171	1.05	28.6	1020	0.94	165
J-88	WR	180.2	1692	3	159-166	163	0.82	28.6	930	0.62	158
J-88	WR	168.3	2186	3	164-176	169	1.04	28.6	1000	0.94	161
H-57	WR	176.6	593	3	89-91	90	0.26	29.5	274	0.48	88
D-63A	RW	229.5	400-500	1	70	70	0.09	27.0	176	0.34	69
D-63B	RW	231.5	400-500	2	75-79	77	0.11	27.0	215	0.37	76
D6AC	--	212[2]	--	1	96	96	0.10	--	--	--	95
J-79	WR	144	--	2	252	252	1.31	29.5	2150	1.40	233

[1] Plastic zone correction included in calculation.

[2] This value represents WR fracture direction.

* Calculated without plastic zone correction factor.

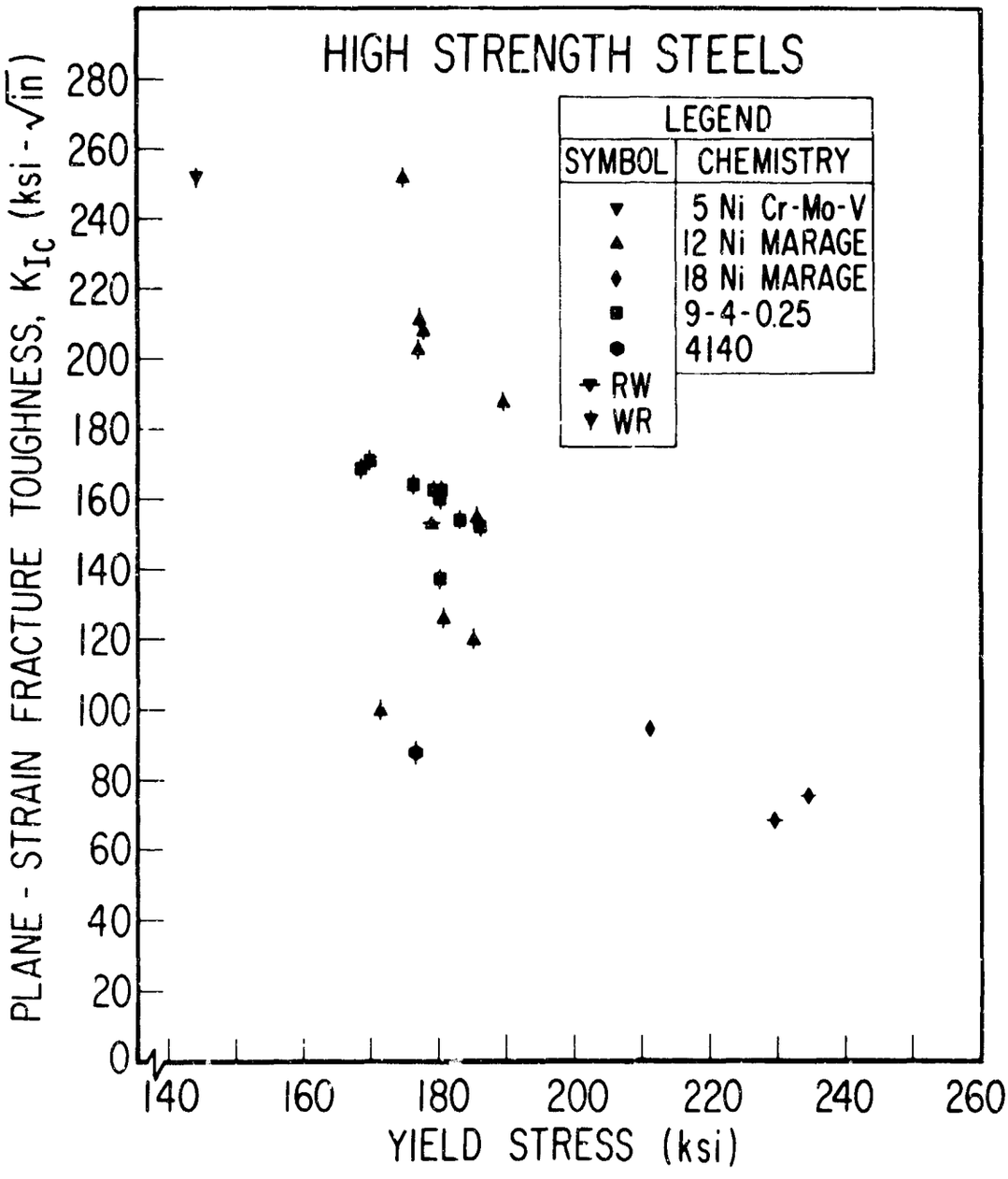

Fig. 46 - K_{Ic} plotted against yield strength for a variety of high strength steels

of the K_{Ic} values obtained from that particular alloy and heat treatment.

The plot of K_{Ic} versus DWTT energy is found in Figure 47. Although some scatter is present, it is evident that a direct correlation exists; an increase in K_{Ic} values corresponds directly with an increase in DWTT energy. The vertical line drawn at 3500 ft-lb on the DWTT energy scale represents the approximate value at which the fracture surface of the DWTT specimen becomes 100 percent slant fracture. The line serves a second purpose in that at this point the nominal-to-yield-stress ratio in the K_{Ic} test approaches 1.0. Beyond this value, the crack may be extending under conditions of gross yielding rather than by linear elastic fracture mechanics.

There are several factors which might affect the accuracy of this preliminary correlation. Since K_{Ic} is a function of strain rate, the high rate of applied strain in the DWTT may cause the specimen to fracture with a lower toughness indication than would be expected if the strain rates of the two tests were similar. However, as the steels tested are relatively insensitive to strain rate effects, this factor should not be too significant.

An energy loss is inherent in the fracture of the brittle, crack-starting weld. Although the loss is small, it might be a significant portion of the recorded energy of the most brittle DWTT specimens. It would be expected that this factor should cause the curve to intersect the abscissa at some finite value of DWTT energy rather than zero DWTT energy. This may be demonstrated when more data are obtained.

A third and perhaps most important point is that as the crack tears through the DWTT specimen, it may initially be governed by a plane strain state of stresses but in the tougher materials it will propagate primarily under mixed mode conditions. The mixed mode is probably caused by the lateral expansion of the crack at the same time that it moves forward. The lateral movement would effectively decrease the constraint around the crack tip and cause the stress intensity factor to rise since plane-strain conditions no longer exist. Thus, the plastic zone would increase in this region of mixed mode fracture, and this would eventually produce surface relaxation evidenced by shear lips. The result is that the energy measured in the DWTT would, for tough materials, represent mixed mode while the stress intensity

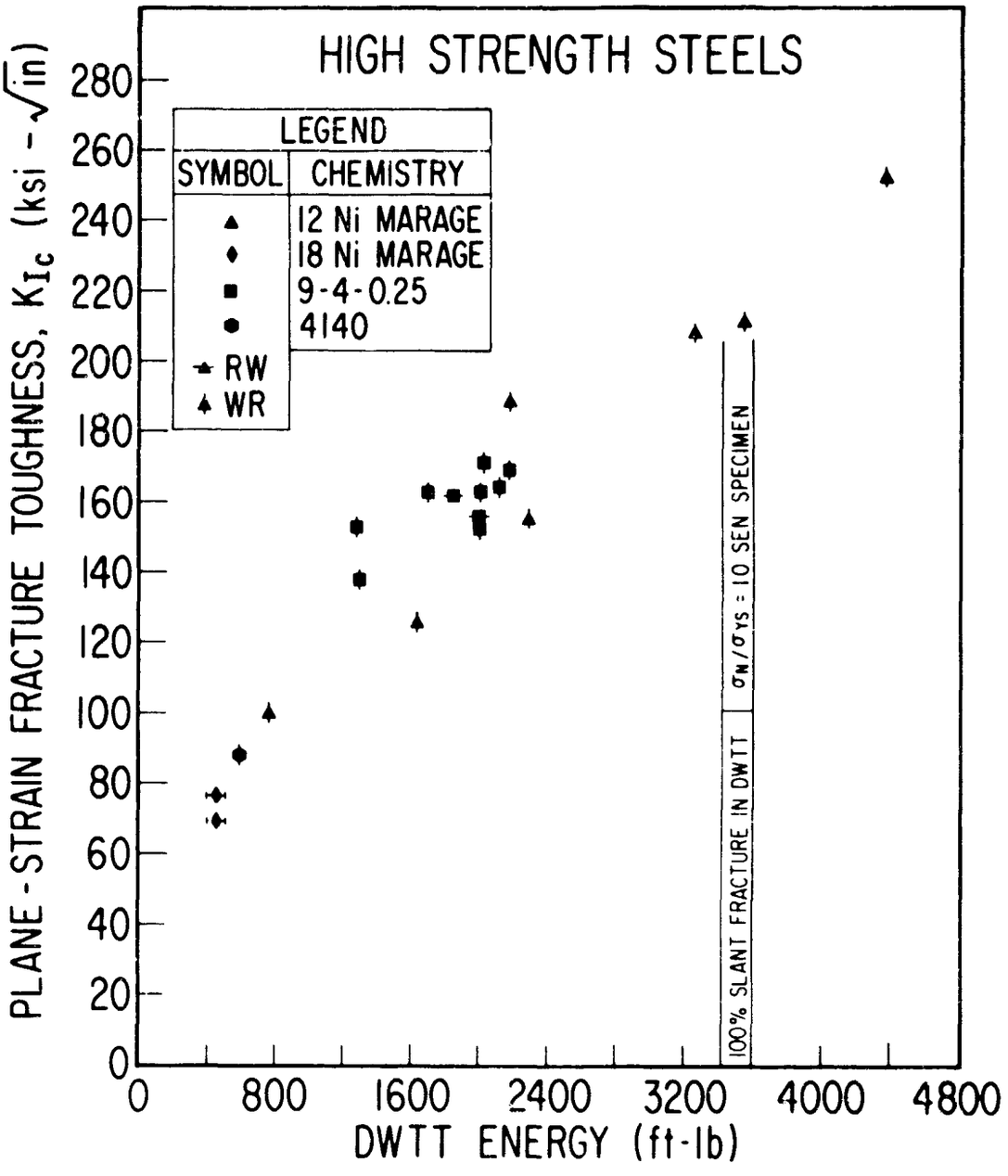

Fig. 47 - Preliminary correlation of K_{Ic} with drop-weight tear test energy

factor determined in the K_{Ic} test would apply to plane-strain conditions. This discrepancy may result in an increase of the correlation scatter at higher DWTT energy values.

The DWTT energy is plotted against β_{Ic} in Figure 48. In both tests the resistance of the metal to crack propagation is a function of the plastic zone size, and β_{Ic} is an indication of this factor for the K_{Ic} investigation. The normalization of K_{Ic} by the yield stress may reduce the degree of scatter.

In Figure 49, the strain energy release rate, $\mathcal{G}_{Ic}$, is compared to the DWTT value divided by the nominal fracture area (excluding the brittle weld). This plot was drawn in order to compare similar quantities on each axis (in-lb/in^2). The least amount of scatter in any of the figures is indicated in this curve.

In conclusion, it should be emphasized that these are preliminary correlations based on a limited amount of data. As more information is accummulated and the degree of scatter that can be expected is better defined, the usefulness of these correlations in permitting predictions of K_{Ic} from DWTT energy values will become better established.

ALUMINUM ALLOYS

(R.W. Judy, Jr. and R.J. Goode)

*STRESS CORROSION CRACKING

Exploratory stress-corrosion-cracking (SCC) studies have been conducted on aluminum alloys in a manner similar to that used for titanium alloys, which is described in an earlier section of this report. Previous studies (5, 7) have shown that these methods do not yield meaningful results when applied to aluminum alloys except for specimens oriented in the "TW" or "TR" (14) position; therefore, these studies of aluminum alloys have been confined to the "TW" or short transverse orientations. Specimens of the proper orientation were obtained from one inch plate by welding tabs to a 1 in. x 1 in. bar and cutting the 1 in. x 1/2 in. x 1 in. specimens from the welded assembly.

Stress-corrosion-cracking data and some mechanical properties of three alloys tested are shown in Table 15 and Figures 50 through 52. Two of the alloys, 7079-T6 (A13) and 7075-T7351 (A14) were relatively sensitive to SCC, having K_{Iscc} values of 11 and K_{Ix} values of 22.8 and 25.3 ksi $\sqrt{in}$, respectively. The 7005-T63 was insensitive with a K_{Iscc} value of 27.5 and K_{Ix} of 27.5 ksi $\sqrt{in}$. The tests were continued over a long time period in a stagnant 3.5% salt water

*This research was supported by the Advanced Research Projects Agency as part of the ARPA Coupling Program on Stress-Corrosion Cracking.

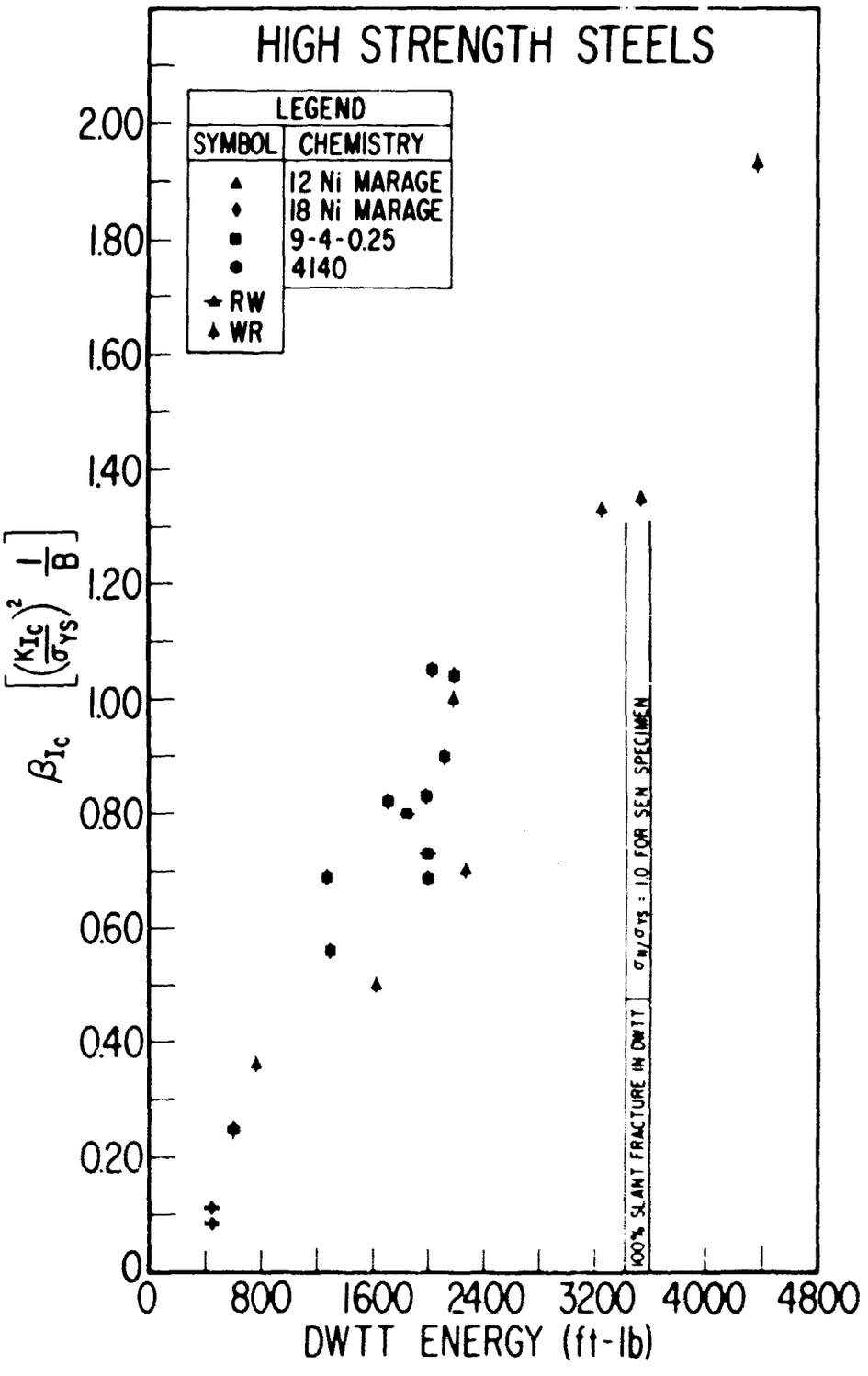

Fig. 48 - Preliminary correlation of β_{Ic} with drop-weight tear test energy

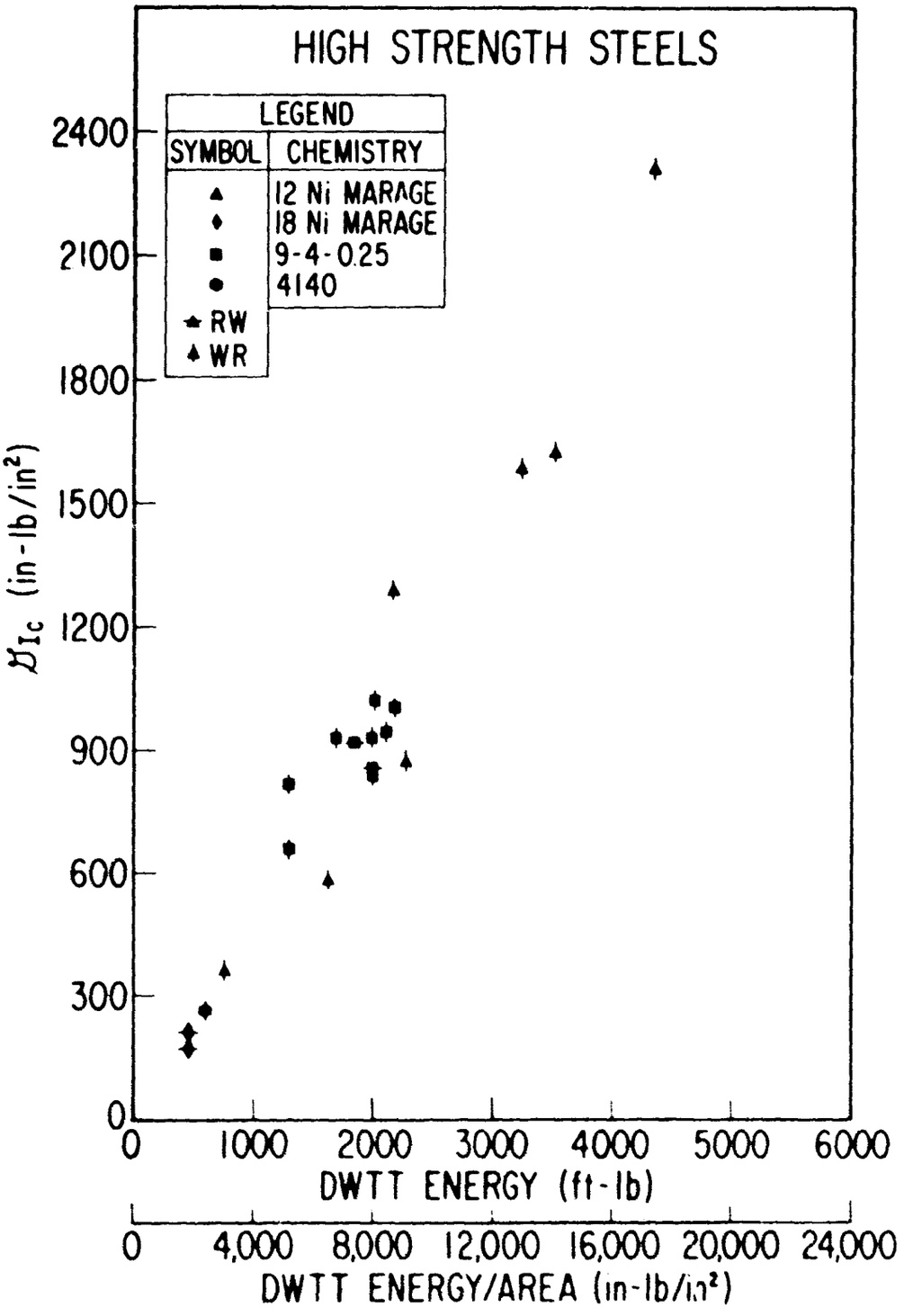

Fig. 49 - Preliminary correlation of strain energy release rate, $\mathcal{G}_{Ic}$ with drop-weight tear test energy results.

TABLE 15

STRESS CORROSION CRACKING OF ALUMINUM ALLOYS

Alloy	Code	YS (ksi)	DWTT (ft-lb)	K_{Ix} (ksi$\sqrt{in}$)	K_{Iscc} (ksi$\sqrt{in}$)	Specimen Depth (in)	Specimen Width (in)
7079-T6	A13	74.9	111	22.8	11	1	1/2
7075-T7351	A14	52	514	25.3	11.5	1	1/2
7005-T63	A15	45.9	870	29	27.5	1	1/2

NOTE: YS and DWTT shown for WR fracture orientation

K_{Ix} and K_{Iscc} shown for TW fracture orientation

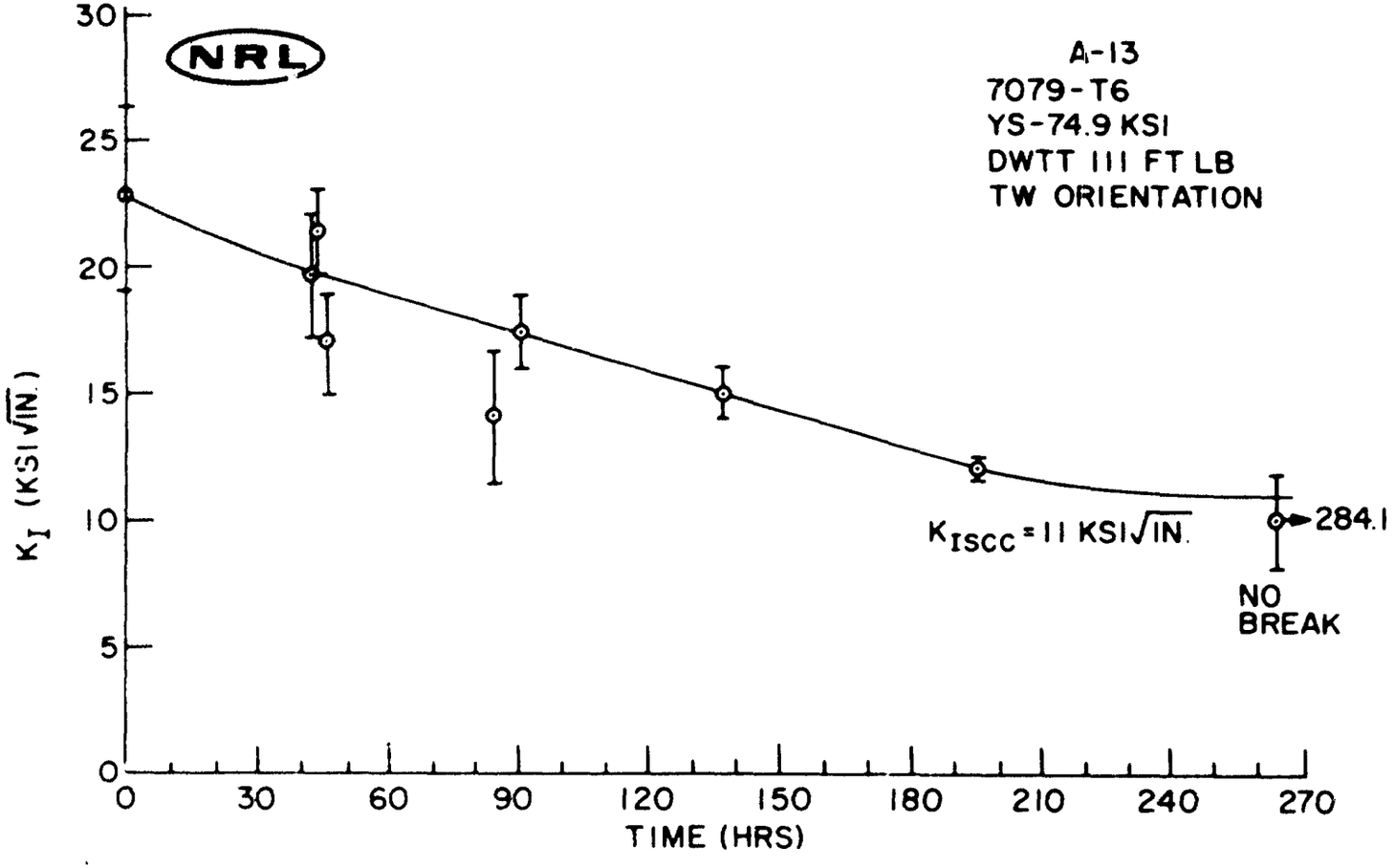

Fig. 50 - Salt water SCC characteristics of aluminum alloy 7079-T6 (A-13)

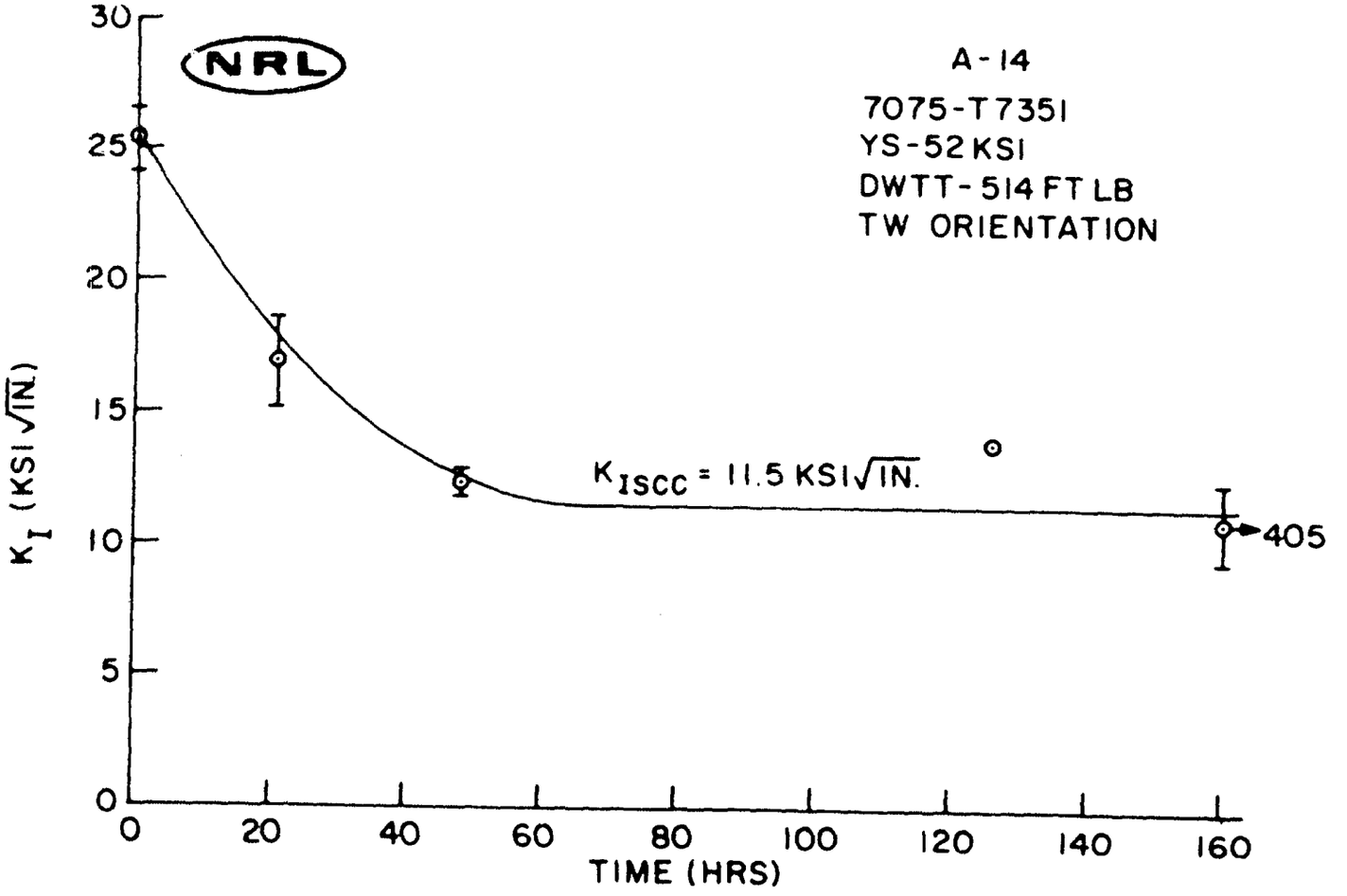

Fig. 51 - Salt water SCC characteristics of aluminum alloy 7075-T7351 (A-14)

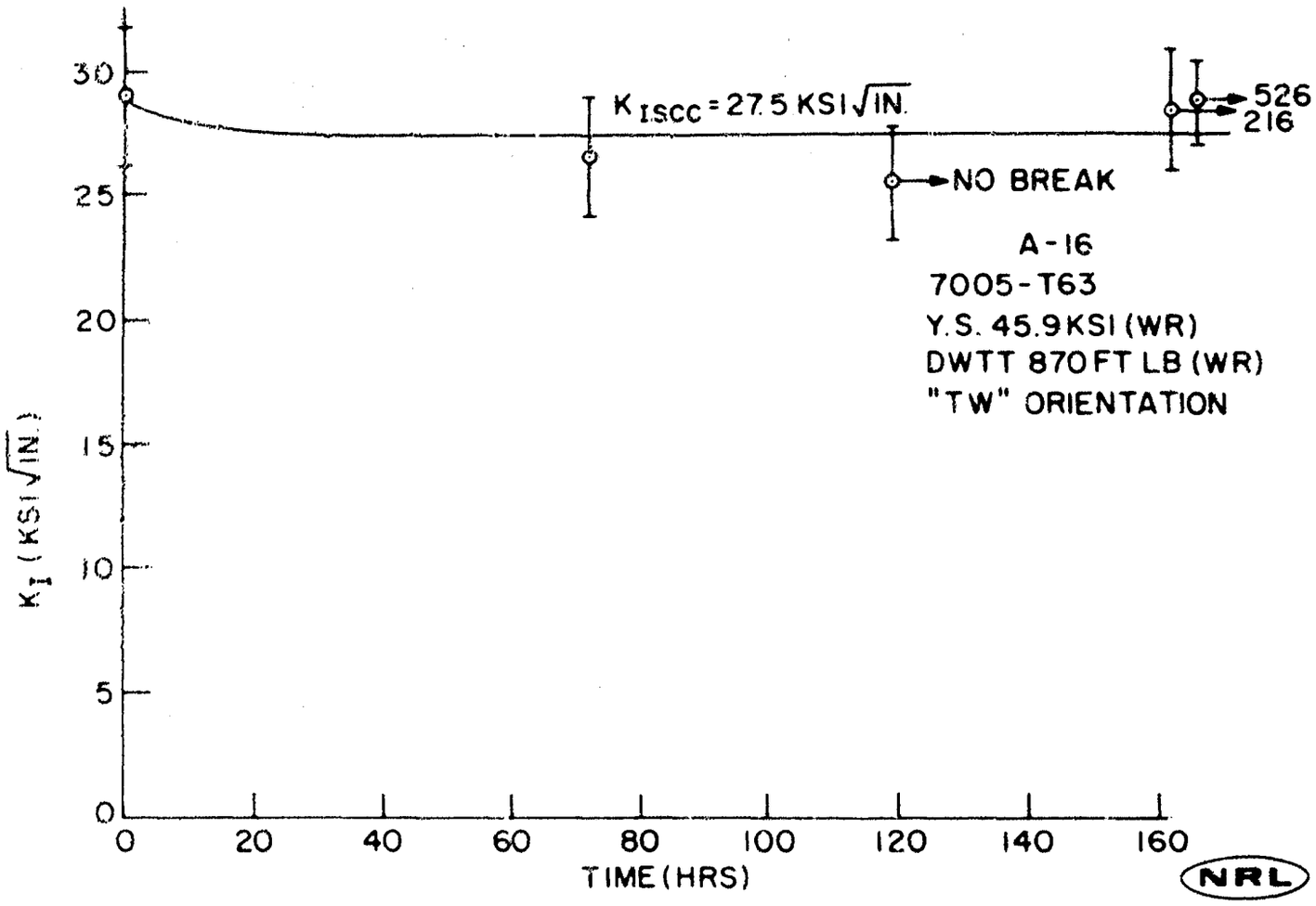

Fig. 52 - Salt water SCC characteristics of aluminum alloy 7005-T63 (A-16)

solution which was changed twice daily, possibly affecting the absolute K_{Iscc} values obtained; however, the general indication of relative sensitivity or insensitivity is considered to be valid.

FRACTURE TOUGHNESS INDEX DIAGRAM FOR ALUMINUM

The fracture toughness index diagram (FTID) for aluminum is shown in Fig. 53. No additions or modifications of these FTID have been made for some time including the period covered by this report. It is being presented now for the benefit of those who have recently become acquainted with this report series since it was not covered in the Eleventh Quarterly. The aluminum FTID reflects the correlation of drop-weight tear test (DWTT) and explosion tear test (ETT) performance with yield strength (YS). The optimum materials trend line shows the limiting or optimum values in the weak fracture direction with respect to the principal rolling direction in commercially provided plate. Correlations of ETT performance with DWTT energy values are shown on the left of the diagram. Alloys with DWTT energies that fall below the elastic-plastic transition band (~300-400 ft-lb DWTT energy) can be expected to support rapid crack propagation (catastrophic fracturing) at elastic stress levels. Increasing DWTT energies above this transition band indicate increasing plastic strain capabilities before a crack will propagate. Above 60 ksi YS all alloys would be expected to be "brittle" and fracture mechanics techniques will be required to characterize fracture toughness. Below about 50 ksi YS a wide variety of alloys should be available that require extreme amounts of plastic strain for fracture.

HIGH STRENGTH STEELS
(P. P. Puzak)

The fracture toughness characteristics of steels and welds of approximately 130 to 200 ksi yield strength have been studied. In this report are the results obtained for 3/4 to 4-in. thick plates of a 5Ni-Cr-Mo-V steel and 1-in. thick plates of a 9Ni-4Co-0.2C (9-4-0.2C) quenched-and-tempered (Q&T) alloy steel. Fracture toughness investigations were also conducted for producer fabricated manual (STICK) and metal-arc inert gas (MIG) welds of the nominal 2Mn-2Ni alloy composition developed for welding the 5Ni-Cr-Mo-V steel, and NRL fabricated, fully-automatic, tungsten-arc inert gas (TIG) welds of the 9Ni-4Co-0.2C alloy and 12Ni-3Cr-3Mo and 17Ni-2Co-3Mo maraging steel weld metal compositions.

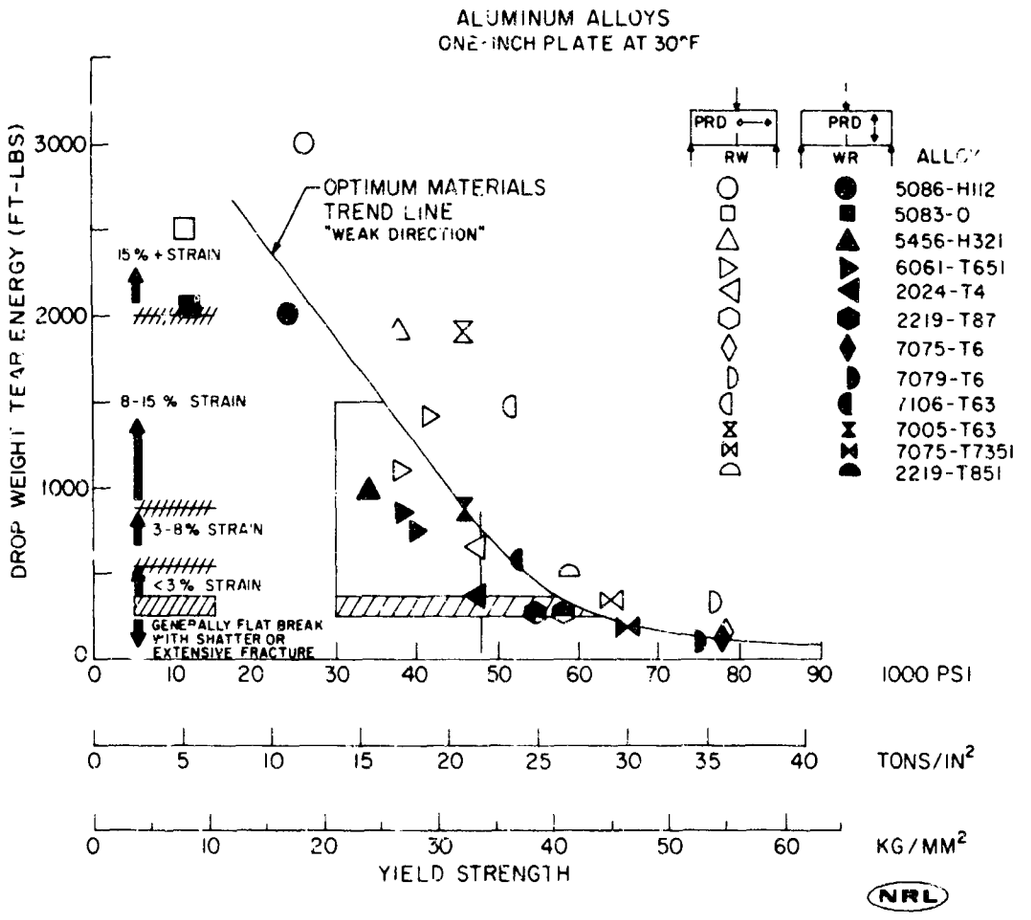

Fig. 53 - Fracture toughness index diagram for 1-inch thick aluminum alloy plates representative of commercial practice

FRACTURE TOUGHNESS INDEX DIAGRAM FOR STEELS

The principal fracture toughness test method employed in NRL studies of high strength steels has been the drop-weight tear test (DWTT) as correlated with results obtained in the large structural prototype element explosion-tear test (ETT). These methods and the correlation procedure have previously been described in detail (1). From the spectrum investigation of 1-in. thick steels, a simplified Fracture Toughness Index Diagram (FTID) which indexes the DWTT fracture toughness characteristics of a steel in terms of ETT performance of the material has been evolved. The FTID chart relating specifically to all 1-in.-thick steel plates evaluated to date is presented in Fig. 54.

The FTID given in Fig. 54 has been updated to present the latest information. Previous studies have emphasized the point that the fracture toughness characteristics of a metal at a given level of YS are highly sensitive to process history, thickness, etc. in addition to chemical composition. A rational evaluation of process history effects is depicted in Fig. 54 by the various curves designated "optimum materials trend line" (OMTL). These curves separate the data illustrated into characteristic groups relating to mill processing variables (melting practice and/or cross-rolling) of the steels. The OMTL may be recognized as the reference "yardstick" for evaluation of new steels with respect to the practicable upper limits of fracture toughness for any given YS level as a function of conventional or special processing variables. All steel data relating to the limiting ceiling OMTL curve have involved vacuum-induction-melt (VIM) or a double vacuum practice of VIM plus vacuum-arc remelt and the illustrated ceiling OMTL curve represents the current estimate of the optimum limits attainable with special VIM and 1 to 1 cross-rolling practices.

The significance and interpretation of the FTID data given in Fig. 54 will not be repeated here since they have been covered in detail in Refs. 2, 7, 24, 25, and 27. Wherever possible, new data (to be described) are reported in charts containing the basic curves and correlation features of the FTID for 1-in. thick steels to illustrate a ready comparison of results for the new steels with previously tested and reported data.

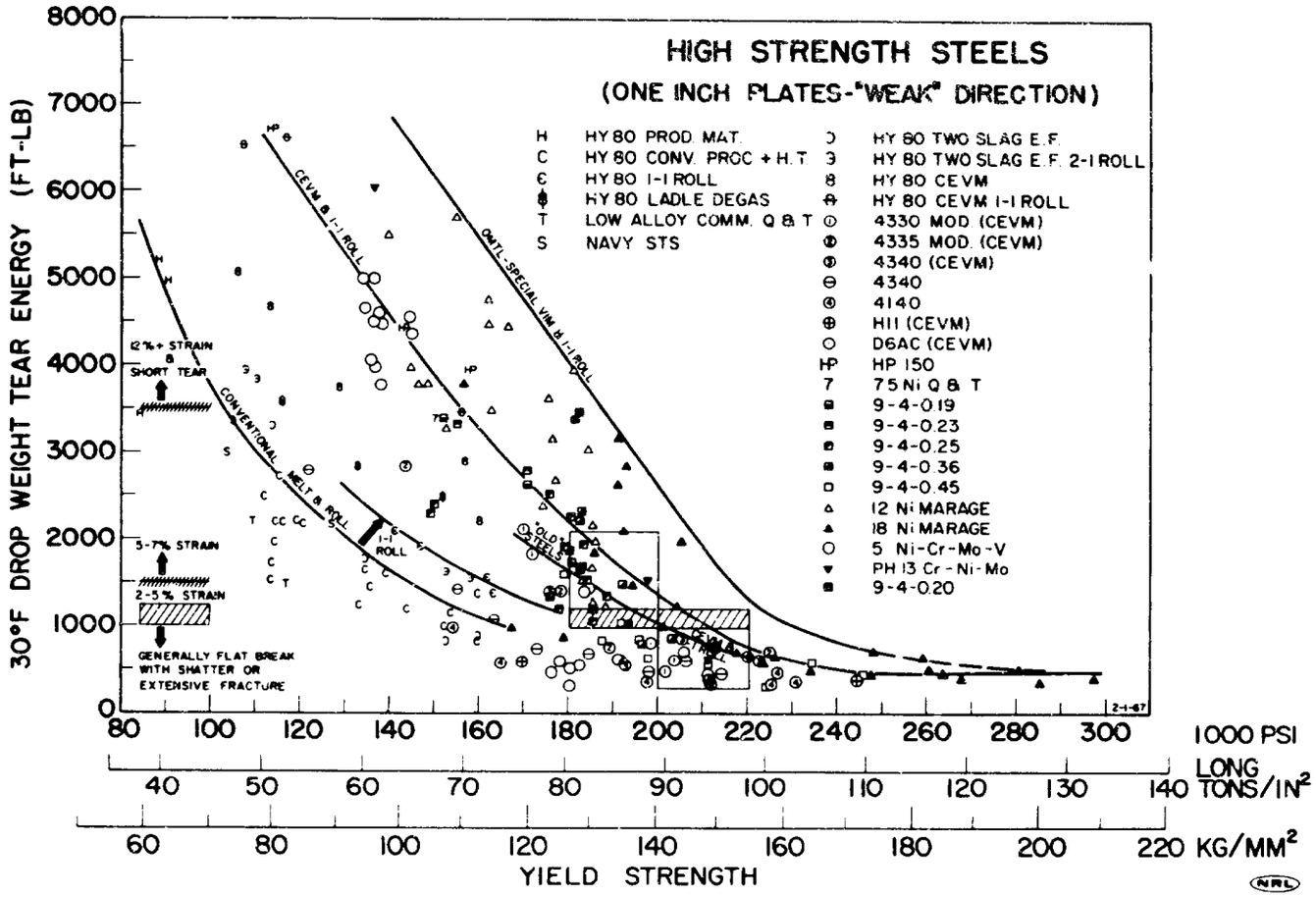

Fig. 54 - Fracture Toughness Index Diagram (FTID) derived from all 1-in. thick high strength steels tested. The explosion-tear test (ETT) correlations and the optimum-materials-trend lines (OMTL) for various mill practices are included.

DROP-WEIGHT TEAR TESTS (DWTT) OF 5Ni-Cr-Mo-V STEEL PLATE [HY-130(T)]

A total of twelve 80 ton electric furnace heats (half of which were vacuum degassed) of the 5Ni-Cr-Mo-V steel were produced. Plates ranging from 3/4 to 4-in. thick from six of these heats (including the first and eleventh) considered to be representative of the production experience of this material have been studied at NRL. The tensile and fracture toughness properties of these plates are given in Table 16.

A graphical summary of the data given in Table 16 is depicted in Fig. 55, as referenced to the FTID features for 1-in. thick steels. For the 1 and 2-in. thick HY-130(T) plates, (open symbols in Fig. 55) the standard DWTT energy values are noted to range from approximately 3500 to 5000 ft-lb which is essentially equivalent to the DWTT values developed by 1-in. thick HY-80 hull steels. (See Fig. 54.) In all cases the DWTT fractures for the 1 and 2-in. thick steels were found to exhibit full shear (45° slant fracture) characteristics (Fig. 56) at 30°F.

The data given in Fig. 55 for the 2 to 4-in. thick plates represent DWTT values obtained for specimens machined to 1-in. thickness.

The 2400 to 4200 ft-lb range of standard DWTT energy values obtained for the 3 and 4-in. thick HY-130(T) steels still implies a relatively high level of fracture toughness. This may be observed by noting the ETT correlation index levels of plastic strain for fracture propagation given by the basic FTID chart. At this stage of development, it is not intended to emphasize the specific values obtained for YS and DWTT energy of these steels or that the variability depicted in Fig. 55 in through-thickness properties is necessarily representative of the expected properties in all "properly heat-treated" 3 and 4-in. thick plates of the HY-130(T) steel.

The results of this study emphasize the need for methods and criteria for evaluation of heavy section plates. This need was recognized, and the DWTT was devised as a laboratory tool for measuring the full thickness fracture toughness by integrating the through-the-plate-thickness quality gradients. Full thickness DWTT of a variety of 2 to 4-in. steels are underway and equipment, instrumentation and specimens are being assembled to facilitate the testing of pressure vessel steels with thicknesses up to

TABLE 16

TEST DATA FOR HY-130(T) STEEL ALLOY (5Ni-Cr-Mo-V) PLATES
[All specimens in "weak" (WR) orientation]

NRL No.	Thick-ness (in.)	0.505" Diam Tension Test Data 0.2% YS (ksi)	UTS (ksi)	El.in 2" (%)	RA (%)	Charpy V @ 30°F (ft-lb)	Drop-Weight Tear @ 30°F * (ft-lb)
H14	3/4	151.3	158.3	18.0	61.3	83	2958
H13	1	145.0	153.5	18.7	63.5	30	4558
H98	1	133.7	141.5	18.8	64.0	93	>5000
J21	1	134.8	140.1	18.8	64.1	79	4636
J86	1	138.3	146.3	18.3	58.5	76	4478
J93	1	138.4	144.7	17.5	58.8	54	3775
J94	1	137.8	145.3	18.0	60.1	-	4596
J95	1	137.3	144.1	18.0	60.4	-	3966
J96	1	136.7	145.3	17.5	69.9	-	4052
J97	1	137.2	146.7	18.0	64.5	-	>5000
J98	1	137.1	145.9	18.0	64.2	-	4494
K11	1	136.5	143.0	18.7	63.7	57	--
K20	1	137.6	143.2	19.0	64.4	54	--
K21	1	137.4	156.8	17.5	59.0	52	--
G73	2	144.9	156.7	18.0	64.6	55	3557
G74	2	149.2	157.1	18.0	59.9	71	3843
H12	2	146.7	158.3	18.3	58.3	70	4175
H99	2	141.8	148.6	17.5	60.2	66	3775
J75	3	140.6	147.7	18.0	61.1	65	4188(Top Surface)
		143.3	149.4	12.5	37.6	55	3584(Centerline)
		120.2	150.5	17.5	56.4	44	3609(Bot.Surface)
J74	4	151.3	155.2	17.0	55.2	43	2618(Top Surface)
		143.9	153.7	17.5	52.7	53	3333(Centerline)
		140.7	156.6	17.0	56.2	42	2412(Bot.Surface)

*No. H14 tested as 3/4-in.-thick by standard DWTT specimens; all 2, 3, and 4-in.-thick steels were split and tested as standard 1-in.-thick DWTT specimens.

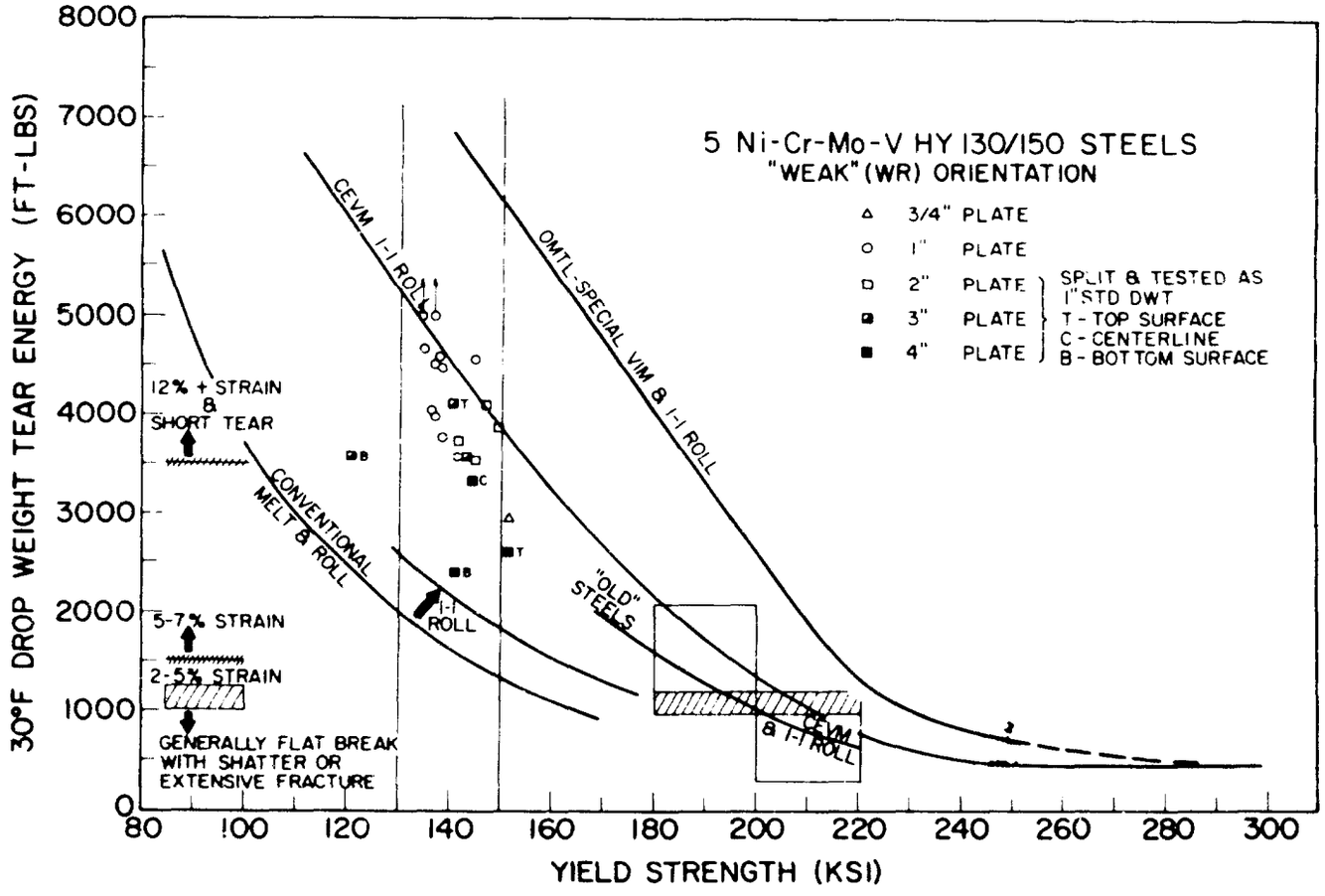

Fig. 55 - Summary of standard (1-in. thick) drop-weight tear test (DWTT) - yield strength (YS) relationships for HY-130(T) (5Ni-Cr-Mo-V) steel plates as referenced to the basic FTID-OMTL data for 1-in. thick steels

Fig. 56 - Drop-weight-tear test fracture faces of a 1-in. thick HY-130(T) steel alloy (J-95) illustrating full shear (45° slant fracture) characteristics found to be typical for 30°F standard DWTT for 1 to 2-in. thick HY-130(T) plates

12-in. Preliminary results obtained for 2 and 3-in. thick HY-130(T) steels are described below.

FULL THICKNESS DWTT OF 2-3-IN. THICK HY-130(T) STEELS

The single pendulum impact machine used at NRL for making direct energy absorption measurements on DWTT specimens is equipped with replaceable tups that provide for a capacity of either 5,000 or 10,000 ft-lb. The smaller capacity tup has proved to be adequate for the testing of most 1-in. thick steels for fracture propagation in the "weak" (WR-orientation) direction (See Fig. 54). However, the 10,000 ft-lb capacity machine has been required for "strong" (RW-orientation) direction tests of 1-in. thick steels, and also for the 2 to 3-in. thick steels characterized by "low" to "moderate" fracture toughness properties. Heavy section steels of "high" fracture toughness properties could not be evaluated with the single pendulum impact machine.

Initial studies of high toughness, heavy section steels required the use of the 1 ton (22,000 ft-lb capacity) or the 6 ton (180,000 ft-lb capacity) NRL drop-weight machines. These early studies also required that several specimens be tested at a given temperature to establish the amount of energy required for complete fracture, i.e., by a "bracketing" technique which was the method originally employed (and hence the name, DWTT) when the test was first conceived. The size of the specimens required for DWTT of 2 to 3-in. thick steels (T x 8 x 28-in.) made the materials requirement for a single determination by the "bracketing" technique prohibitively excessive, and it was necessary to look to other means for conducting DWTT of heavy section steels. A solution to this problem was achieved by adapting the existing drop-weight machines with auxiliary equipment comprising photographic equipment and an instrumented impact transducer to record load signal on either a cathode-ray oscilloscope or a tape recorder. This enables the force-time data to be permanently recorded during an impact test and provides for the indirect calculation of energy absorption through the relationships involving the impulse of the force acting on the specimen and the change in linear momentum. The details of this technique will be described in a future report.

The preliminary results of the full thickness DWTT of the 2 and 3-in. thick HY-130(T) steels are presented in Table 17. It is apparent that both of the HY-130(T)

TABLE 17

TEST DATA FOR FULL THICKNESS DWTT OF HY130(T) STEELS
(All Specimens in "weak" (WR) orientation)

NRL No.	Thickness (in.)	Test Temperature (°F)	Full Thickness DWTT (ft-lb)	Full Thickness DWTT Area (ft-lb/in.^{2})	1-In. DWTT (ft-lb)	1-In. DWTT/Area (ft-lb/in.^{2})
H-99	2	75	21,974	2,197	---	---
		30	19,109	1,911	3,775	1,258
		0	14,121	1,412	---	---
J 75	3	30	20,841	1,389	4,188 (Top)	1,396
				---	3,584 (Center)	1,195
				---	3,609 (Bottom)	1,203
		0	20,058	1,337	---	---

steels exhibit relatively high fracture toughness characteristics at 30°F. However, these data also suggest that both of these steels are within their "transition temperature range" for tests at 0°F. It is also noted that the data given in Table 17 implies that on the basis of "nominal-net-section-test-area" the 2-in. thick HY-130(T) steel (10 sq. in. of "test"area) is considerably higher at 30°F and essentially equal at 0°F to the DWTT fracture toughness properties of the 3-in. thick HY-130(T) steel (15 square inches of "test" area).

The fracture appearances of the full thickness DWTT specimens of the 2 and 3-in. thick HY-130(T) steel tested at 30°F are shown in Fig. 57. Apparent in these fractures are indications of centerline segregations of nonmetallic inclusions which result in longitudinal ruptures in planes parallel to the rolled surfaces of the plates. This condition is partly attributable to the melting and deoxidation practices used for the HY-130(T) steels. Extensive studies by the producer are underway to develop refinements of melting and deoxidation practices to alieviate or eliminate the tendency to promote centerline planes-of-weakness for fracture propagation parallel to the rolled plate surfaces.

DROP WEIGHT TEAR TEST STUDY OF 2%Mn-2%Ni WELD METALS DEVELOPED FOR FABRICATING HY-130(T) STEEL WELDMENTS

Weldments, 2 to 3 ft. in length, representative of each electrode and weld procedure under development by subcontractors in the NAVSHIPSYSCOM HY-130 steel program with U.S. Steel were furnished NRL to investigate their fracture toughness characteristics. These weldments are considered representative of the best 2%Mn-2%Ni filler wire and procedures developed during the first phase of the program. Details of the welding processes and procedures used are given in Table 18. The results obtained in this investigation are summarized in Table 19.

Figure 58 presents a summary of the 30°F DWTT energy values and YS relationships obtained for the 2%Mn-2%Ni welds in Table 19, as referenced to the FTID for 1-in. thick steel plates. The shaded region given in this illustration encompasses the range of DWTT-YS values developed with 1-in. thick DWTT specimens from the 1 to 2-in. thick HY-130(T) steel plates (described previously in Fig. 55). It is noted that the 2%Mn-2%Ni welds are characterized by generally lower DWTT fracture toughness values than that exhibited by the HY-130(T) plates.

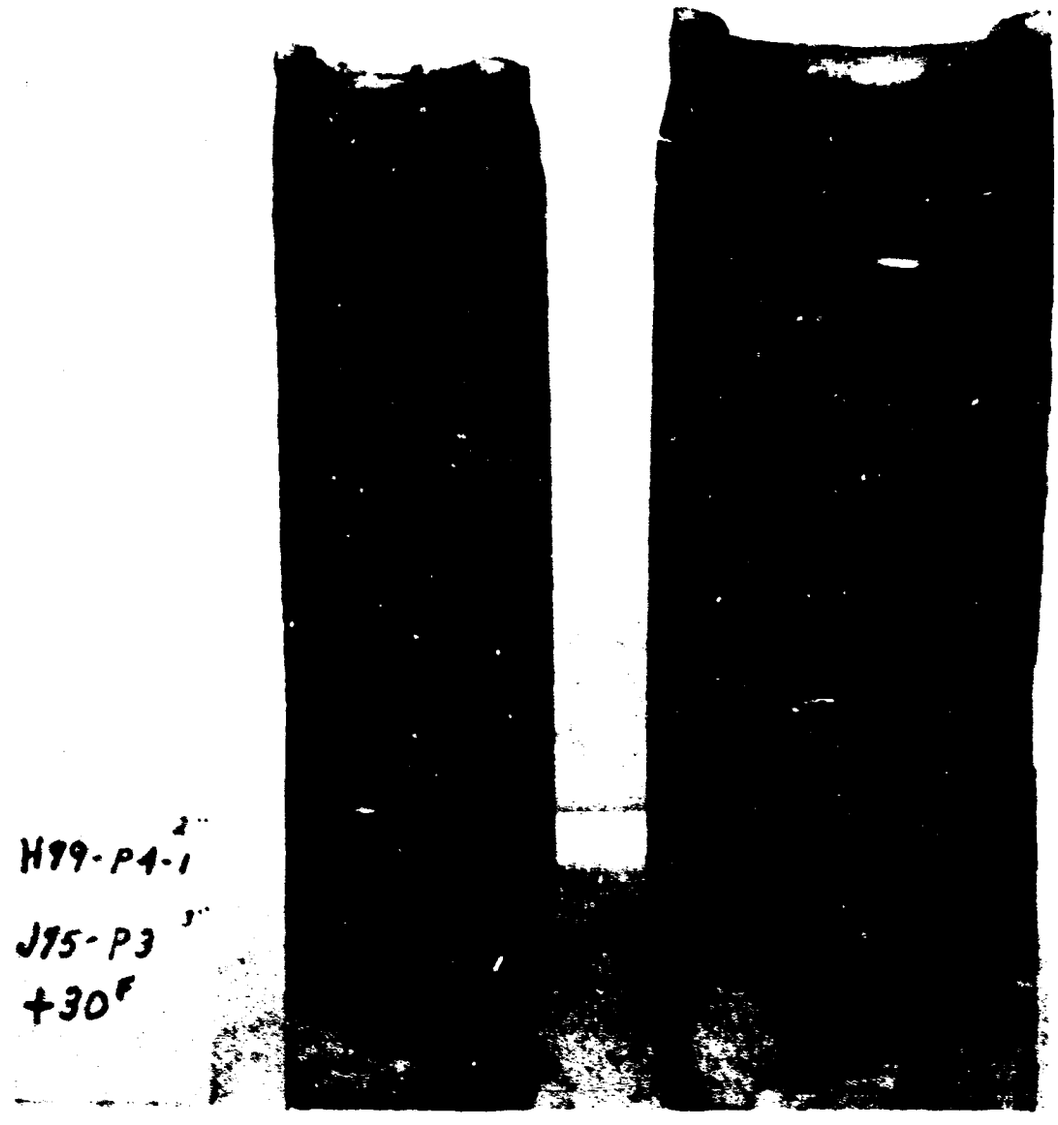

Fig. 57 - Illustrating the 30°F drop-weight-tear-test fracture faces of the 2 and 3-in. thick HY-130(T) steel alloys reported in Table 17

TABLE 18

WELDING PROCEDURES DATA FOR 1-IN.-THICK HY-130(T) (5Ni-Cr-Mo-V) WELDMENTS

NRL No.	Process	Position	Wire	Gas	Preht.&I.P.	Av. Ht. Input (J/in.)
J86	MIG-Spray Arc	Flat	L-150 (Vac.Ht.ORO 440) 1/16-in. diam (%C - high)	A+2O_2	250°F	38,500
J96	MIG-Spray Arc	Flat	AX-140 (Air Ht.IP0047) 1/16-in. diam	A+1O_2	200/225°F	45,700
J93	MIG-Interrupted Arc	Vert.-Up	L-150 (Vac Ht ORO 440) 0.035-in diam (%C - high	60He+38A+2O_2	250°F	37,800
J97	MIG-Interrupted Arc	Vert Up	AX-140 (Air Ht IP0047) 0.045-in diam	70He+26A+4CO_2		50,800
J98	MIG-Interrupted Arc	Vert -Up	AX-140 (Vac Ht 50325) 0.045-in diam (%Ti - low)	70He+26A+4CO_2	200/225°F	49,000
J94	Manual-Stick	Flat	HY-140 (A-046) 5/32"x14"	Covered	225/250°F	27,800
J95	Manual-Stick	Vert -Up	HY-140 (A-046) 5.32"x14"	Covered	200/225°F	49,300
K11	Manual-Stick	Flat	HY-140 (IP0419) 3/16"x14"	Covered	275°F	34,400
K20	Manual-Stick	Vert.-Up	HY-140 (IP0419) 5/32"x14"	Covered	275°F	40,600-53,400
K21	Manual-Stick	Vert.-Down	HY-140 (IP0419) 5/32"x14"	Covered	275°F	25,400

TABLE 19

TEST DATA FOR 1-IN.-THICK HY-130(T) (5Ni-Cr-Mo-V) WELDMENTS

NRL No.	Location	0.2% YS (ksi)	UTS (ksi)	El in 2" (%)	RA (%)	Av. DWTT @ 30°F (ft-lb)	Av. C_v @ 30°F (ft-lb)	Av. C_v @ 80°F (ft-lb)
J86	MIG-Flat							
	All Weld	146.5	155.7	18.0	61.8	1720	51	69
	Trans. Weld*	140.0	149.4	13.0	37.4	-	-	-
	Plate (WR)	138.3	146.3	18.3	58.5	4478	76	76
J96	MIG-Flat							
	All Weld	144.9	154.1	18.0	64.5	1723	53/65**	53/72**
	Trans. Weld*	141.5	150.9	11.0	63.9	-	-	-
	Plate (WR)	136.7	145.3	17.5	69.9	4052		
J93	MIG-Vert.-Up							
	All Weld	-	-	-	-	3400	62	68
	Trans. Weld*	140.7	147.7	14.0	51.5	-	-	-
	Plate (WR)	138.4	144.7	17.5	58.8	3775	54	55
J97	MIG-Vert.-Up							
	All Weld	140.4	151.9	18.0	64.6	2325	51/59**	55/66**
	Trans. Weld	139.2	151.9	14.0	64.3	-	-	-
	Plate (WR)	137.2	146.7	18.0	64.5	>5000		
J98	MIG-Vert.-Up							
	All Weld	140.1	152.6	18.0	64.4	4000	64/83**	64/86**
	Trans. Weld	139.2	150.4	15.0	64.3	-	-	-
	Plate (WR)	137.1	145.9	18.0	64.2	4494		
J94	Stick-Flat							
	All Weld	136.5	137.9	19.0	63.6	3333	59	69
	Trans. Weld	134.1	138.3	15.5	60.3	-	-	-
	Plate (WR)	137.8	145.3	18.0	60.1	4596		
J95	Stick-Vert.-Up							
	All Weld	134.7	140.1	17.0	58.8	3201	54	60
	Trans. Weld	133.2	139.2	16.0	63.3	-	-	-
	Plate (WR)	137.3	143.1	18.0	60.4	3966		
K11	Stick-Flat							
	All Weld	140.7	144.2	17.5	60.9	1905	55	55
	Trans. Weld	-	-	-	-	-	-	-
	Plate (WR)	136.5	143.0	18.7	63.7	-	57	57
K20	Stick-Vert.-Up							
	All Weld	140.7	151.6	18.0	59.0	1326	45	50
	Trans. Weld	-	-	-	-	-	-	-
	Plate (WR)	137.6	143.2	19.0	64.4	-	54	54
K21	Stick-Vert.-Down							
	All Weld	140.2	140.2	16.0	55.8	-	53	60
	Trans. Weld	-	-	-	-	-	-	-
	Plate (WR)	137.4	156.8	17.5	59.0	-	52	52

* Tensile fracture outside of weld in Plate-HAZ area.
** Charpy V values for TOP/BOTTOM of weld deposit.

108

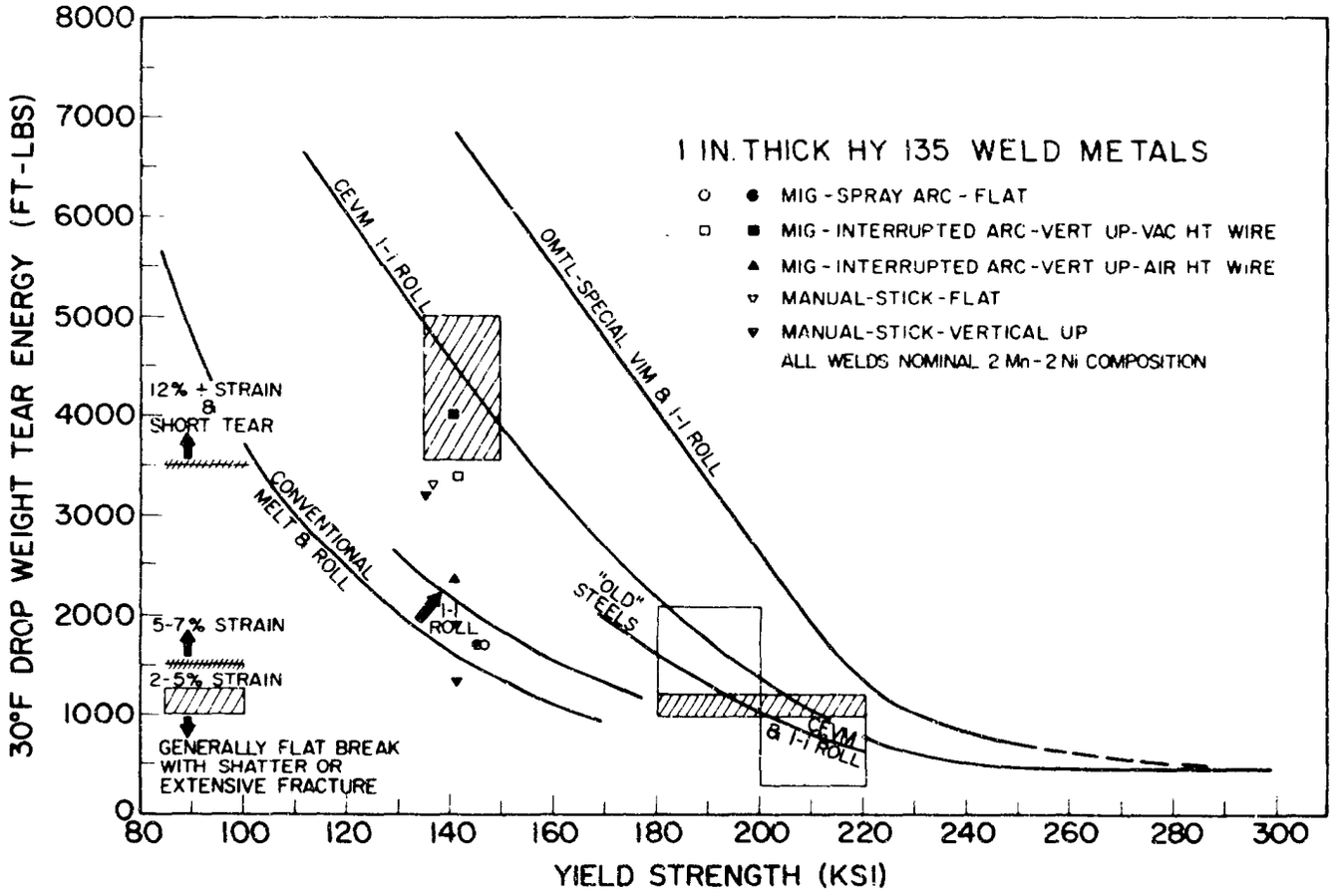

Fig. 58 - Summary of standard drop-weight-tear-test - yield strength relationships for 2%Mn-2%Ni weld metals, as referenced to the basic FTID-OMTL data for 1-in. thick steel plates

Depending upon the electrode and welding procedure, the YS values of the 2%Mn-2%Ni welds range from 134.7 to 146.5 ksi; and the DWTT values range from 1326 to 4000 ft-lb. It should also be noted that a DWTT value is not reported for the manual-STICK weldment fabricated in the vertical-down position. Difficulties encountered in electron-beam weld preparation of specimens from this weldment resulted in subsequent DWTT fractures involving significant amounts of the HY-130(T) plate metal, with the concomitantly "high" DWTT energy values considered to be more representative of the plate rather than the weld.

The data given in Table 19 and Fig. 58 indicate an extremely large variation in DWTT values for the 2%Mn-2%Ni welds despite the fact that the chemical compositions of these welds were reported to be essentially similar. Of particular significance is the observation that the MIG-spray-arc flat-position welds are characterized by relatively low (approximately 1700 ft-lb) DWTT values at 30°F compared with the significantly higher DWTT values (approximately 3400 ft-lb) obtained with the same heat of weld wire used in MIG-interrupted arc-vertical up position welds. On the basis of C_V results for these 2%Mn-2%Ni welds (described below) the "low" DWTT values for the MIG-Flat welds cited above, and the similarly "low" DWTT results obtained for some of the manual-STICK welds depicted in Table 19 and Fig. 57 are considered to reflect transition temperature range aspects of these weld metals.

CHARPY V (C_V) FRACTURE TOUGHNESS OF HY-130(T) PLATES AND 2%Mn-2%Ni WELD METALS

The average C_V energy absorption curves for 1 and 2-in. thick HY-130(T) steels are depicted in Fig. 59. It should be noted that these data represent tests in the "weak" (WR orientation) fracture direction. The 1-in. thick steels exhibit C_V shelf level values ranging from 52 to 93 ft-lb at 30°F. In general, the shelf level values are maintained for these steels to test temperatures at 0°F and for several 1-in. thick steels to subzero test temperatures. The one 2-in. thick steel which does not exhibit C_V shelf level energy values at 30°F (No. G-73, Fig. 59, bottom) represents data for material cut from one end of a 2-in. thick plate produced from the first production heat of HY-130(T) steel. In the production of this plate, a malfunction of the heat treatment and quenching facilities was encountered and reported by the producer; but the specific plate was shipped without requiring the plate to be recycled through the continuous

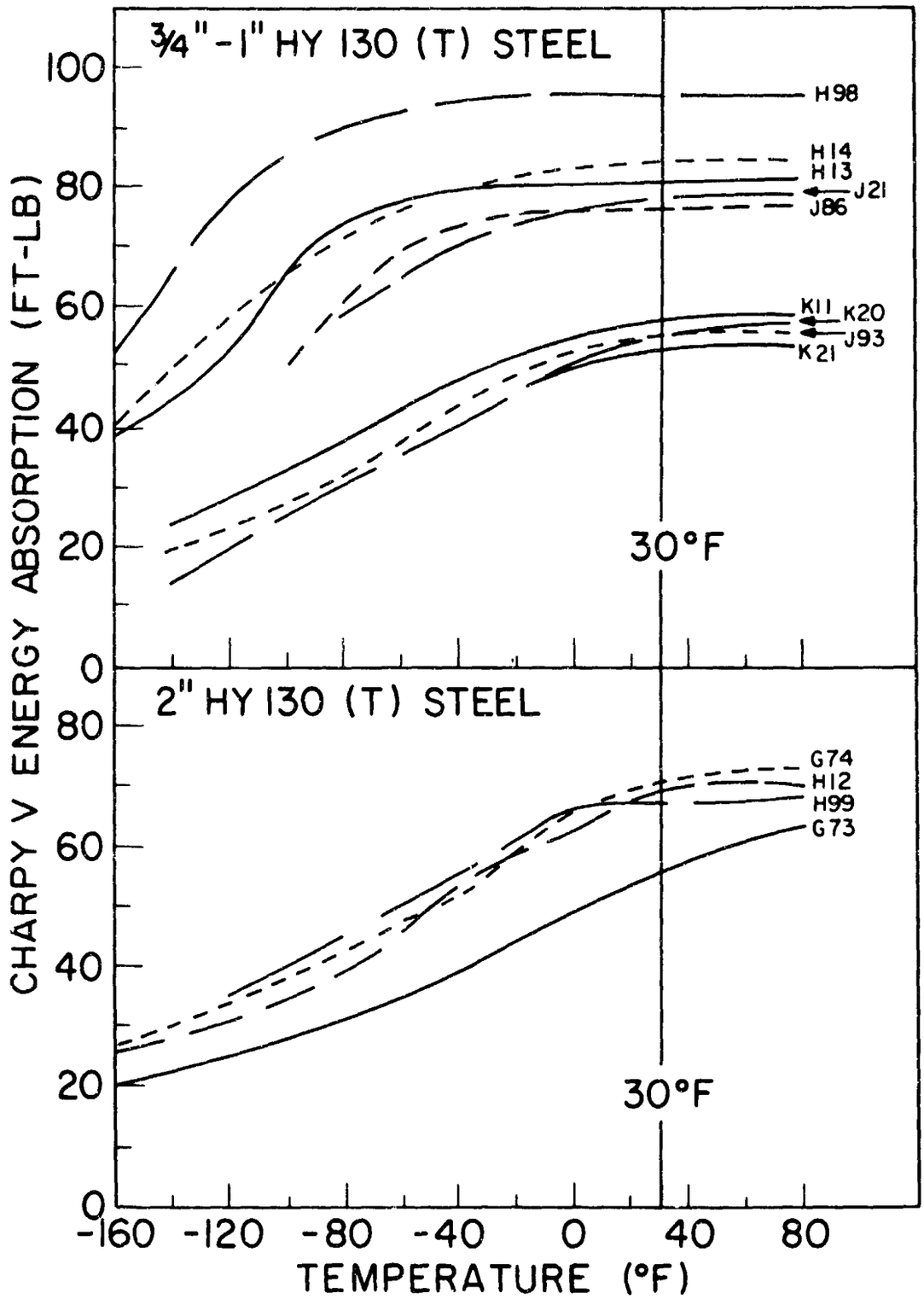

Fig. 59 - Summary of the average Charpy V (C_V)energy absorption curves for 1 and 2-in. thick HY-130(T) steel plate alloys. The data relate to "weak" (WR orientation) fracture direction tests.

heat treating line to insure the development of optimum properties. Laboratory heat treatment of small plate samples of the G73 plate resulted in the development of C_V properties essentially equal to those shown in Fig. 59, bottom, for the G74 plate which also represents another 2-in. thick plate produced from the first production heat of HY-130(T) steel.

The C_V data developed by NRL for the 3 and 4-in. thick HY-130(T) steel plates are given in Figs. 60 and 61. It is noted that the significant variation in surface and centerline properties previously described for these steels by results of standard DWTT are similarly indicated by the illustrated results for C_V tests. Both the 3 and 4-in. thick steels are characterized by C_V shelf level values at 30°F. However, depending on the location and orientation of the C_V specimen, it is apparent that C_V shelf level values below the 50 ft-lb minimum shelf level energy specified as the aim for HY-130(T) steels are developed by the "improperly" heat treated 3 and 4-in. thick HY-130(T) steels.

The average C_V energy absorption curves for the various 2%Mn-2%Ni MIG and STICK welds studied in this investigation are depicted in Figs. 62 and 63. All weldments were fabricated with a wide gap (1-in.), single V joint preparation (required for DWTT of weld metals) as shown in Fig. 62, top, right. This results in the evaluation of essentially undiluted weld metal. As noted in the illustration, C_V test specimens were machined so as to study top and bottom portions of the 1-in. thick weldments. For those weldments fabricated with back-up strips (Nos. J96, J97, J98, K21), dilution of the weld metal with the HY-130(T) steel is noted to result in relatively higher C_V energy values for the "bottom" specimens compared with the C_V values obtained for undiluted weld metal in the top portion of the welds.

Generally, all of the illustrated 2%Mn-2%Ni weld metals are noted to develop average C_V values of 40 ft-lb or more in tests at 30°F. However, the characteristic shape of the C_V energy absorption curves indicates that several of these weld metals are within their transition temperature range at 30°F; and the relatively low DWTT values described previously for these weld metals would seem to confirm this fact. This raises a question concerning the 0°F fracture toughness characteristics of these weld metals if the HY-130(T) weldment is used as contemplated in surface ship applications to gain desired fabrication experience prior to use in submarines.

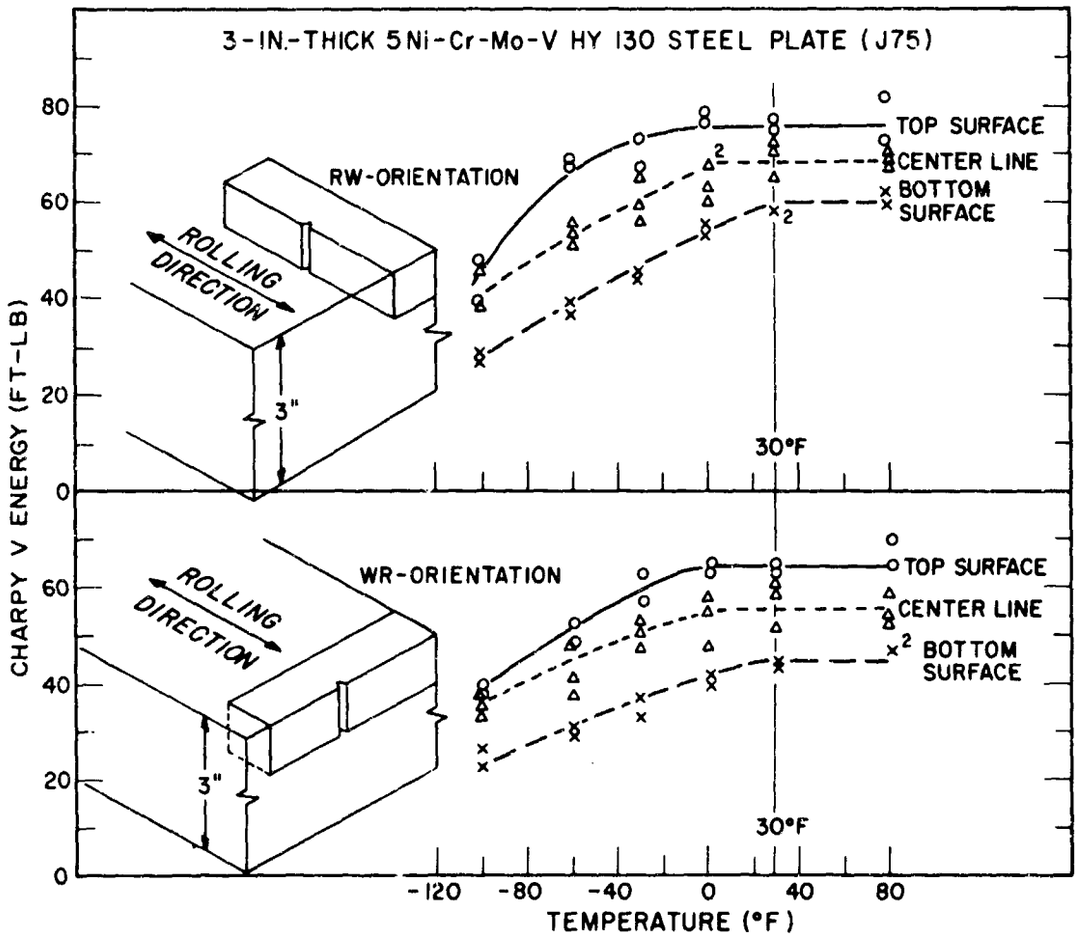

Fig. 60 - Charpy V energy absorption curves for both surfaces and centerline locations in a 3-in. thick HY-130(T) alloy (No. J-75)

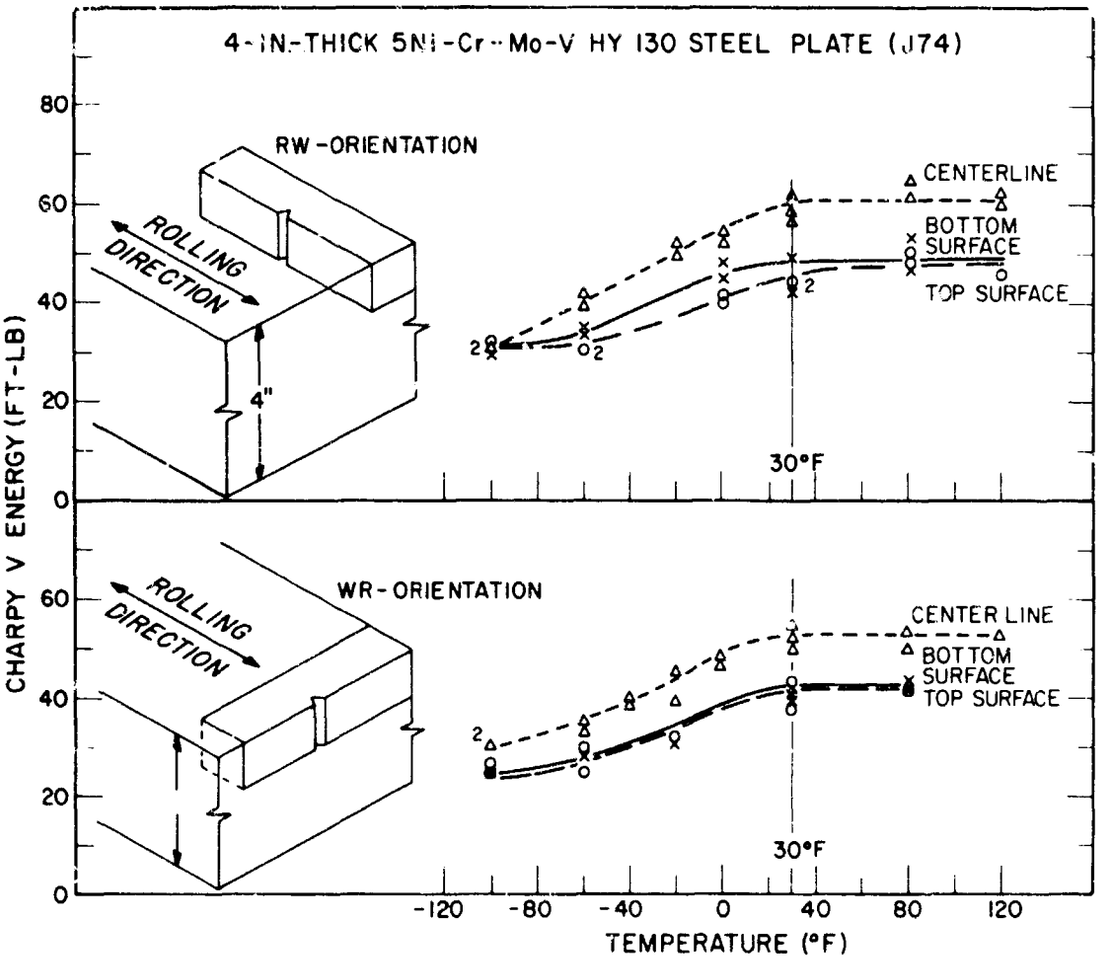

Fig. 61 - Charpy V energy absorption curves for both surfaces and centerline locations in a 4-in. thick HY-130 (T) alloy (No. J-94)

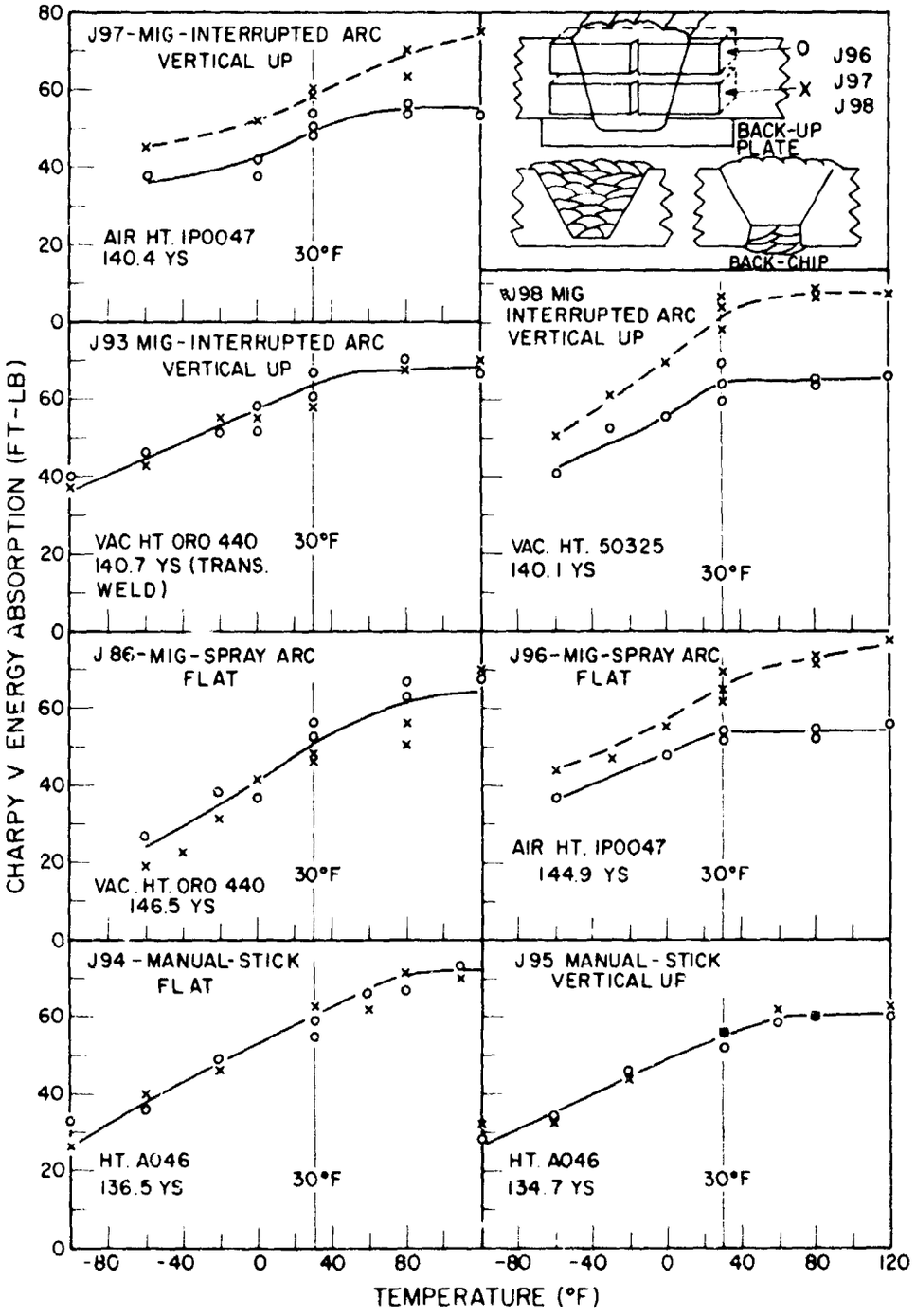

Fig. 62 - Charpy V energy absorption curves for 2%Mn-2%Ni weld metals deposited by MIG and STICK processes in HY-130 (T) steel plate

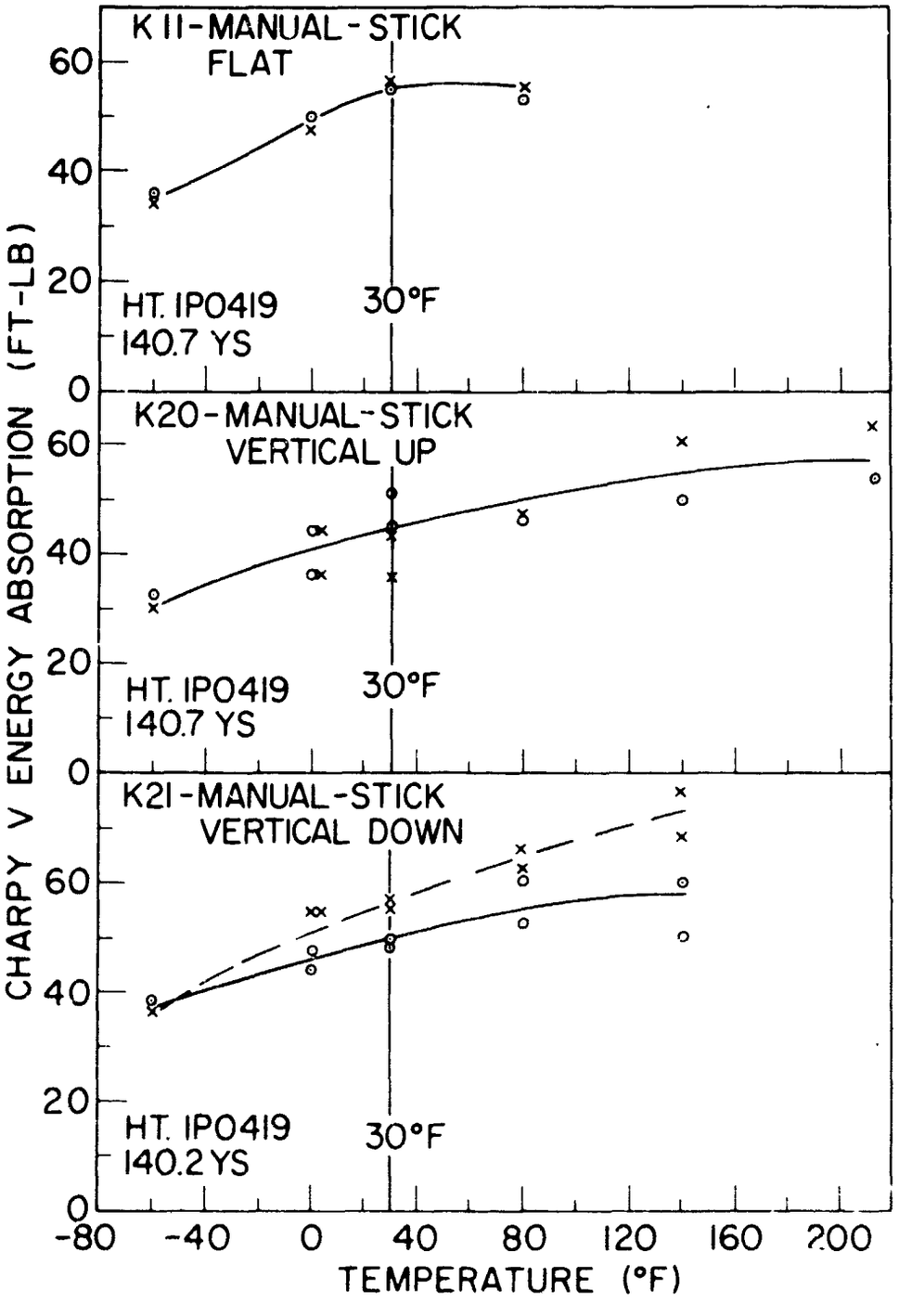

Fig. 63 - Charpy V energy absorption curves for 2%Mn-2%Ni weld metals deposited by STICK processes in HY-130(T) steel plate

All of the HY-130(T) weldments described herein were fabricated with filler metals from large (7-1/2 to 17 ton) production heats of vacuum melted and air melted 2%Mn-2%Ni MIG wires, and covered (STICK) electrodes were produced on a production basis. Initial quantities of the "production-lot" electrodes were found to be lacking in one or more aimed for "optimum" characteristics, e.g., useability characteristics, root pass cracking difficulties, small deviations from aimed for composition, etc. These problems were generally ameliorated by reprocessing and vacuum annealing of the filler metals to achieve better surface conditions on the MIG wires (free of oxide and/or die-lubricant contamination) and by modifications of the coating or flux formulations used on the STICK electrodes. The general experience gained with these initial production heats of 2%Mn-2%Ni weld metals is expected to result in the production of "improved" versions of the 2%Mn-2%Ni filler metals which will be studied extensively along with the recently available "matching" 5%Ni-Cr-Mo-V filler metal.

DWTT OF "NEW" 9Ni-4Co-0.20C ALLOY HIGH STRENGTH STEELS

Fracture toughness data for several grades of the recently developed Ni-Co family of alloy compositions (designated 9-4-0.XXC) were presented in previous investigations (22, 23, 24). These have involved plates of the two basic compositions (available commercially since 1962) containing 0.25%C and 0.45%C as well as several "experimental" versions of the basic alloy containing lower carbon and increased chromium and molybdenum contents from that specified for the basic 9-4 alloys (AMS 6540 through AMS 6546). The proprietary designation of 9-4 may be partly misleading in that the steels of this alloy family are all reported to contain 7.0 to 8.5%Ni and produced to a specification range of 7.0 to 9.0%Ni. The basic 9-4 composition can be adjusted or the heat treatment varied to develop YS levels ranging from approximately 150 to 250 ksi as required for specific applications. Composition modifications or "rebalancing" of the alloy by the producer to secure better combinations of strength and toughness than that developed by the commercially available grades of the 9-4 alloys resulted in a new member of this Ni-Co alloy family, designated 9-4-0.20C and aimed at 180 ksi minimum YS, being made commercially available in the latter half of 1966.

In all cases, commercial production of the 9-4 steels have involved special melt practices involving vacuum arc remelt (VAR) practice of electrode ingots

produced from a basic electric furnace (EF) air melt heat. The initial EF melting is performed without the use of strong deoxidizers, and the resulting electrode ingot product is relatively high in oxygen content in the form of oxides. In subsequent vacuum arc remelting at sufficiently low pressures, the carbon acts effectively as a deoxidizer capable of reducing oxygen to very low levels providing the oxygen is not tied up as highly stable oxides. The producer has designated the term "VAR-C-DOX" to signify "vacuum-arc-remelt, carbon-deoxidation." During vacuum arc remelting, a carbon "boil" is experienced and results in the evolution of CO gas during the remelting operation. The specific special melt practices used for the 9-4 steels are aimed at producing material essentially "free" of deoxidation product inclusions ("dirt") and of a considerably lower gas (O_2, H_2 and N) content than that produced by conventional practices. Present VAR facilities are limited to electrode ingot sizes from approximately 5 to 15 tons. Usually ten (10) or more electrode ingots are poured from the initial EF (70-80 ton) melt; however, the producer considers the product from each VAR ingot as separate "production" heats of the 9-4 alloy.

Small plate sections (approximately 1 x 18 x 36-in.) from two of the VAR heats of material produced from the first large (70 ton) EF heat of the "new" 9-4-0.20C alloy steel were received in the mill quenched-and-tempered (Q&T) heat treatment condition for evaluation studies by NRL. It is apparent from the C_V curves established for the "weak" (WR) and "strong" (RW) orientations of fracture in these plates, Fig. 64, that both plates had been produced with relatively high (essentially 1 to 1) degrees of cross rolling. The average 0.505-in. diameter tension test data also shown for these steels in Fig. 65 indicate that both steels developed YS levels slightly above the 180 ksi minimum YS specified for these steels. Fracture appearance ratings of these steels could not be established from macro features of the C_V test specimens; however, the energy absorption curves suggest that C_V shelf energy values are developed by these steels at temperatures of 0°F and higher. The procurement of additional plates of "new" 9-4-0.20C steels is planned to develop the DWTT energy absorption versus temperature behavior of these steels and, thus, establish the significance of the relatively high (in excess of 50 ft-lb) C_V values noted in Fig. 64 for subzero temperatures.

A summary of the DWTT-YS relationships for all of the 9-4 steels evaluated to date is presented in Fig. 65.

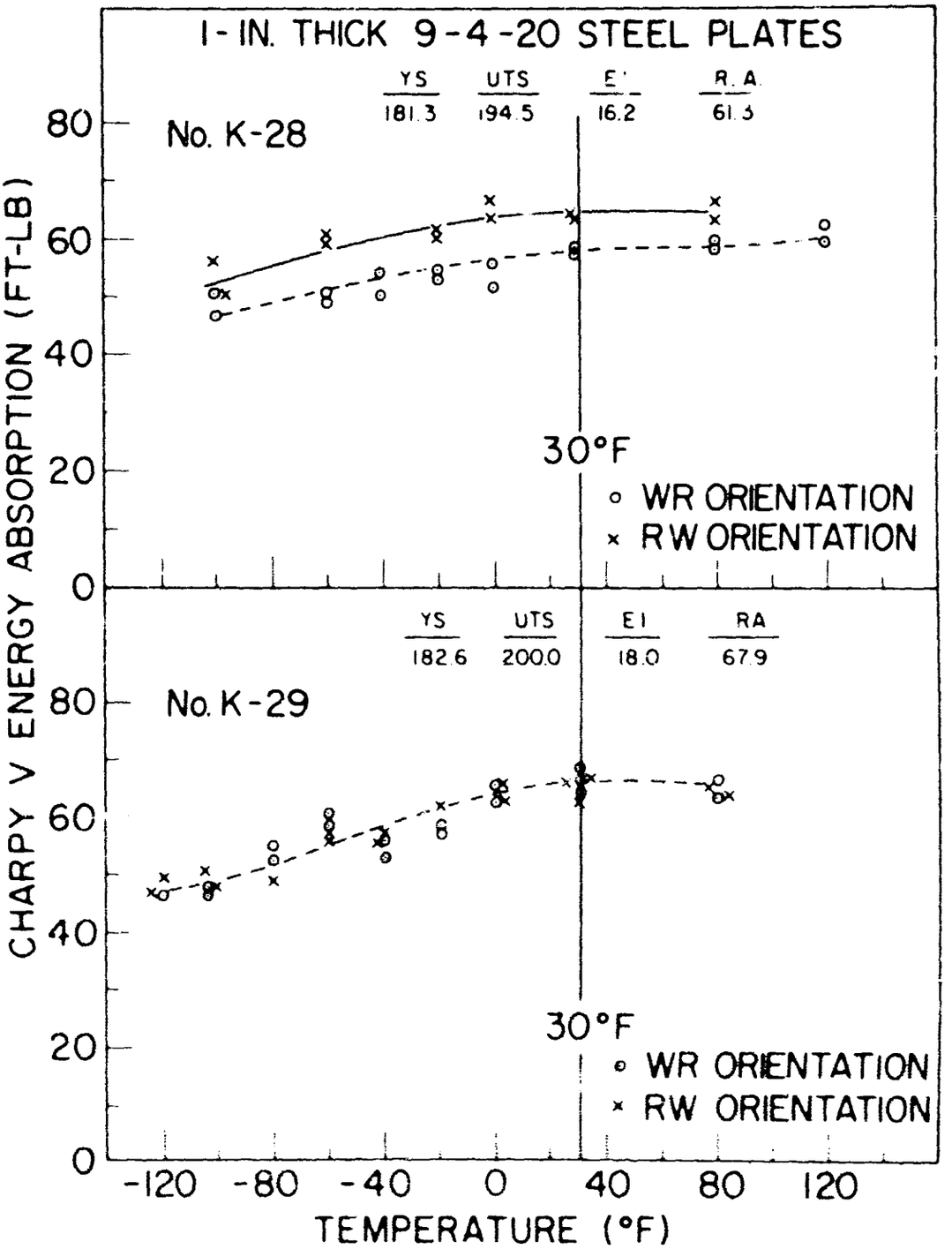

Fig. 64 - Charpy V energy absorption curves for two 1-in. thick plates of the "new" 9-4-0.20C steel alloy

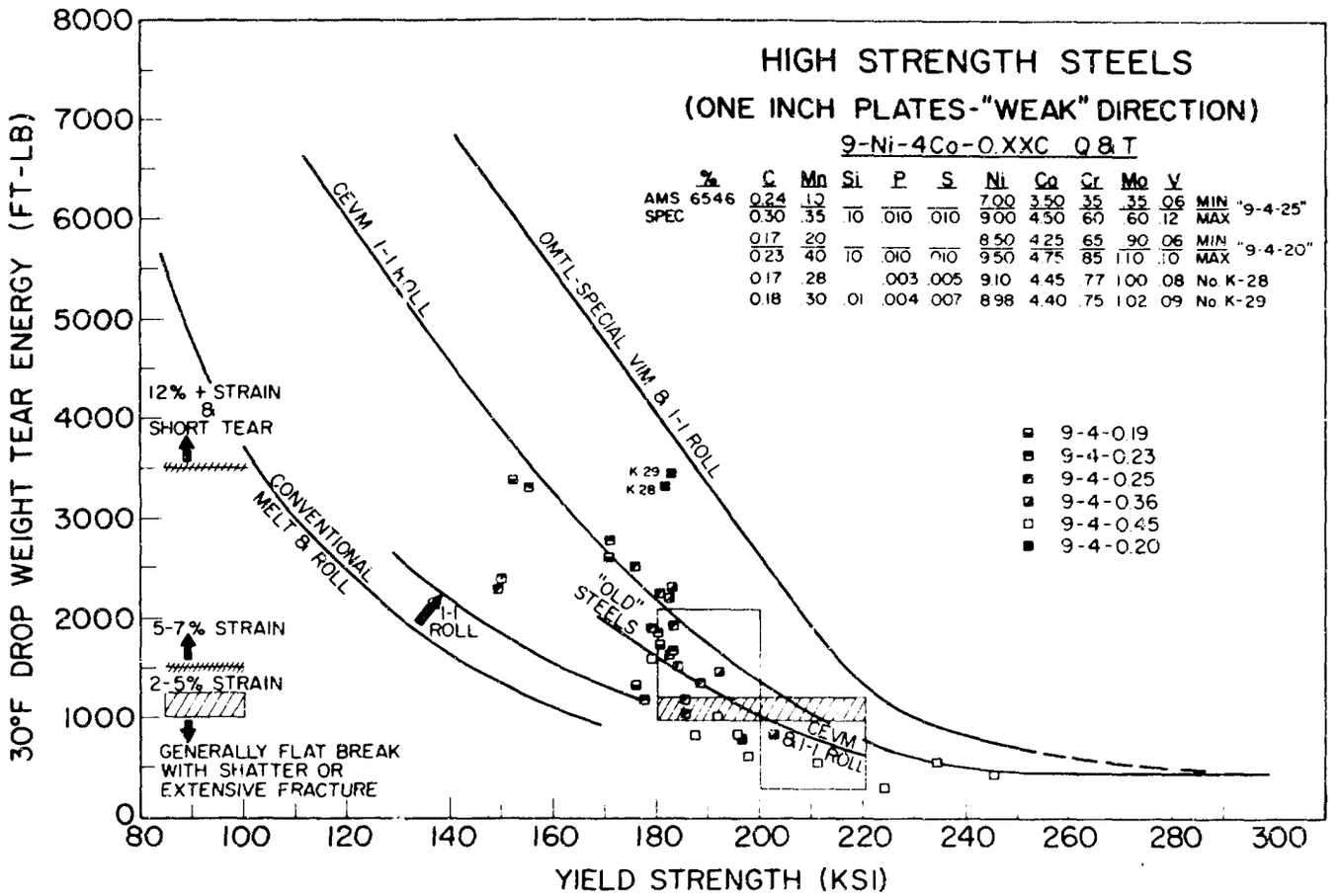

Fig. 65 - Spectrum view of standard drop-weight-tear-test - yield strength relationships for all 9Ni-4Co steel alloys studied to date, as referenced to the basic FTID-OMTL data for 1-in. thick steel plates

Also shown in this illustration is a comparison of the chemical compositions specified for the basic 9-4-0.25C (AMS 6546) alloy with that of the "new" 9-4-0.20C steel. Both of these grades of the 9-4 alloy are designed to develop 180 ksi minimum YS. Except for carbon content, the compositions are noted to be similar; however, significantly higher contents of Ni, Co, Cr, and Mo are specified for the "new" 9-4-0.20C alloy than that expected for "average" composition of the 9-4-0.25C basic alloy. The specific mill heat analyses given in the illustration for the two plates (Nos. K28 and K29) evaluated in this investigation are noted to represent low carbon, low residual Mn, Si, P, S, and high Ni, Co, Cr, Mo, V versions of the "new" 9-4-0.20C alloy. The similarity in composition of these plates from two VAR "production" heats suggests that the basic composition of the initial EF melt predominates and controls the resulting composition of the various VAR ingot heats produced from a given EF melt.

The "new" 9-4-0.20C steels (Nos. K28 and K29) are noted in Fig. 64 to be characterized by considerably higher DWTT fracture toughness than any of the previously tested 9-4-0 steels for yield strengths of approximately 180 ksi. Previously studied experimental versions of this "new" alloy (designated 9-4-0.19C and 9-4-0.23C) contained considerably lower Ni (6.81 and 7.13% respectively) and higher Cr and Mo contents than those now illustrated for the "rebalanced" alloy. The "experimental" lower nickel and carbon content and higher Cr-Mo content versions of the basic 9-4-0.25C alloy are noted to exhibit lower YS levels and higher fracture toughness than those obtained by the basic 9-4-0.25C alloys. At a 180 ksi minimum YS level, the DWTT fracture toughness values of various basic 9-4-0.25 steel plates ranged from 1000 to 2200 ft-lb compared to approximately 3300-3500 ft-lb for the "new" 9-4-0.20C alloy steels (Nos. K28 and K29). The high carbon content (9-4-0.45C) alloy steel is noted to be capable of propagating fractures at elastic stress levels for all heat treatment conditions studied except that of Q&T 1100°F. For this heat treatment condition, however, the YS of the 9-4-0.45C alloy is noted to be below the 180 ksi minimum YS level developed by the basic 9-4-0.25C and the "new" 9-4-0.20C steels.

DWTT OF 9Ni-4Co AND MARAGING STEEL WELD METALS

The 9-4-0.25C steels and the 12-5-3 maraging steels have appeared promising for nominally 180 ksi minimum YS structural applications. Weld wires for these alloys, however, have not been generally available commercially. Preliminary evaluations of producer-fabricated, TIG process, 180 ksi YS weldments using "experimental" electrodes produced

from small (150 lb) research quality heats were reported to be highly encouraging for weldments in both of these alloy steels (24, 25). For further studied required for the characterization of critical properties of such weldments, weld wires representative of semiproduction heats (1000 lb) were procured. Specifications for these weld metals were based upon producers recommendations to obtain the "best" weld wire product possible. The 9Ni-4Co filler metal procured for this investigation was melted to an aim chemical composition representing that of the "best" of the experimental filler metals developed for welding the basic 9-4-0.25C alloy steel as described recently by Ries and Poole (29). The composition is similar but lower in Ni and Co to that of the new composition specified for the 9-4-0.20C alloy steel.

As described in earlier reports (5, 7, 24), two weld metals have been evolved for fabricating the 12Ni-5Cr-3Mo maraging steels. These comprise a nominal 12Ni-3Cr-3Mo (12-3-3) wire composition, expected to develop a 160 ksi minimum YS upon aging, and a nominal 17Ni-2Co-3Mo (17-2-3) wire composition expected to develop a 180 ksi minimum YS upon aging. Preliminary studies with manual TIG weldments indicated that both of these weld compositions developed optimum C_V toughness-strength relationships upon aging for relatively long times (10 to 24 hr) at 850°F and that short time aging at 900°F resulted in the development of YS levels 15 to 20 ksi below the 160 and 180 ksi YS "expected" respectively for the 12-3-3 and the 17-2-3 weld metals (7). For comparison with continuing weldment evaluation studies of these two weld metals, a limited amount of a "matching" composition filler metal (containing 12Ni-5Cr-3Mo-0.3Ti-0.3Al) was procured from the INCO Research Laboratory facility. This filler metal was produced by converting sections of 2-in. thick rolled plates from a VIM heat of the 12-5-3 alloy into weld wire.

A series of enlarged (1-in. wide) single "V" joint preparation weldments were fabricated by NRL to provide material for DWTT of the various filler metals described above. The automatic tungsten-arc-inert-gas (TIG) cold wire feed process was used for all welding in this study. Generally, producers' recommendations for optimum welding procedures were followed; and these resulted in similar conditions and weld heat inputs (44 to 46 kilojoules per inch) for both the 12-5-3 maraging and the 9-4-0.25C Q&T steels. Argon at a flow rate of 40 cfh was used as shielding gas (no auxiliary shielding was used) and all weldments were started without preheat and finished with 200-225°F maximum interpass temperature control.

The maraging steel weldments were aged after fabrication. A summary of the data developed in this investigation is given in Table 20. Figure 65 presents a summary of the DWTT-YS relationships for these high strength weld metals, as referenced to the FTID-OMTL chart for 1-in. thick steel plates.

From the summary of data given in Table 20 and Fig. 66, it is generally noted that the 12-3-3 weld metal is characterized by the lowest strength and highest DWTT fracture toughness values. The 9Ni-4Co weld metals are observed to develop significantly higher YS levels and concomitantly lower DWTT fracture toughness levels than the 12-3-3 and the 17-2-3 maraging steel weld metals. Surprisingly, the "matching" composition 12-5-3 weld metal which displays 50 ft-lb C_V energy at 30°F is noted to develop the lowest DWTT energy value for all of the weldments evaluated. Additional C_V specimens of the 12-5-3 weld metal were tested at 120° and 160°F with resulting values of 63 and 68 ft-lb respectively. The implications for C_V data and low DWTT value for the 12-5-3 matching composition weld metal suggests that this weld may be within its transition temperature range at 30°F. Examination of the C_V data given in Table 20 for all maraging steel weld metals suggests that the long time aging treatment at 850°F may be responsible for developing transition temperature range aspects in the maraging weld metals.

The data developed in this investigation for the 17-2-3 weld metal, Table 20, tends to oppose the conclusion drawn previously that optimum strength-toughness relationships are developed by the 17-2-3 weld metal by long time aging at 850°F. It is noted that 3 hr aging at 900°F resulted in the development of YS levels slightly lower than the 180 ksi YS "expected" for the 17-2-3 weld composition with DWTT toughness values essentially equivalent to those developed by long time 850°F aging treatments. Continuing weldment evaluation studies in this program are expected to explore the effects of long time 850° and 900°F aging treatments on transition temperature behavior of the maraging weld metals and to establish weld metal properties of maraging and 9Ni-4Co weldments fabricated with lower weld heat inputs than those used in this investigation.

TABLE 20

TEST DATA FOR ONE-INCH-THICK TIG WELDS FOR MARAGING AND 9Ni-4Co FILLER METALS

			0.505-in.-diam. Tensile Test Data All Weld Metal Specimens						
NRL No.	Type	Aging (°F/hr)	YS (ksi)	UTS (ksi)	El. (%)	RA (%)	C_v at 30°F	C_v at 80°F	DWTT at 30°F
M 11*	12-3-3	850/24	163.7	170.9	15.0	61.8	72	82	3228*
M 12*	17-2-3	850/24	180.5	193.0	15.0	60.0	48	52	2560*
M 13	"	850/12	164.8	175.6	14.5	59.9	47	57	2560
M 19	"	900/3	174.0	183.4	15.0	59.0	50	50	2733
M 20	"	900/3	179.3	187.0	14.0	55.8	45	47	2501
M 5	12-5-3	850/12	179.0	188.0	16.0	62.4	48	48	--
M 7*	"	850/24	181.1	188.5	13.0	58.2	50	56	1356*
M 14	9-4-25	None	193.5	222.3	16.5	35.2	40	40	1905
M 16	"	"	204.1	220.9	17.0	46.6	43	45	1601
M 17	"	"	198.1	217.8	20.0	56.8	44	48	--
M 18**	"	"	216.3	221.7	12.0	60.7	36	38	1662

* Two-in. thick weldments evaluated in DWTT with standard 1 x 5 x 18-in. specimens. All other weldments were 1-in. thick.

** Filler metal from production vacuum arc remelted ingot heat No. 3931006 of the basic 9-4-0.25C alloy composition.

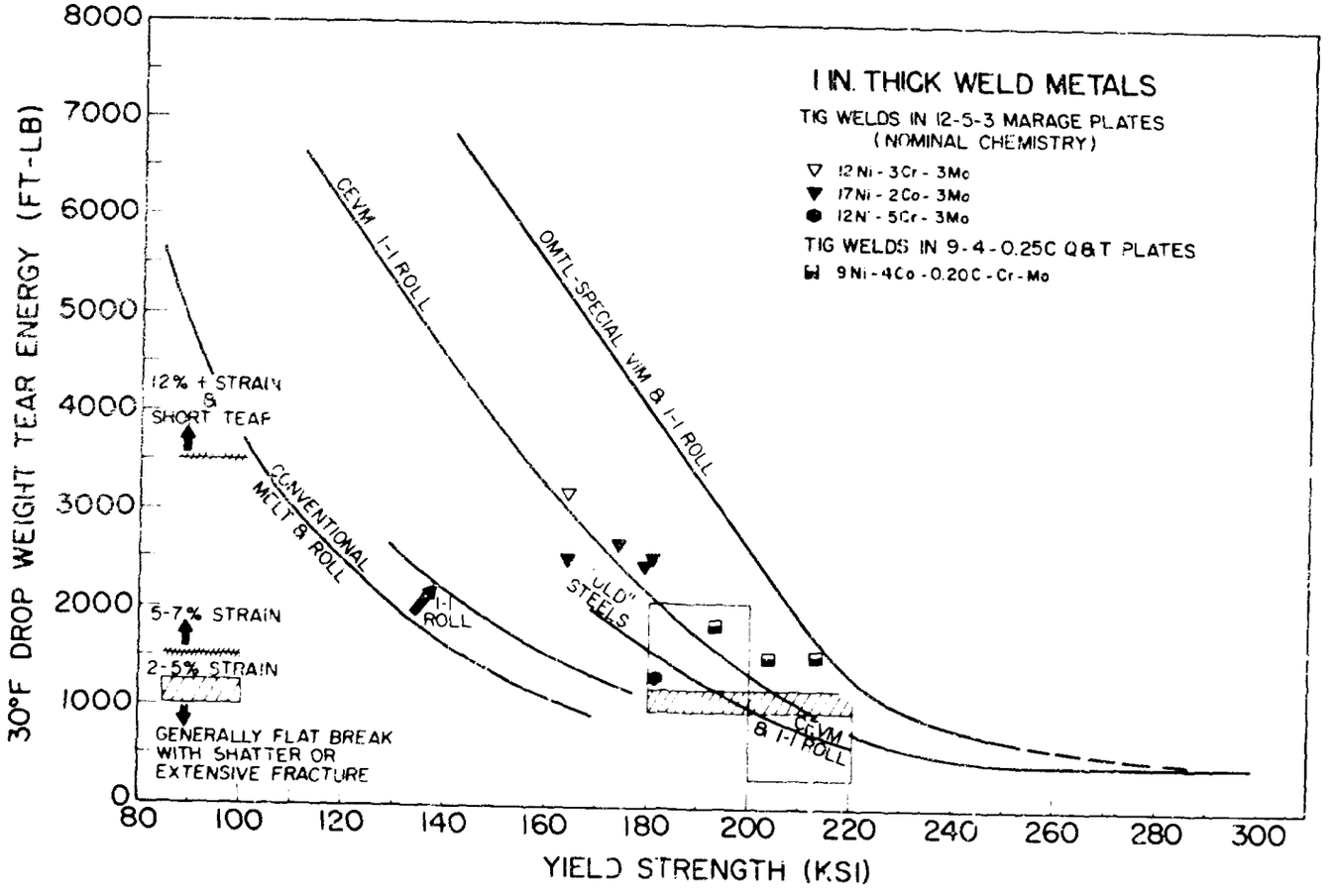

Fig. 66 - Summary of drop-weight-tear test - yield strength relationships for high strength TIG weld metals of the 9Ni-4Co alloy steel and maraging steel alloys, as referenced to the basic FTL-OMTL data for 1-in. thick steel plates

REFERENCES

1. Pellini, W. S., et al., "Review of Concepts and Status of Procedures for Fracture-Safe Design of Complex Welded Structures Involving Metals of Low to Ultra-High Strength Levels," NRL Report 6300, June 1965

2. Goode, R J., et al., "Metallurgical Characteristics of High Strength Structural Materials (Ninth Quarterly Report)," NRL Report 6405, November 1965

3. Goode, R. J. and Huber, R.W., "Fracture Toughness Characteristics of Some Titanium Alloys for Deep-Diving Vehicles,"Journal of Metals, August 1965

4. Howe, D. G., "Effects of Heat Treatment on the Stress-Corrosion-Cracking Resistance of Several Ti-Al-Mo-V Alloys", Report of NRL Progress, February 1966, pp.14-18.

5. Goode, R. J., et al., "Metallurgical Characteristics of High Strength Structural Materials (Tenth Quarterly Report),"NRL Report 6454, April 1966

6. Howe, D. G., "Effect of Heat Treatment on the Stress-Corrosion-Cracking Resistance of Several Titanium Alloys", Report of NRL Progress, July 1966, pp. 20-21

7. Puzak, P.P., et al., "Metallurgical Characteristics of High Strength Structural Materials (Eleventh Quarterly Report)",NRL Report 6513, August 1966

8. Howe, D. G., "Properties of Ultra High Strength Alloys (Effect of Heat Treatment on the Stress-Corrosion-Cracking Resistance of Several Titanium Alloys)", Report of NRL Progress, September 1966, pp. 25-27

9. Howe, D. G., "Effects of Heat Treating Environmental Conditions on the Stress-Corrosion-Cracking Resistance of Several Titanium Alloys", Report of NRL Progress, February 1967

10. Brown, B. F. and Beachem, C. D., "A Study of the Stress Factor in Corrosion Cracking by Use of the Precracked Cantilever Beam Specimen", Corrosion Science, Vol. 5, No. 11, 1965, pp. 745-750

11. Kies, J. A., et al., "Fracture Testing of Weldments" in Fracture Toughness Testing and Its Applications, ASTM STP 381, American Society for Testing and Materials, 1965

12. Brown, B.F., "A New Stress-Corrosion Cracking Test Procedure for High Strength Alloys," ASTM Materials Research and Standards, Vol. 66, No. 3, March 1966

13. Brown, B. F., et al., "Marine Corrosion Studies, (Third Interim Report of Progress)" NRL Memo Report 1634, July 1965

14. ASTM Materials Research and Standards, Vol. 1, No. 5, May 1961

15. Judy, R. W., Jr., and Crooker, T. W., et al., "Fractographic Analysis of Ti-7Al-2Cb-1Ta and Ti-6Al-4V Fractures Developed in 'Wet' Fatigue," NRL Report 6330, January 1966

16. Lange, E.A., and Klier, E.P., "A Study of Fracture Development and Materials Properties in PVRC Vessels 1 and 2," Welding Journal Research Supplement, Vol. 27, No. 2, February 1962

17. Lange, E.A., et al., "Failure Analysis of PVRC Vessel No. 5," Welding Research Council Bulletin, No. 98, August 1964

18. Pellini, W.S., and Puzak, P.P., :Fracture Analysis Diagram Procedures for the Fracture-Safe Engineering Design of Steel Structures," NRL Report 5920, March 1963

19. Kooistra, L.F., Lange, E.A., and Pickett, A.G., "Full-Size Pressure Vessel Testing and Its Application to Design," TRANS of the ASME Journal of Engineering for Power, Vol. 86, Series A, No. 4, October 1964

20. Crooker, T.W., and Lange, E. A., "Low Cycle Fatigue Crack Propagation Resistance of Materials for Large Welded Structures", Proceedings, ASTM Fatigue Crack Propagation Symposium, Atlantic City, N.J., June 30-July 1, 1966 (publication pending)

21. Crooker, T.W., and Lange, E.A., "Corrosion Fatigue Crack Propagation in Modern High Performance Structural Steels," AIME Symposium, The Effect of Environment on the Mechanical Properties of Metals, Chicago, Illinois, October 31, 1966 (publication pending)

22. Goode, R.J., et al., "Metallurgical Characteristics of High Strength Structural Materials (Fourth Quarterly Report)", NRL Report 6137, June 1964

23. Puzak, P.P., Lloyd, K.B., Goode, R.J., Huber, R.W., Howe, D.G., Crooker, T.W., Lange, E.A., Pellini, W.S., "Metallurgical Characteristics of High Strength Structural Materials, (Third Quarterly Report),"NRL Report 6086, January 1964

24. Puzak, P.P., Lloyd, K.B., Goode, R.J., Huber, R.W., Howe, D.G., Judy, R.W., Jr., Crooker, T. W., Morey, R.E., Lange, E.A., and Freed, C.N., "Metallurgical Characteristics of High Strength Structural Materials, (Eighth Quarterly Report)", NRL Report 6364, August 1965

25. Goode, R.J., et al., "Metallurgical Characteristics of High Strength Structural Materials, (Seventh Quarterly Report)", NRL Report 6327, May 1965

26. The ASTM Committee on Fracture Testing of High-Strength Metallic Materials, "The Slow Growth and Rapid Propagation of Cracks"(Second Report), ASTM Materials Research Standards, Vol. 1, No. 5, May 1961

27. Pellini, W.S., et al., "Metallurgical Characteristics of High Strength Structural Materials, (Sixth Quarterly Report), NRL Report 6258, December 1964

28. Pellini, W.S. and Puzak, P.P. "Factors that Determine the Applicability of High Strength Quenched and Tempered Steels to Submarine Hull Construction", NRL Report 5892, December 5, 1962

29. Ries, G.D. and Poole, S.W., Welding Journal Research Supplement, October 1966, Vol. 31, No. 10, p. 465-S

Security Classification

DOCUMENT CONTROL DATA - R & D

Security classification of title, body of abstract and indexing annotation must be entered when the overall report is classified

1 ORIGINATING ACTIVITY (Corporate author) Naval Research Laboratory Washington, D. C. 20390	2a. REPORT SECURITY CLASSIFICATION Unclassified 2b. GROUP

3 REPORT TITLE

METALLURGICAL CHARACTERISTICS OF HIGH STRENGTH STRUCTURAL MATERIALS (Twelfth Progress Report)

4 DESCRIPTIVE NOTES (*Type of report and inclusive dates*)

Progress report on the project

5 AUTHOR(S) (*First name, middle initial, last name*)

Goode, R.J., Huber, R.W., Howe, D.G., Judy, R.W., Jr., Crooker, T.W., Lange, E.A., Freed, C.N., and Puzak, P.P.

6 REPORT DATE	7a. TOTAL NO OF PAGES	7b. NO OF REFS
September 1967	133	29

8a. CONTRACT OR GRANT NO	9a. ORIGINATOR'S REPORT NUMBER(S)
NRL Problem Nos. F01-17 b. PROJECT NO M01-05 M01-18 c M03-01 M04-08B d.	NRL Report 6607 9b. OTHER REPORT NO(S) (*Any other numbers that may be assigned this report*)

10 DISTRIBUTION STATEMENT

This document has been approved for public release and sale; its distribution is unlimited.

11 SUPPLEMENTARY NOTES	12 SPONSORING MILITARY ACTIVITY
	Special Projects-Department of the Navy Office of Naval Research Advance Research Projects Agency

13 ABSTRACT

A progress report covering the research studies in high strength structural metals conducted during the period July 1966 through January 1967 is presented. The report includes fracture toughness studies on some new titanium alloys as well as results of an initial feasibility study aimed at raising the optimum strength and toughness limits for titanium alloys through an approach involving thick section composites. The results of salt water stress-corrosion-cracking studies on a number of titanium alloys are described including a study concerning the effect of vacuum heat treatment on stress-corrosion-cracking resistance of titanium alloys. Fatigue crack propagation studies in air and in salt water on the pressure vessel steels A302B, A201B, and A517F are discussed; and the results compared to the actual service performance of these same materials in PVRC program studies. Preliminary fracture toughness correlation diagrams are presented for high strength steels based upon fracture mechanics and engineering test methods. The latest versions of the Fracture Toughness Index Diagrams for steels, titanium alloys and aluminum alloys, a usual feature of this report series and which are based upon engineering test methods, are presented and the significance of the features briefly discussed. Fracture toughness studies on thick plates of 5Ni-Cr-Mo-V, and a "new" 9Ni-4Co steel are reported. In addition, the results are presented for similar studies on welds of 2Mn-2Ni in 5Ni-Cr-Mo-V steels and welds of 9Ni-4Co, 12Ni-3Cr-3Mo and 17Ni-2Co-3Mo compositions.

DD FORM 1 NOV 1473 (PAGE 1)

S/N 0101-807-6801

Security Classification

Security Classification

14 KEY WORDS	LINK A		LINK B		LINK C	
	ROLE	WT	ROLE	WT	ROLE	WT
High-strength structural metals Fracture toughness studies High-strength titanium alloys Heat treatments Stress-corrosion-cracking resistance of titanium alloys Low cycle fatigue crack propagation in pressure vessel steels Aluminum alloys						

DD FORM 1 NOV 1473 (BACK)
(PAGE 2)

Security Classification

GPO 931-308